UNIVERSITEIT·STELLENBOSCH·UNIVERSITY
jou kennisvennoot • your knowledge partner

Design Procedures for Series and Parallel Feedback Microwave DROs

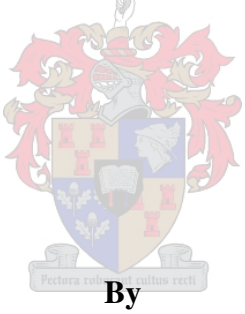

By

Nauwaf Alaslami

Thesis presented in partial fulfilment of the requirements for the degree of Master of Science in Engineering at the University of Stellenbosch

Supervisor:

Prof. JB de Swardt

December 2007

Decliration

I, the undersigned, hereby declare that the work contained in this assignment/thesis is my own original work and that I have not previously in its entirety or in part submitted it at any university for a degree.

Signature: ..... Date: .....

Acknowledgements

I would like to thank the following persons who helped me in various ways during the completion of my thesis

Professor J.B. de Swardt, my study leader. Thank you for your guidance, patience, knowledge and understanding.

Wessel Croukamp and Ulrich Buttner: I admire your technical ability and your patience with my last minute alterations. The excellence of your work has never stopped amazing me.

Ashley: Thank you for making my PCBs. And for making my final PCBs in one afternoon

M.J. Siebers: Thank you for helping me with my measurements and for organizing the fifth floor lab.

All the guys and girl in E212: It has been a pleasure to work with you and thank you for all your help.

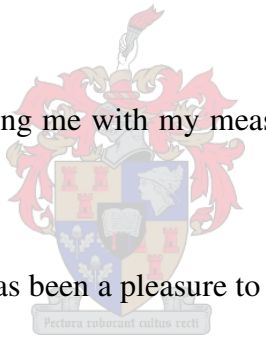

Abstract

Clear procedures for designing dielectric resonator oscillators (DROs) are presented in this thesis, including built examples to validate these design procedures. Both series and parallel feedback DROs are discussed and the procedures for building them are presented. Two examples at different frequencies for each type of DRO are constructed and tested with the results shown. The first is at a frequency of approximately 6.22 GHz and the second for the higher frequency of 11.2 GHz. The DROs for the desired frequencies are designed using the Microwave Office (MWO) software by AWR with the design based on the small-signal model (scattering parameters). Oscillators are produced using the negative resistance method. The circuit achieves low noise by using a dielectric resonator with a high Q factor. Both the series and parallel feedback DRO circuits can be mechanically tuned around the resonant frequency to maximize performance.

Opsomming

Duidelike prosedures vir die ontwerp van diëlektriese resoneerder ossillators (DROs) word ten toon gestel in hierdie tesis beskryf en voorbeelde word gebruik om hierdie prosedures te illustreer. Serie en parallelle terugvoer DROs is bespreek en die vervaardiging van beide word ondersoek. Twee voorbeelde van beide tipes DRO word vervaardig en getoets by twee verskillende frekwensies en die resultate word getoon. Die een frekwensie is ongeveer 6.22 GHz en die ander ’n hoër frekwensie van ongeveer 11.2 GHz. Die DROs is ontwerp deur gebruik te maak van die Microwave Office (MWO) sagteware pakket deur AWR en die ontwerp is gebaseer op die kleinseinmodel (weerkaatsparameters). Ossillators is vervaardig deur gebruik te maak van die negatiewe weerstand metode. Ruis in die stroombaan is laag omdat ’n diëlektriese resoneerder met hoë Q faktor gebruik is. Beide die serie en parallelle terugvoer DRO stroombane kan rondom die resonansfrekwensie meganies verstel word vir optimale werking.

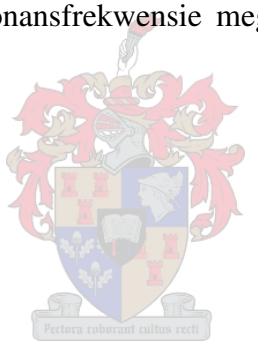

List of Figures

List of Tables

List of abbreviations and symbols

dB	decibel
Hz	Hertz
GHz	Giga Hertz
MHz	Mega Hertz
kHz	Kilo Hertz
PCB	Printed circuit board
dBm	Decibel with reference to 1 mW
dBc/Hz	Decibel with respect to the carrier frequency per hertz
DC	Direct current
RF	Radio frequency
VCO	Voltage controlled oscillator
Z_0	Characteristic impedance of the system (usually 50Ω)
Q	Quality factor
Q_0	Unloaded quality factor
Q_L	Loaded quality factor
Γ	Reflection losses
β	Coupling factor
dBc	Decibel with respect to the carrier frequency
mA	Milliampere
DR	Dielectric resonator
LMDS	Local Multipoint Distribution Service
DRO	Dielectric resonator oscillator
PLDRO	Phase-locked dielectric resonator oscillators
UHF	Ultra High Frequency
VHF	Very High Frequency
MIC	Microwave integrated circuit
$\mathbf{f_t}$	transition frequency
GBW	gain bandwidth

Si	silicon
GaAs	gallium arsenide
SiGe	silicon germanium
BJT	bipolar junction transistors
FET	field effect transistor
HBT	hetero junction bipolar transistors
HEMT	high electron-mobility transistors
MESFET	Metal-Semiconductor-Field-Effect-Transistor
B1	stability measure
K	Rollet stability factor
ε_r	dielectric constant
kΩ	Kilo ohm
f_o	Resonance frequency
DRA	Dielectric Resonant Antenna
RLC	Resistor inductor capacitor
TE	Transverse electric
L_0	Insertion loss
λ_g	wavelength
CST	Microwave Studio software
MWO	Microwave office software
L	Length
$\lambda/4$	Quarter wavelength
Ro	Outer radius of the stub
W	Microstrip line width
Wg	Width of crossing of stub and microstrip line
δ	Delta
G_A	Amplifier gain
L_F	Feedback circuit loss
φ_A	Phase shift of the transistor
Rext	External resistance

Qext	External quality factor
N	Transformer Turn ratio
L (f_m)	Phase noise

CHAPTER 1

Introduction

1.1 Brief Historical Background

R.D. Richtmyer showed in 1939 that unmetallized dielectric objects can function similarly to metallic cavities which he called dielectric resonators (DRs) [1]. Practical applications of DRs to microwave circuits, however, began to appear only in the late 60's as resonating elements in waveguide filters [2]. Recent developments in ceramic material technology have resulted in improvements including small controllable temperature coefficients of the resonant frequency over the useful operating temperature range, and very low dielectric losses at microwave frequencies. These developments have revived interest in DR applications for a wide variety of microwave circuit configurations and subsystems [3, 4].

Armstrong had made the first electronic oscillator in September of 1912 using Lee DeForest's new device, the audion, which is now known as the triode vacuum tube. Microwave oscillators started with vacuum tubes and ruled this field for about three decades starting in 1940. Gunn and IMPATT diode oscillators dominated signal generation applications before 1970. By the mid 1970s, the three terminal devices took over. Dielectric resonator oscillators came into use by the late 1970s [5].

1.2 Motivation for the study

High performance oscillators are in high demand for modern microwave and millimetre-wave systems. They are used for local multipoint distribution services (LMDS), fixed satellites, digital point-to-point radio services, automotive radars, wireless LANs, and others. The high cost of licensed spectrum has promoted the introduction of new point-to-point and point-to-multipoint communication systems operating at the higher millimetre wave frequencies, such as the local multipoint distribution services (LMDS) operating at 28/38 GHz [6, 7].

On the other hand, the microwave radar technology has been encouraged in the field of sensor applications [8], such as tank level and contactless vehicle speed and distance measurements [9, 10]. Sensor technology will benefit from a higher operating frequency, which guarantees smaller sensor size and improved resolution. There has therefore been a shift for level measurement applications from the traditional 5.8and10 GHz frequencies to the 24 GHz range [9]. In the automobile industry, anti-collision radar systems operating at 24, 77 and 94 GHz frequency range have already been reported [10, 11]. These systems need frequency sources with low near-carrier noise and little frequency drift with time.

Stabilized oscillators also provide a lower pushing which is reducing the frequency drift due to power supply changes and higher frequency stability. Dielectric resonators (DR's) have traditionally been the choice for oscillation stabilization. For digital communications and broadcasting via satellites, the ground stations usually use dielectric resonance oscillators (DRO) or phase locked dielectric resonance oscillators (PLDRO) as the stable microwave frequency source. Phase-locked dielectric resonator oscillators (PLDROs) with superior phase-noise performance and low cost were also applied to local multipoint distribution systems (LMDS) and other point-to-multipoint systems that employ higher order M-ary modulation schemes and operate at millimetre frequencies of 24 GHz and above [12].

For these purposes, DR's are placed either directly on MIC's [13] or on an adjacent substrate [14]. However, they are not fully monolithic and the circuits still require careful post-fabrication attention. This is to position the dielectric puck onto the main substrate or onto a second adjacent substrate. High placement accuracy is required in the final assembly, especially at higher frequencies. The demanding factors of cost, size and reliability made by the developing collision-avoidance radar market still point toward a fully monolithic solution to the problem [15]. Dielectric resonators have found extensive applications in modern electronic systems e.g. as key elements of UHF, VHF and microwave filters, stabilising elements of microwave oscillators and as part of material property measurement fixtures [16].

Dielectric resonator oscillators are also used widely in today's electronic warfare, missile and radar systems. They find use both in military and commercial applications. The DROs are characterized by low phase noise, compact size, frequency stability with temperature, ease of integration with other hybrid MIC circuitries, simple construction and the ability to withstand harsh environments. These characteristics make DROs a natural choice both for fundamental oscillators and as the sources for oscillators that are phase-locked to reference frequencies, such as crystal oscillators.

Since it is clear that there is a definite need for improved DROs, so there is a need for a clear and uncomplicated design procedure.

1.3 The Aim of the Thesis

The aim of this study is to develop a clear procedure for designing dielectric resonator oscillators. A general overview of oscillator design and considerations will be discussed to give the reader essential information about oscillators and oscillator designs. Some aspects of dielectric resonators are investigated including coupling and modes. Thereafter, the two common dielectric resonator oscillator configurations are examined and examples of each design are given.

1.4 Thesis Organization

This thesis concentrates on the design procedures of dielectric resonator oscillators of the two most common topologies of DROs which are the series and parallel feedback topologies.

Chapter 2 will give some necessary information that is needed to be known about oscillators. The types, configurations, and topologies of oscillators will be presented as well as the basic procedure of designing oscillators. The choice of the active part is also discussed. This chapter will also give an overview of dielectric resonator oscillators design approach.

Since the main focus of the thesis is DROs, chapter 3 will give an overview of dielectric resonators. The important properties of dielectric resonator oscillators will be .measured. The extraction of the electric model of the dielectric resonator is done using s-parameters measurements.

Chapter 4 will discuss a design procedure of the series feedback dielectric resonator oscillator in detail. Two examples were designed and built to verify the procedure. The first example is centred at a frequency of approximately 6.22 GHz and the second is centred at a frequency of roughly 11.2 GHz.

In chapter 5, the design procedure of parallel feedback dielectric resonator oscillators is discussed. In this chapter several parallel dielectric resonator oscillators are used to demonstrate the effect of spacing between the dielectric resonator and the microstrip lines.

Chapter 6 will summarize the work which has been done in the past and some future recommendations will be stated.

CHAPTER 2

Oscillators

2.1 Introduction

Wave generators play a big role in the field of electronics. They generate signals from a few hertz to several gigahertz. Modern wave generators use many different circuits and generate outputs such as sinusoidal, squire, rectangular, sawtooth and trapezoidal waveshapes.

A sinusoidal oscillator produces a sine-wave output signal. Ideally, the output signal is of constant amplitude with no variation in frequency. In fact, something less than the ideal is always obtained. The degree to which the ideal is approached depends on some factors such as amplifier characteristics, frequency stability and amplitude stability.

Sine-wave oscillators produce signals ranging from low audio frequencies to ultrahigh radio and microwave frequencies. Most low frequency oscillators use resistors and capacitors to form their frequency determining networks and are referred to as RC oscillators. They are widely used in the audio-frequency range.

The second type of sine-wave generator uses inductors and capacitors for its frequency determining network. This type is known as LC oscillators. LC oscillators, which use tank circuits, are commonly used at higher radio frequencies. They are not suitable for use as very low frequency oscillators because the inductors and the capacitors would be large in size, heavy and costly to manufacture and they can be used at very high frequencies.

The third type of sine-wave oscillator is the crystal oscillator. It provides excellent frequency stability and is used from the middle of the audio range through the radio frequency range.

At higher frequencies there are several other types of resonators that can be used such as YIG, transmission lines, cavity, and dielectric resonators. The dielectric resonator will be discussed in detail in the chapter 3.

Some of the known types of oscillators according to their frequency determining network (resonator) are summarized in table 2.1.

Table 2. 1 Some known types of oscillators

Resonator	Oscillator Name
Cavity	High Q or stable oscillator
YIG	YTO (YIG tuned oscillator)
Varactor	VTO (Voltage tuned oscillator)
Transmission lines	Distributed or Microstrip oscillator
Lumped element	LC and RC oscillator
Crystal	crystal oscillator
Dielectric	DRO (dielectric resonator oscillator)

An oscillator can be thought of as an amplifier that provides itself with an input signal using feedback. By definition, the oscillator is a nonrotating device which produces alternating current and the output frequency is determined by the characteristics of the device. The primary purpose of the oscillator is to generate a given waveform at a constant peak amplitude and specific frequency and to maintain this waveform within certain limits of amplitude and frequency.

At least one component in an oscillator must provide amplification In an oscillator, a portion of the output is fed back to sustain the input. Enough power must be fed back to the input circuit for the oscillator to drive itself. To cause the oscillator to be self driven, the feedback signal must also be regenerative (positive). Regenerative signals must have enough power to compensate for circuit losses and maintain oscillations.

Virtually, every piece of equipment that uses an oscillator has two stability requirements, amplitude stability and frequency stability. Amplitude stability refers to

the ability of the oscillator to maintain constant amplitude of the output waveform. The more constant the amplitude of the output waveform is, the better the amplitude stability. Frequency stability refers to the ability of the oscillator to maintain its operating frequency. The less the oscillator varies from its operating frequency, the better the frequency stability.

A constant amplitude and frequency can be achieved by taking care to prevent variation in load, bias, and component characteristics. Load variation can greatly affect the amplitude and the frequency stability of the output of the oscillator. Therefore, maintaining the load as constant as possible is necessary to ensure a stable output. Bias variations affect the operating point of the transistor and may also alter the amplification capabilities of the oscillator circuit. A well regulated power supply and bias stabilizing circuit are required to ensure a constant, uniform signal output.

2.2 Oscillator configurations

There are three main configurations of the amplifier part in oscillators. These configurations are common base/gate, common collector/drain, and common emitter/source.

2.2.1 Common base/gate configuration

The power gain and voltage gain of the common base/gate configuration are high enough to give satisfactory operation in oscillator circuits. The wide range between the input resistance and the output resistance make impedance matching slightly harder to achieve in the common base/gate circuits than common collector/drain circuits. An advantage of the common base/gate configuration is that it exhibits better high frequency response than common collector/drain configuration.

2.2.2 Common emitter/source configuration

The common emitter/source configuration has high power gain and is used in low frequency applications. The feedback network of a common emitter/source oscillator must provide a phase shift of approximately 180 degrees for the energy, which is fed back from the output, to be in phase with the energy at the input. An advantage of the emitter/source configuration is that the medium resistance range of input and output simplifies the job of impedance matching.

Table 2. 2 Advantages and disadvantages of the common source/emitter and common gate/base topology

Types	Advantages	Disadvantages
Common emitter	High output power	Difficulties to get conditional stable bias point
Common base	High stability in the bias point	Required a negative supply

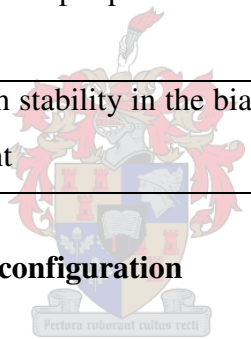

2.2.3 Common collector/drain configuration

Since there is no phase reversal between the input and the output circuits of common collector/drain configuration, the feedback network does not need to provide a phase shift. Although the voltage gain is less than unity and the power gain is low, the common collector/drain configuration is used in oscillator circuits.

2.3 Oscillators design methods

There are three main analysis or design approaches of oscillators. The first is only using a linear (small signal) approach. This approach uses only the s-parameters of the transistor which is usually available or can be measured. The second method of analysis is the quasi non-linear (large signal) technique [17]. In this technique the large signal operation is not accurate. The final analysis uses an accurate large signal model.

Since the large signal model is not always available for all transistors, the linear approach will be taken.

A typical oscillator design procedure is:

a) Choose a transistor with enough gain at the required frequency.

b) Select a circuit that gives K (Stern's stability factor) < 1 at the operating frequency. Add feedback if this is not satisfied.

c) Design an output port matching circuit that gives $|S_{11}|>1$ in the desired frequency range.

d) Place a resonator at the input port so that the value of S_{22} is greater than one.

2.4 Negative resistance in oscillators

The negative resistance theory accurately predicts the oscillation frequency and the ability of an oscillator to oscillate by simple calculation of the centre frequency and loss of the resonator and negative resistance of the transistor. However, the calculation of the loaded Q factor of the negative resistance topology is difficult. The load seen by the resonator is negative and the resulting loaded Q would be infinite if taken in this context [18]. Other analysis is done using negative resistance simply neglect loaded Q as in [19]. Loaded Q is found as a measured quantity, but not predicted in [20]. Another method must be used to predict and optimise loaded Q in a negative resistance topology for low noise oscillator design.

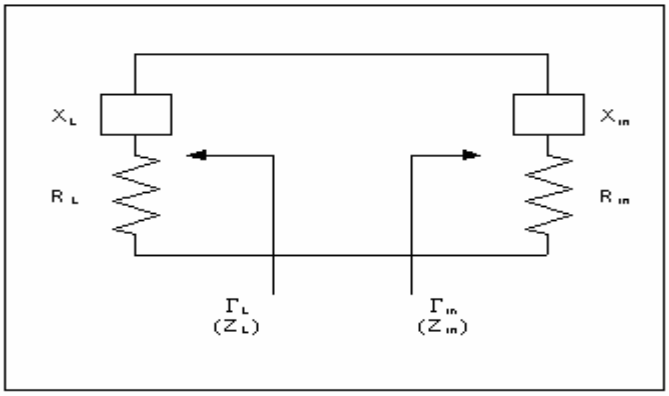

Figure 2. 1 A one port oscillator block diagram

For the circuit in figure 2.1

$$Z_{in} = R_{in} + jX_{in} \tag{2.1}$$

and

$$Z_L = R_L + jX_L \tag{2.2}$$

By KVL

$$(Z_{in} + Z_L) \times I = 0 \tag{2.3}$$

Therefore the requirement for oscillation is

$$R_L = -R_{in} \tag{2.4}$$

and

$$X_L = -X_{in} \tag{2.5}$$

Since the load is passive $R_L > 0$ so $R_{in} < 0$

$$\Gamma_L = \frac{Z_L - Z_o}{Z_L + Z_o} = \frac{-Z_{in} - Z_o}{-Z_{in} + Z_o} = \frac{Z_{in} + Z_o}{Z_{in} - Z_o} = \frac{1}{\Gamma_{in}} \tag{2.7}$$

Because R_{in} will become less negative as the oscillation builds up, it is important to choose R_L so that $R_L + R_{in} < 0$ for start-up condition..

In practice, according to [21] the value of R_L should be

$$R_L = -1/3(R_{in}) \tag{2.8}$$

or and according to [22, 23] and [24] R_{in} should be 20 percent more than R_L

$$R_{in} = -1.2(R_L) \tag{2.9}$$

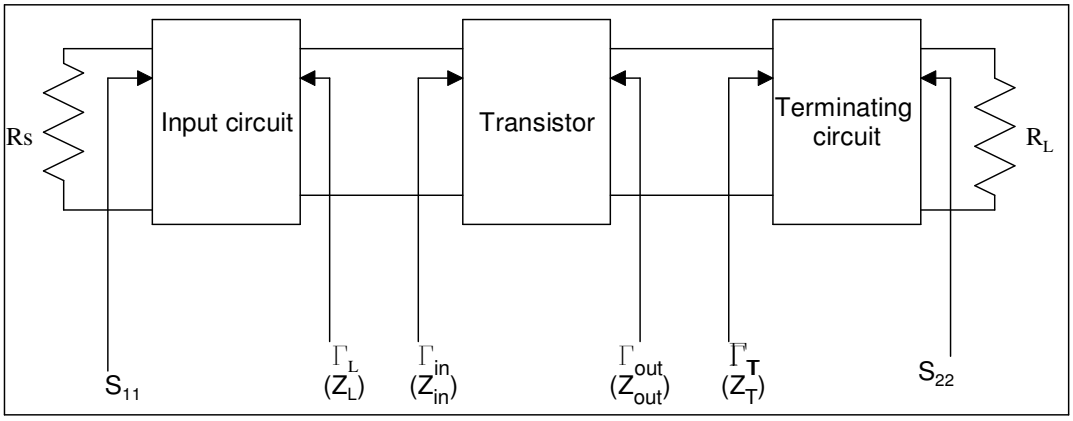

Figure 2. 2 A two port oscillator block diagram

Shown in figure 2.2, a two port oscillator circuit, will now be considered. When oscillation occurs between the input circuit and the transistor, oscillation will also occur at the output port simultaneously. For steady state oscillation at the input port, we must have $\Gamma_{in}\Gamma_L = 1$, as derived in (3.7). Then, we have

$$\frac{1}{\Gamma_L} = \Gamma_{in} = S_{11} + \frac{S_{12}S_{21}\Gamma_T}{1 - S_{22}\Gamma_T} \tag{2.10}$$

Solving for Γ_T gives,

$$\Gamma_T = \frac{1 - S_{11}\Gamma_L}{S_{22} - \Delta\Gamma_L} \tag{2.11}$$

where $\Delta = S_{11}S_{22} - S_{12}S_{21}$

Then

$$\Gamma_{out} = S_{22} + \frac{S_{12}S_{21}\Gamma_L}{1 - S_{11}\Gamma_L} = \frac{S_{22} - \Delta\Gamma_L}{1 - S_{11}\Gamma_L} \tag{2.12}$$

Which shows that $\Gamma_T\Gamma_{out} = 1$. Thus, the condition of oscillation of the terminating network is satisfied [21, 25].

2.5 Noise in oscillators

The classical approach to optimise the phase noise in a dielectric resonator oscillator consist of minimising the dielectric resonator coupling in order to obtain high Q values[26]. The relation between the phase noise and Q factor is given by

$$L(f_m) = 20\log \frac{f_0 \times \Delta\varphi_T}{2\sqrt{2} \times Q_L \times f_m} \tag{2.13}$$

Where $\Delta\varphi_T$ is the residual phase fluctuation of the active device (rad/√Hz).

f_o is the oscillation frequency.

Q_L is the resonator loaded quality factor.

f_m is the noise offset frequency.

Clearly, from equation (2.13), we can see that by increasing Q_L the phase noise will be reduced.

2.5.1 Minimising phase noise and jitter

It is possible to highlight the main causes in order to be able to minimise phase noise and jitter. In order to minimise the phase noise of an oscillator we thus need to ensure the following:

a) Maximise the Q-factor of the resonator network.

b) Maximise the power in the resonator. This will require a high RF voltage across the resonator and will be limited by the breakdown voltages of the active devices in the circuit.

c) Use an active device with a low noise figure.

d) Phase perturbation can be minimised by using high impedance devices such as GaAs FET's and HEMT's, where the signal-to-noise ratio or the signal voltage relative to the equivalent noise voltage can be very high[18].

e) Reduce flicker noise. The intrinsic noise sources in a GaAs FET are the thermally generated channel noise and the induced noise at the gate. There is no shot noise in a GaAs FET, however the flicker noise (1/f noise) is significant below 10 to 50MHz. Therefore it is preferable to use bipolar devices for low-noise oscillators due to their much lower flicker noise. The 2N5829 Si Bipolar transistor has a flicker corner frequency of approximately 5 kHz with a typical value of 6 MHz for a GaAs FET device. The effect of flicker noise can be reduced by RF feedback, e.g. an un-bypassed emitter resistor of 10 to 30 ohms in a bipolar circuit can improve flicker noise by as much as 40 dB[18].

f) The energy should be coupled from the resonator rather than another point of the active device. This will limit the bandwidth as the resonator will also act as a band pass filter. Therefore, some of the power must be dissipated in the resonator to minimize phase noise [27].

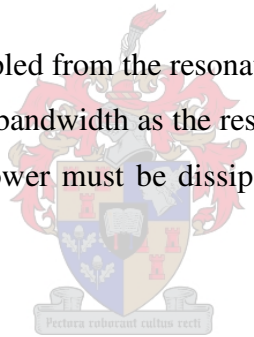

2.6 The active component

2.6.1 Transistor choice

The most important part of the active component is the choice of transistor to be used. The transistor plays a vital role in the power output and the amount of phase noise in the final oscillator, therefore the choice of transistor needs careful consideration. The amplifier provides both the output and feedback power to sustain the oscillation condition.

Table 2. 3 Open loop gain required and temperature

Oscillator use	Temperature Range [11]	Open-Loop Gain (dB)
Laboratory Only	+10 to +40	2 to 3
Commercial	0 to +50	4
Military	-20 to +60	6 to 8
Military	-40 to +60	8 to 10
Military	-40 to +70	10 to 12

Table 2.3 shows the open loop gain required for a stable amplifier is shown in table 2.3 [28]. The open-loop gain of the amplifier plays a large role in the phase noise performance of the final oscillator –too high an open-loop gain will give excessive signal compression, which causes increased phase noise. If the open-loop gain is too low, though, oscillator start-up will be a problem at the temperature extremes and power output will vary excessively [28]. Since DROs can be used in hash environment application, it was decided to design for an open-loop gain of around 8 dB.

The three main properties of an amplifier that must be carefully considered are noise, power output and gain at the desired frequency. The amplifier will contribute to the oscillator's noise with three kinds of noise, namely thermal-, shot- and flicker noise [28].

The thermal and shot noise affects the signal to noise ratio far from the carrier while the flicker affects the oscillator noise close to the carrier. One of the most important tradeoffs in an amplifier is between gain and power output. The gain of an amplifier is limited by the manufacturing process. A common measure of the limit is known as the transition frequency (f_t) or gain bandwidth product (GBW). Power output can be determined by increasing the size of the device. Power output and gain are carefully balanced to provide the optimum performance.

All three of these parameters are heavily dependent on the transistor types and technology type. Common semiconductor technologies are silicon (Si), gallium arsenide (GaAs) and silicon germanium (SiGe). Typical device types are bipolar

junction transistors (BJT), field effect transistors (FET), hetero junction bipolar transistors (HBT) and high electron-mobility transistors (HEMT) [25].

The phase noise performance of bipolar transistors greatly exceeds that of field-effect transistors. Semiconductor surface noise currents cause 1/f noise and as FET's are surface devices their 1/f noise will be much greater than that of a bipolar device. Differences of 15 dB at 6.5 GHz are not uncommon [28].

A great deal of work has been done on comparing the performances of the high electron mobility transistor (HEMT), the MESFET transistor and the hetero junction bipolar transistor (HBT). It was reported in 1988 that MESFET's perform better than HEMT's at room temperature with the phase noise of the MESFET measured as –95 dBc at 10 kHz offset from the carrier and HEMT's measured –85 dBc at 10 kHz offset [29]. These results were confirmed in 1993 by [3]. Two different HEMT's were used, a pseudomorphic HEMT (PHEMT) and a specially manufactured device not commercially available, which they call a SLHEMT. At room temperature the phase noise measurements were comparable to those measured in 1988, with the SLHEMT bringing up the rear. At cryogenic temperatures, however, the MESFET showed negligible improvement, while the PHEMT improved by 15 dB to –101 dBc at 10 kHz offset from a 4 GHz carrier. At room temperature the low frequency generation-recombination noise component in HEMT devices is responsible for the poor phase noise performance. At cryogenic temperatures the g-r traps time constants are so large that this noise becomes subordinate to the 1/f noise. The superior 1/f noise generation of the HEMT gives it an advantage over MESFET devices at cryogenic temperatures.

A comparative study [30] between HEMT's and HBT's in 1995 shows that HBT's can also be used in low phase noise oscillators with great effect. Although HEMT devices have a lower noise up-conversion factor than HBT's, they do have higher low frequency noise levels. Both these factors play a large role in the overall phase noise performance of the final oscillator. Unfortunately, information pertaining to the cryogenic performance of HBT's is still pending.

The decision was made to use a HEMT device: a 2 – 18 GHz Ultra Low Noise Pseudomorphic HEMT (ATF-36077) from Agilent, due to its good performance and its availability. This device has a typical noise figure of 0.5 dB and 12 dB associated gain at 12 GHz. The data sheet for the device is available in Appendix A.

2.6.2 Transistor stability

Transistor stability is usually defined in terms of two parameters: the stability factor K (Rollet stability factor) and the stability measure B1 [31]. Generally, transistor stability can be categorised as one of three states:

a) Unconditionally stable ($K > 1$ & $B1 > 0$).
b) Conditionally stable (potentially unstable) ($K < 1$ & $B1 > 0$).
c) Unstable ($K < 1$ & $B1 < 0$).

2.7 Overview of the DRO design approach

A DRO uses a dielectric resonator to set the oscillating frequency. The dielectric resonator is a small disc of high permittivity, low loss material that has a fundamental resonant frequency set by its relative dielectric constant (ε_r) and its physical dimensions. Its resonance is a result of reflections at the air/dielectric boundary, in an analogous manner to the resonance of metallic cavities. The resonant frequency is also affected by the presence of grounded metal walls in close proximity. A more detailed explanation of dielectric resonators and their applications can be found in [32]. In order to utilize a dielectric resonator to set the frequency of a microwave oscillator it is normally placed in close proximity to an unshielded transmission line. The transmission line is coupled to the dielectric resonator, which can be conveniently modelled as a parallel RLC resonator. The typical configuration of the puck coupling to a microstrip transmission line is depicted in figure 2.3 together with the electric equivalent circuit. A transformer is used to model the coupling between the dielectric resonator and the transmission line. The closer the dielectric resonator is to the microstrip line, the higher the turns ratio of the transformer.

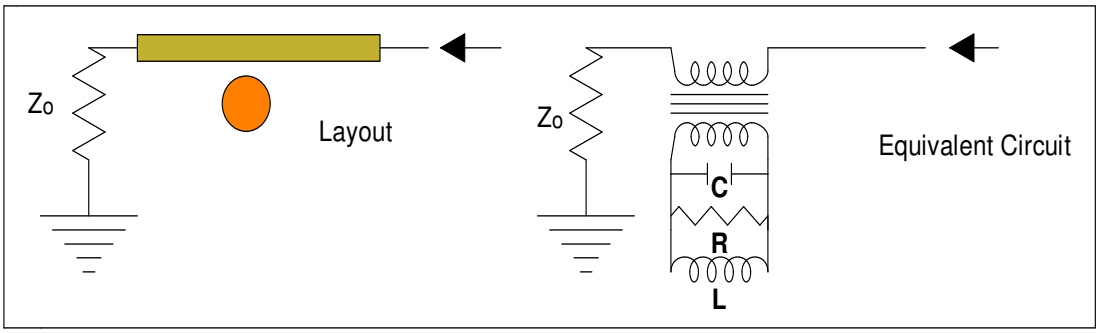

Figure 2. 3 Resonator schematic and its equivalent circuit

Because the puck is a high Q (low loss) resonator the value of R is very high and the phase noise of the resultant oscillator is low. At resonance the reactance of the L and the C are equal and opposite and the equivalent circuit of the dielectric resonator is simply the high value resistor R. The frequency of resonance is thus given by equation 2.14.

$$f_0 = \frac{1}{2\pi\sqrt{LC}} \tag{2.14}$$

2.8 Oscillator topologies

Oscillators may be classified by name, such as Armstrong, Hartley, Colpitts, or by the manner in which the power is fed back [25].

The two main topologies used are parallel feedback and series feedback as shown in figure 2.4. The parallel feedback is based on a transmission amplifier (S_{21}>0) and the series feedback is based on a reflection amplifier (S_{11}>0). In the case of parallel feedback, we need to match the transistor to achieve a sufficient margin of gain around the frequency of interest. Previous work has shown that by increasing the open loop gain, the open loop phase fluctuations that degrade the final phase noise performance of the oscillator increases [26]. In addition, it has been previously reported that the best

trade-off between high gain and low phase noise can be achieved with the series feedback configuration [26, 28].

In this thesis, both configurations have been used. There are two possible topologies of the series configuration which are: a) common gate/base and b) common source/emitter. The decision was made to use only the common source one in order to compare it to the parallel feedback topology. To create the negative resistance, an open stub is placed on the base (in common gate/base mode) or on the emitter (in common source/emitter mode). The location of the gain peak is easily controlled by the stub length. These configurations present advantages and disadvantages which are described in the Table 2.2.

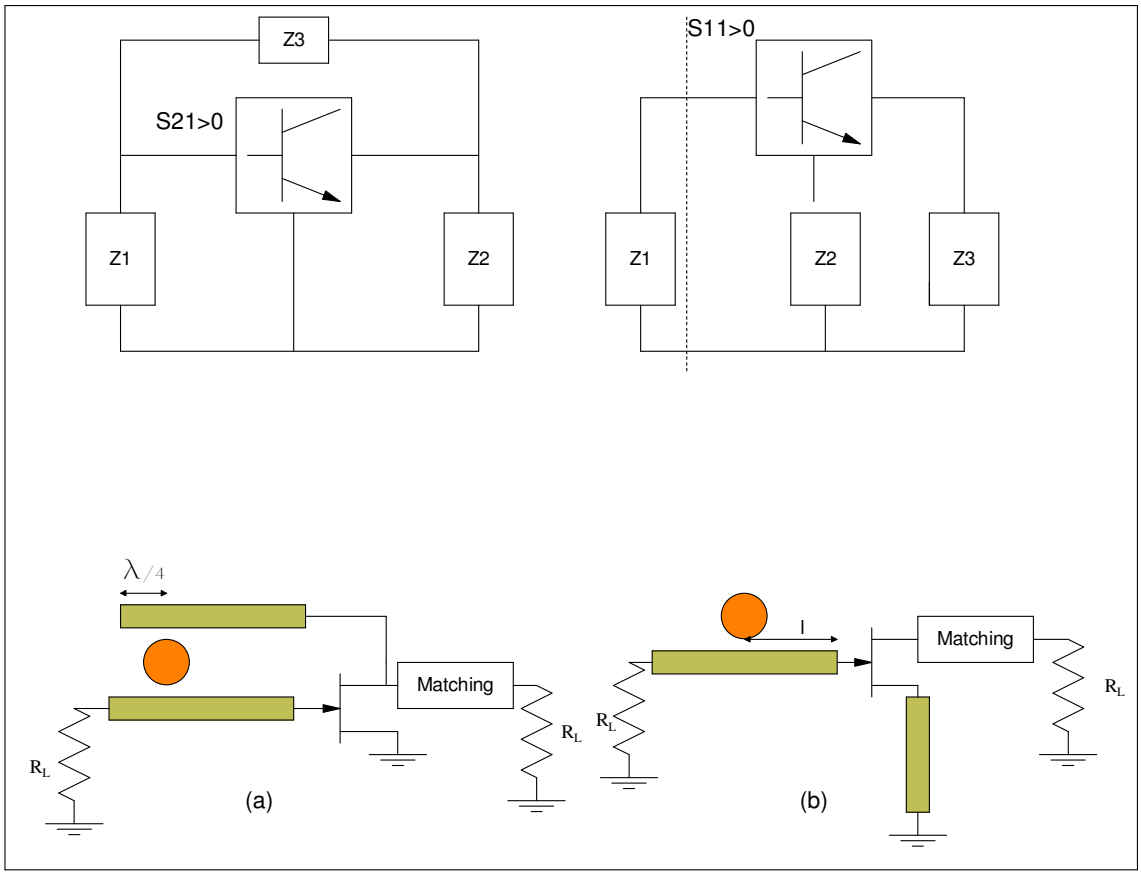

Figure 2. 4 (a) Parallel- and (b) series feedback topologies

2.9 Conclusion

This chapter highlights the main issues of oscillators. It shows some known types, names and configurations of oscillators. Oscillators typical design procedure and negative resistance in oscillators. The start-up conditions for oscillation were shown. Noise in oscillators and how to minimize it were stated. The active component choices, stability and configurations were shown. Overview of .DROs design approach and topologies were shown.

CHAPTER 3

Dielectric Resonators

3.1 Introduction

Since the decision was made to use a dielectric resonator as the frequency determining device, the dielectric resonator itself will be dealt with in this chapter.

Resonators are the basic building blocks of microwave oscillators and filters. Like many other circuit components, resonators should be tested experimentally in order to determine their properties. There are three important characteristics of RF resonators that have to be determined by measurement, which are:

a) Resonator frequency
b) Coupling factor
c) Unloaded and Loaded quality factors

The unloaded quality factor is usually given by the manufacturer as a function of frequency.

Specialised instruments, such as Q meters and grid-dip meters, were used in the past to test RF resonators. At microwave frequencies, the Q factor used to be determined by precision slotted lines. They have all been replaced by more universal test precedure which are based on network analysers [32].

There are two possible circuit configurations which are used to measure Q factors: reaction type and transmission type. Both types will be discussed. The reaction type will be used to measure the resonator's three fundamental characteristics as well as for extracting the electric model of the resonator and this type will be described in detail later in the chapter.

3.2 Dielectric Resonators

A dielectric resonator is an electronic component that exhibits resonance for a narrow range of frequencies, generally in the microwave band. The resonance is similar to that of a circular hollow metallic waveguide, except that the boundary is defined by a large change in permittivity rather than by a conductor. Dielectric resonators generally consist of a "puck" of ceramic that has a large dielectric constant and a low dissipation factor. The resonant frequency is determined by the overall physical dimensions of the puck and the dielectric constant of the material.

A dielectric resonator is generally enclosed in an RF shield to prevent it from radiating. An unshielded dielectric resonator can be used as an antenna. This type of antenna is usually called a DRA (Dielectric Resonant Antenna).

Dielectric resonators function by trapping energy in an extremely small band of frequencies within the confines of the resonator volume. The method of resonance closely approximates that of a circular waveguide. Energy is reflected back into the resonator resulting in negligible radiation losses by presenting a large change in permittivity at the boundary of the resonator. The actual resonant frequency is determined by the mechanical dimensions of the puck [32].

Dielectric resonators have a very high quality factor (Q) (up to 10000) at microwave frequencies. The dielectric material is usually of high-dielectric constant and with excellent temperature stability. Nowadays, many ceramic compositions are developed which offer excellent dielectric properties. The important properties of different dielectric materials developed commercially are compared in table 3.1 [26]

Table 3. 1 Dielectric Resonator materials

Composition	ε_r	Quality factor	Temp. coeff	Frequency range	Manufacturer
Ba2 Ti9 O20	40	10000@4GHz	+2	1 to 100GHz	Bell Labs
(Zr-Sn) Ti O4	38	10000@4GHz	-4 to 10	1 to 100GHz	Trans Tech Thomson Murata
Ba (Zn 1/3 Ta 2/3) O2	30	10000@10GHz	0 to 10	4 to 100GHz	Murata
Ba (Mg 1/3 Ta 2/3) O2	25	25000@10GHz	4	4 to 100GHz	Sumimoto
Ba O – PbO-Nd2 O3-Ti O2	88	5000@1GHz	0 to 6	< 4GHz	Murata Trans Tech
Al2 O3	11	50000@10GHz	0 to 6	> 18GH	NTK Trans Tech

Using a high Q tuning network enhances the stability of the oscillator. The Q of other resonators such as lumped elements and microstrip lines is only a few hundred [21].

Although cavity resonators can have Qs in the order of thousands, they are not suitable for microwave integrated circuitry. One of their disadvantages is the frequency drift due to the expansion of the cavity caused by temperature variations. The DRs do not have these disadvantages since DRs have high Qs and have a compact shape that can be easily integrated with planer circuitry. As mentioned earlier, dielectric resonators have excellent temperature stability since they are mostly made of ceramic materials. This is why dielectric resonator oscillators are common over the entire microwave frequency range [21].

Some of the advantages of the substitution of conventional resonators by DRs are:

a) Smaller circuit sizes.

b) A greater degree of circuit and subsystem integration, due to simpler coupling schemes from microwave integrated circuits (MICs) to DRs.

c) Better circuit performance, when compared to MIC line resonators, with regard to both temperature and losses.

d) Reduction of overall circuit cost for comparable performances.

3.3 Basic Properties

The important material properties for dielectric resonators applications are:

a) The temperature coefficient of the resonant frequency, which combines three independent factors: temperature coefficient of the dielectric constant, thermal expansion of the material and thermal expansion of the environment in which the resonator is mounted [16].

b) The unloaded Q factor (Q_0), which depends strongly on both dielectric losses and environmental losses. Q_0 is defined by the ratio between the stored energy to the dissipated energy per cycle. Typical commercial dielectric resonators are made of ceramics having permittivities in the range 30-90 and of products in the range of Q x f of 41000 to 110000 (at room temperatures), where Q is the inverse of the dielectric loss tangent of dielectric material and f is frequency of operation in gigahertz [33].

c) The dielectric constant of the material, which will ultimately determine the resonator dimensions. At present, commercially available temperature stable dielectric resonators materials exhibit dielectric constants of 30 and above [33].

3.4 Coupling

The dielectric resonator is usually coupled to an oscillator circuit by positioning it close to a microstrip line, as shown in figure 3.2. The magnetic field of the microstrip line couples energy to the resonator; the strength of the coupling is determined by the spacing (d), between the DR and microstrip line. Since it is coupled by the magnetic field, the resonator is modelled as a parallel resonant circuit (RLC) and the coupling is modelled as a transformer [21].

The $TE_{01\delta}$ mode is the commonly used mode in cylindrical dielectric resonators. The magnetic field intensity of this mode is shown in figure 3.1.

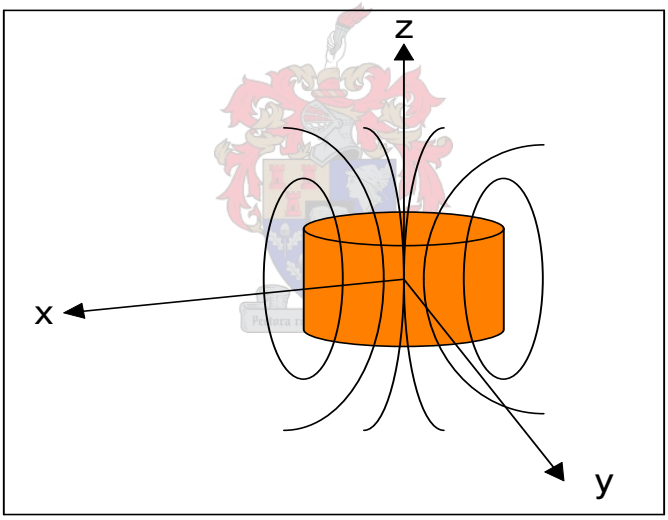

Figure 3. 1 Magnetic field lines of the resonant mode $TE_{01\delta}$

This mode appears as a magnetic dipole, for this reason some call it a magnetic dipole mode instead of using the term $TE_{01\delta}$. The electric field lines are circles concentric with the axis of the resonator.

When the relative dielectric constant is high (more than 30), more than 95% of the stored energy and more than 60% of the stored magnetic energy of the $TE_{01\delta}$ mode are located within the cylinder. The remaining energy is distributed in the area near the resonator and this will give room to couple the resonator to other devices such as microstrip lines. It decays rapidly as the distance from the resonator surface increases [32].

The geometric form of a dielectric resonator is simple, but an exact solution of the Maxwell equation is far more difficult than for a metal cavity. Complex numerical procedures can be used to compute the exact frequency of a resonator mode such as the $TE_{01\delta}$ mode.

The following formula is used to estimate the resonant frequency of the DR to an accuracy of 2% provided that for the $TE_{01\delta}$ mode $0.5< a/L <2$ and $30 < \varepsilon_r < 50$.

$$f_{GHz} = \frac{34}{a\sqrt{\varepsilon_r}}\left(\frac{a}{L} + 3.45\right) \tag{3.1}$$

where *a* is the radius of the DR and L is the length, and both are in millimetres. The frequency is in GHz [32].

Microwave studio (CST) can also estimate the resonant frequency of DRs for the $TE_{01\delta}$ mode as shown in secton 3.7.

The easiest way of using a dielectric resonator in a microwave network is to replace it on a microstrip substrate as shown in figure 3.2. Basically, the distance (d) between the microstrip line and the dielectric resonator determine the amount of coupling between the two. The radiation losses are prevented by enclosing the entire device in a metal box.

3.5 Metal Cavity

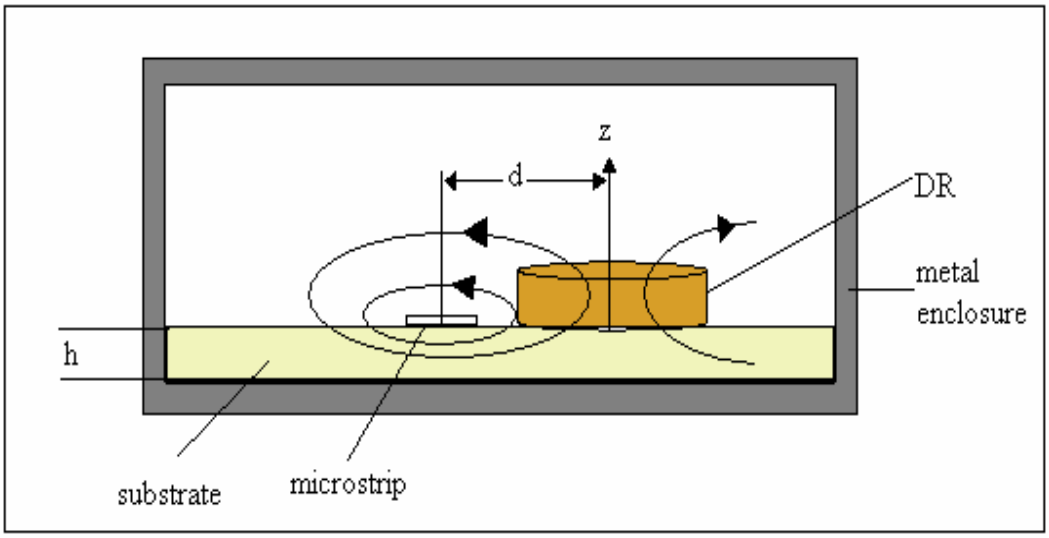

Figure 3. 2 Coupling between a microstrip line and a dielectric resonator

Since a metal enclosure is needed in order for the dielectric resonator to be effective, the effect of the metal enclosure on the dielectric resonator performance has to be discussed.

It has been found that the metal enclosure influences the resonant frequency because by bringing it close to the dielectric resonator, the value of the frequency given by (3.1) is increased. The explanation for this behaviour of the resonant frequency is done by the cavity perturbation theory. It is stated that when a metal wall of a resonant cavity is moved inward, the resonant frequency will decrease if the stored energy of the displaced field is electric. Otherwise, if the stored energy enclosed by the metal wall is predominantly magnetic, as in the case of shielded the $TE_{01\delta}$ mode considered here, the resonant frequency will increase by moving the wall inward [32].

3.6 Parameters of the resonant device

In this section the two types of measurements which are reaction type and transmission type will be discussed but only the reaction type will be measured since it is easier and more accurate[34].

DRs can be modelled as a parallel RLC circuit as show in figure 3.3.

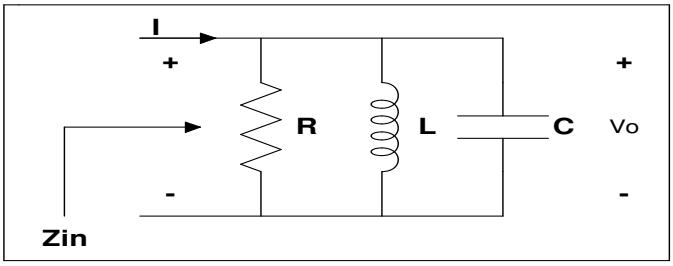

Figure 3. 3 DR parallel RLC model

$$Z_{in} = \frac{V_o}{I} = \left[sC + (sL)^{-1} + (R)^{-1} \right]^{-1} \tag{3.2}$$

At resonance Zin becomes as follows

$Z_{in} = R$ and is shown in figure 3.4.

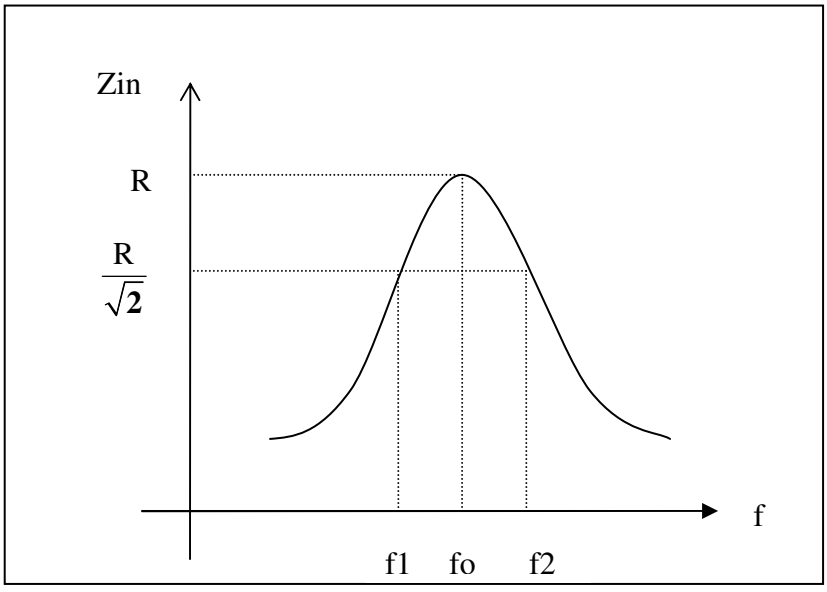

Figure 3. 4 Input impedance magnitude versus frequency

3.6.1 The reaction type measurement

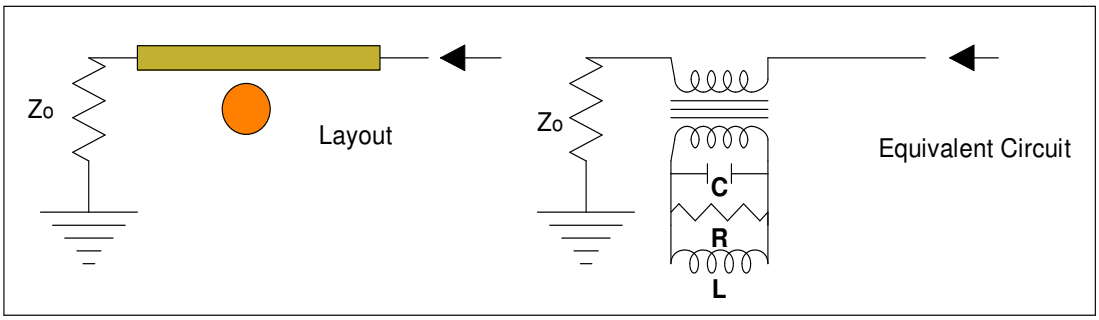

Figure 3. 5 Resonator schematic and its equivalent circuit

The resonant frequency can be defined by the following formula:

$$f_0 = \frac{1}{2\pi\sqrt{LC}} \tag{3.3}$$

$$N^2 = \frac{2Z_o\Gamma}{R - \Gamma R} \tag{3.4}$$

where $\Gamma = \frac{\beta}{1+\beta}$

L- being the modelling equivalent inductive element of the resonator. L can be defined as: Since only the product N^2R is uniquely determined which leave a degree of freedom between N and R [21, 35].

$$L = \frac{R}{\omega_0 Q_L} \tag{3.5}$$

C- being the modelling equivalent capacitive element of the resonator. C can be defined as:

$$C = \frac{Q_L}{\omega_0 R} \tag{3.6}$$

The unloaded $\mathbf{Q_0}$ of a parallel resonator at resonance can be defined as:

$$Q_0 = \frac{R}{\omega_0 L} \tag{3.7}$$

$$\frac{Q_0}{Q_{ext}} = \frac{R}{2Z_0} \tag{3.8}$$

where Q_{ext} is the external quality factor of the DR.

The unloaded $\mathbf{Q_0}$ can be related to the loaded $\mathbf{Q_L}$ by the following formula:

$$Q_0 = (1+\beta)Q_L \tag{3.9}$$

From the above equation, R determines the unloaded $\mathbf{Q_0}$ of a dielectric resonator. The higher the frequency selectivity of the resonator (the unloaded $\mathbf{Q_0}$) is, the better the phase noise.

The coupling coefficient can be written as:

$$\beta = \frac{R}{R_{ext}} \tag{3.10}$$

where R_{ext} is the external resistance seen by the DR.

$$R = 2Z_0\beta \tag{3.11}$$

$$\beta = \frac{R}{R_{ext}} = \frac{R}{2Z_o} = \frac{S_{11}}{1-S_{11}} = \frac{1-S_{21}}{S_{21}} = \frac{S_{11}}{S_{21}} = \frac{Q_0}{Q_{ext}} \tag{3.12}$$

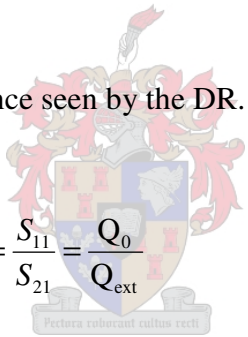

The insertion loss of the resonator can be written as:

$$L_0 = -20\log\left(1 - \frac{Q_L}{Q_0}\right) \tag{3.13}$$

The bandwidth can be written as:

$$BW = \frac{\omega_0}{Q_L} = \frac{1}{RC} \tag{3.14}$$

The frequency deviation can be written as:

$$\delta = \frac{2L}{\lambda_g} \tag{3.15}$$

The wavelength can be written as:

$$\lambda_g = \frac{c}{f_o\sqrt{\varepsilon_r}} \tag{3.16}$$

These equations will be used to calculate the DRs electric models.

3.6.2 The transmission type measurement

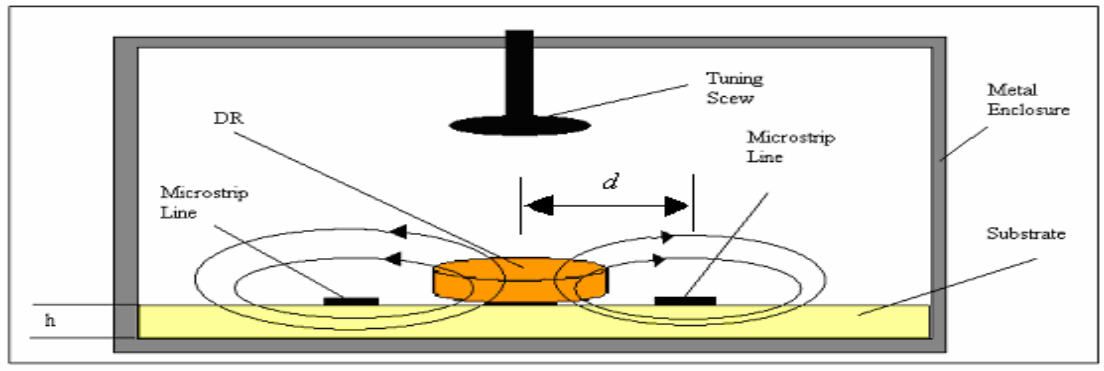

Figure 3. 6 Coupling between two microstrip lines and a dielectric resonator

In figure 3.6 the second way in which the transmission type of measurement is couples the DR to two microstrip lines is shown. From the measurements done with the network analyser, the reflection losses Γ quality factors Q_0 and Q_L can be calculated.

$$S_{21} = \frac{2\sqrt{\beta_1\beta_2}}{1+\beta_1+\beta_2} \times \frac{1}{\sqrt{1+(2\cdot\delta\cdot Q_L)^2}} \tag{3.17}$$

$$\text{where } \delta = \frac{f - f_0}{f_0} \tag{3.18}$$

through a careful placement of the dielectric resonator, the air gaps at both sides must be equal, so that

$$\beta_1 = \beta_2 = \beta \tag{3.19}$$

then the total coupling is equal to 2β and S_{21} becomes

$$S_{21} = \frac{2\beta}{1+2\beta} \times \frac{1}{\sqrt{1+(2\cdot\delta\cdot Q_L)^2}} \tag{3.20}$$

The magnitude of S_{21} at resonance is:

$$S_{21} = \frac{2\beta}{1+2\beta} \tag{3.21}$$

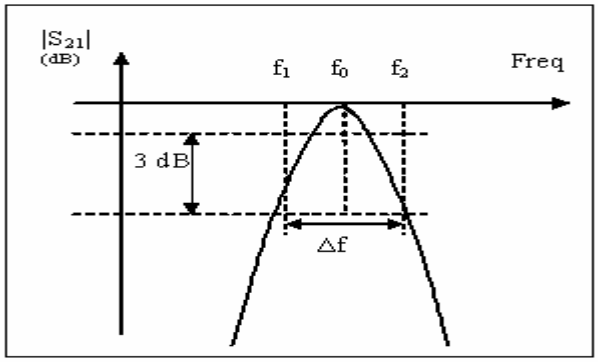

Figure 3. 7 The shape of S_{21}

Where f_0 is the frequency of resonance of the passive circuit, the insertion losses are minimal. f_2 and f_1 are respectively the frequency higher and lower than the resonant frequency at which the insertion loss is 3 dB below the insertion loss at f_0. These frequencies can also be obtained by starting from the measurement of the phase of the resonant device, as indicated in figure 3.8.

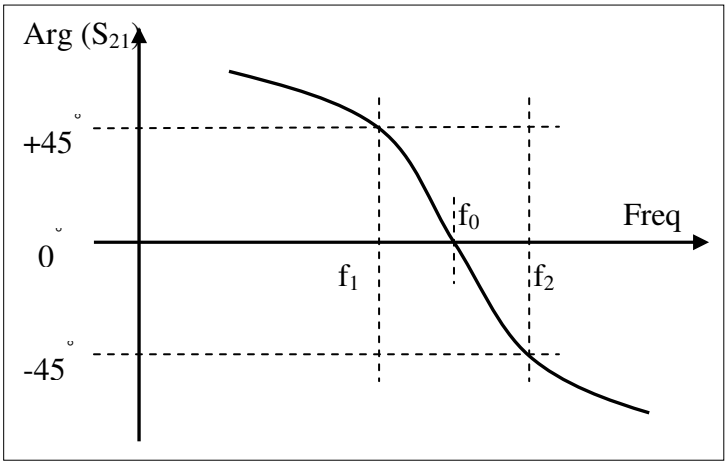

Figure 3. 8 The phase of S_{21}

The insertion loss at resonance can be calculated using the following formula:

$$|S_{21}| = \frac{2\beta}{1+2\beta} \tag{3.22}$$

$$S_{21dB} = 20\log_{10}(|S_{21}|) \tag{3.23}$$

The coupling coefficient β can be derived directly:

$$\beta = \frac{\left|S_{21}\right|}{2\cdot\left(1-\left|S_{21}\right|\right)} \tag{3.24}$$

Always starting from measurement corresponding to figure 3.9, the loaded quality factor can be determined.

$$Q_L = \frac{f_0}{\Delta f} \tag{3.25}$$

Suppose, as an indication, that the electric equivalent of the DR is a parallel RLC circuit specifically. The resonance frequency is calculated as follows:

$$f_0 = \frac{1}{2\pi\sqrt{LC}} \tag{3.26}$$

And the unloaded quality factor is as follows:

$$Q_0 = \frac{R}{|X|} = RC\omega_0 = \frac{R}{L\omega_0} \tag{3.27}$$

From the expressional $S_{21,}$ Q and β can be calculated. Hence, Q_0 is calculated as follows:

$$Q_0 = Q_L(1+2\beta) \tag{3.28}$$

Q_0 corresponds to the loaded quality factor Q_L. One can evaluate the selectivity and thus the purity of the spectral of f_0. When Q_L is high, the spectrum line is narrow, and conversely when Q_L is low, the line is broader and spread out in frequency.

The loaded quality factor Q_L is conditioned mainly by the spacing of d. The more d is, the higher Q_L.

The effect of the spacing d, on Q_L is illustrated in figure 3.9:

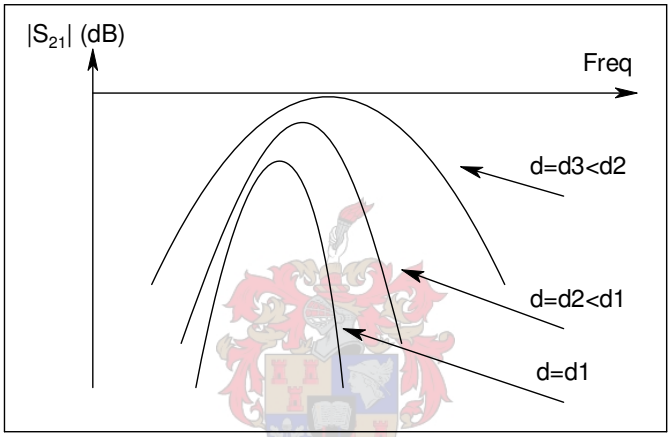

Figure 3. 9 The Effect of changing the gap between the two microstrip lines

For this type of measurement to be accurate, equation (3.18) must be satisfied, requiring that the input and output couple equal each other. In this measurement, there is not electrical verification of this equality. Another important factor is that the accuracy is reduced a lot when coupling is larger than critical. This happens because S_{21} approaches unity as the coupling become strong. Therefore, the bottom part of equation (3.23) becomes the difference of two almost equal numbers, so that even a small error in S_{21} will cause a large error in Q_o even though it has been measured accurately.

The above paragraph gives the reasoning behind using the reaction type measurement instead of using the transmission type measurement in order to get the resonator parameters.

3.7 CST Simulation

The coupling of a dielectric resonator at about 6.22 GHz to a microstrip line was simulated using CST in order to find the resonant frequency. The result is shown in figure 3.11 .

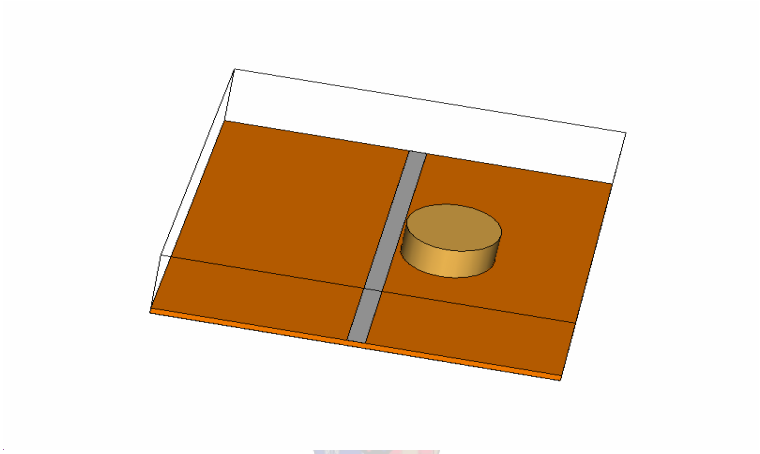

Figure 3. 10 Schematic of dielectric resonator at approximately 6.22 GHz coupled to a microstrip line

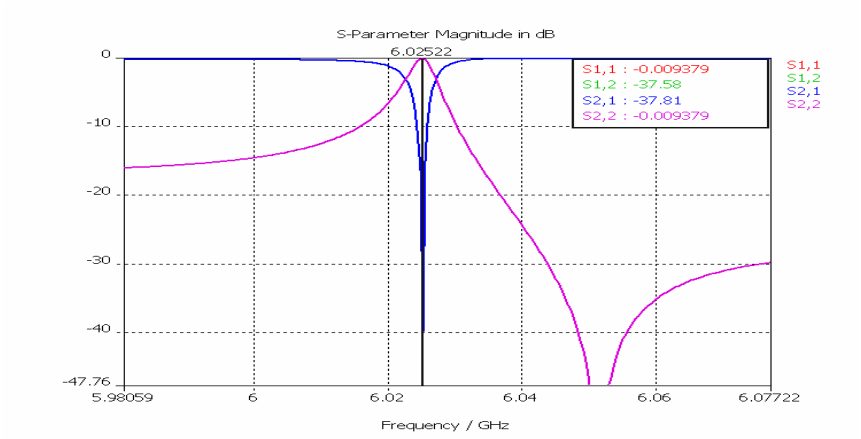

Figure 3. 11 Simulated transmission and reflection of a dielectric resonator of approximately 6.22 GHz coupled to microstrip line

The coupling of a dielectric resonator at approximately 11.2 GHz to a microstrip line was simulated using Microwave Studio (CST). The result is shown in figure 3.13.

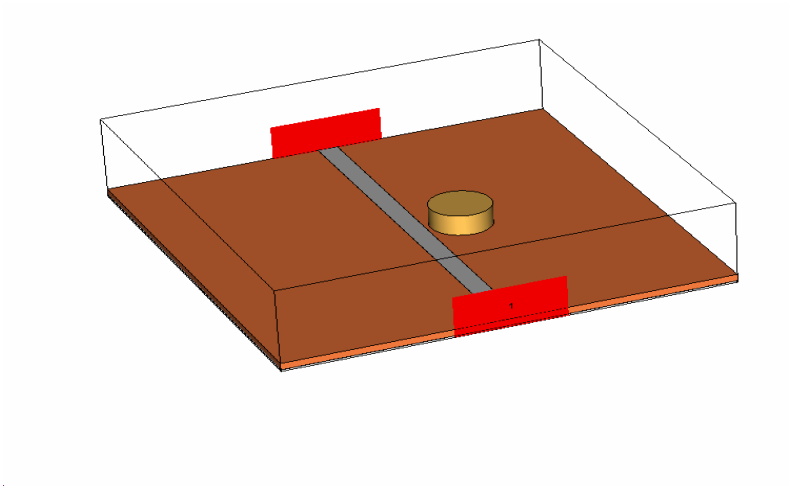

Figure 3. 12 Schematic of dielectric resonator at approximately 11 GHz coupled to a microstrip line

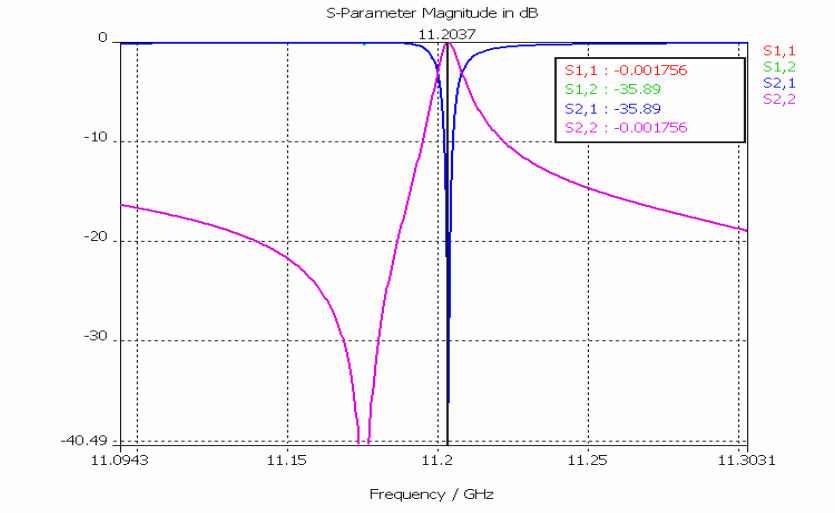

Figure 3. 13 Simulated transmition and reflection of a dielectric resonator at approximately 11.2 GHz coupled to microstrip line

The CST simulation was done to check the size and the frequencies of the tow DRs before they are used.

3.8 Measurement and results

In order to have more understanding of dielectric resonators, it is a good practice to do the measurement and obtain the fundamental characteristics of the dielectric resonator. Two different dielectric resonators were tested; both were samples already available from Trans-Tech. The first is the D8300 series having a resonant frequency of approximately 6.22 GHz and the second is the D8700 series which has a higher resonant frequency of approximately 11.2 GHz.

The test setup consists of several components:

a) Aluminium packaging
b) A substrate with a microstrip line
c) Two SMA connecters
d) Dielectric resonators
e) A network analyzer. (HP 8510C)

The very first step involved the characterization of the microstrip line. A Rogers 4003 substrate was used for the microstrip line. A calibrated HP 8510C network analyser was used to perform the s-parameters measurements.

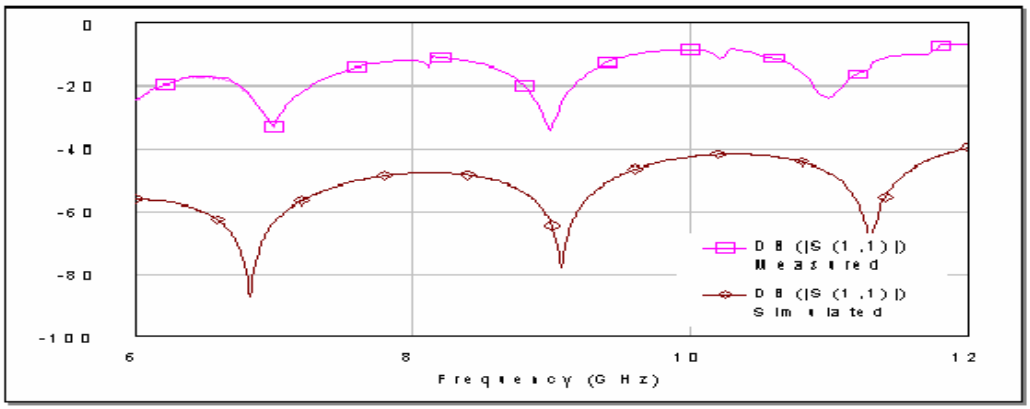

Figure 3. 14 MWO Plot of S_{11} of the measured and simulated microstrip Line

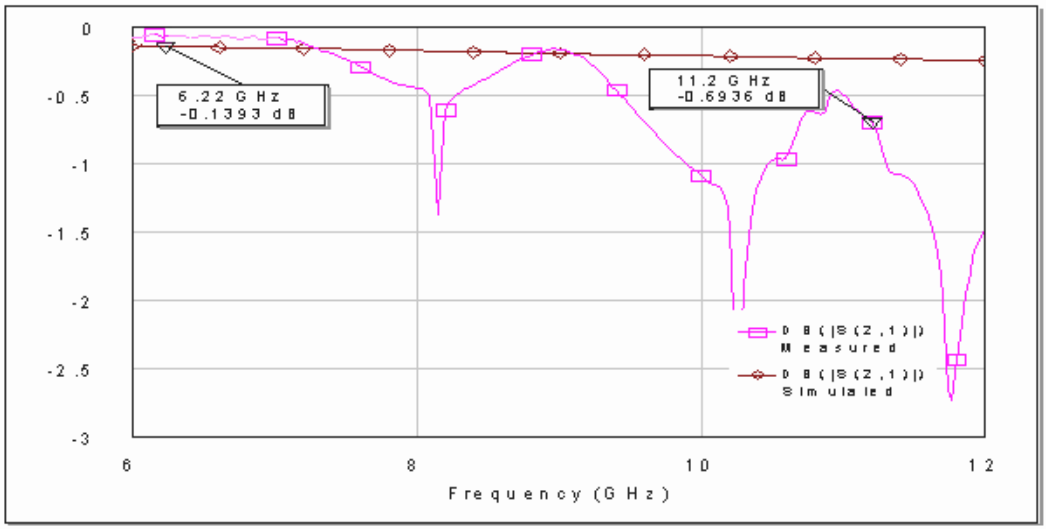

Figure 3. 15 MOW Plot of S_{21} of the measured and simulated microstrip Line

Figure 3.14 and Figure 3.15 show the 2-port s-parameters of the microstrip line. They compare the measured and the simulated data of the board. The measured data is denoted as the plot in pink and the simulated is in brown since the insertion loss is small(less than 0.7 dB) the effect of the line in the measurement is ignored.
The second step involved the characterization of the dielectric resonator puck coupled to the microstrip transmission line using calibrated HP 8510C. An aluminium cavity was designed shown in figure 3.18, in which the dielectric resonator was placed close to the microstrip transmission line.

The first dimensions of the metal cavity that were used were of 40x40x20 mm then in the measurement. The metal cavity resonates at a frequency close to DR resonant frequency as shown in figure 3.16. Matlab was then used to calculate the dimensions of the aluminium cavity to ensure that its resonant frequency is much higher than that of the DR. The height of the cavity was reduced to 10 mm for the 11.2 GHz DRO so that its first resonant mode starts at 16 GHz. The height was also reduced to 10 mm for the 6.22 GHz DRO so that its first resonant mode starts at 16 GHz. The resonant frequency of the different modes of metal cavities can be seen in Appendix C.[21]

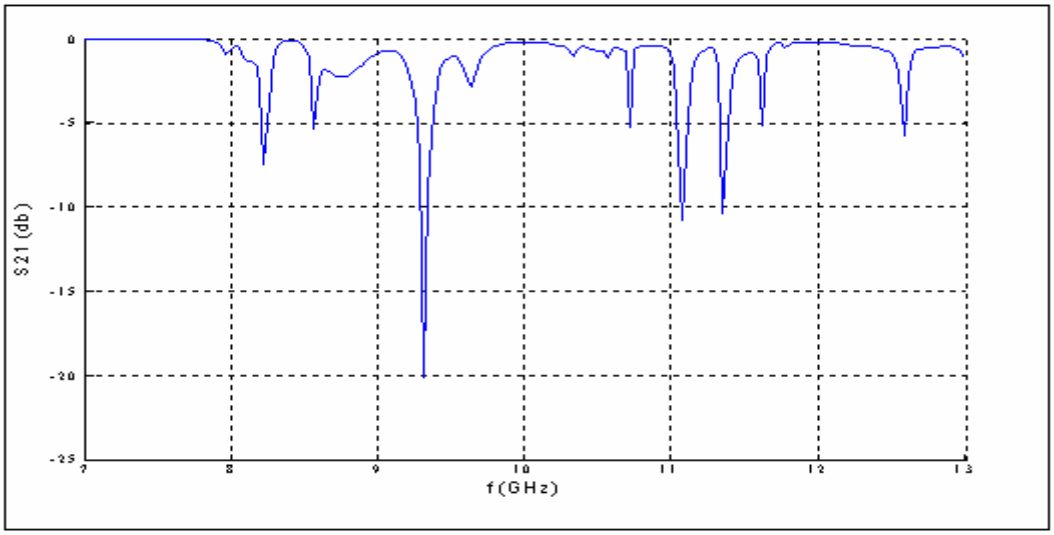

Figure 3. 16 Cavity resonant frequency for 20 mm height

The next step was to characterize the coupling between the DR and the microstrip line. This is done by measuring the s-parameters for different values of d for the coupling as shown in figure 3.17.

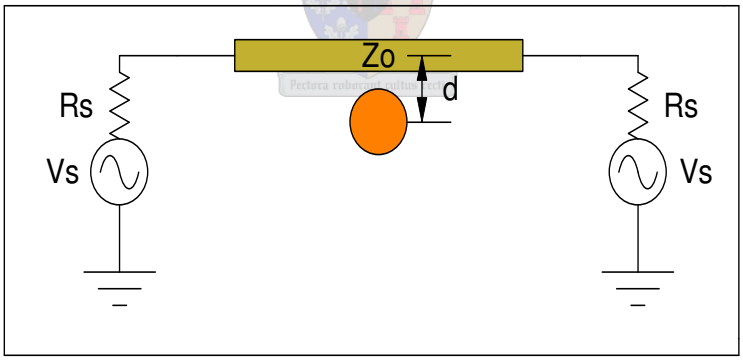

Figure 3. 17 DR coupled to one microstrip line

These measurements are used in MWO to determine the necessary characteristics of the coupling. Some characteristics can be read directly such as the resonant frequency f_o and the resonator resistance R. The rest of the parameters like coupling and the loaded Q must be calculated using the formulas which are given in section 3.7.

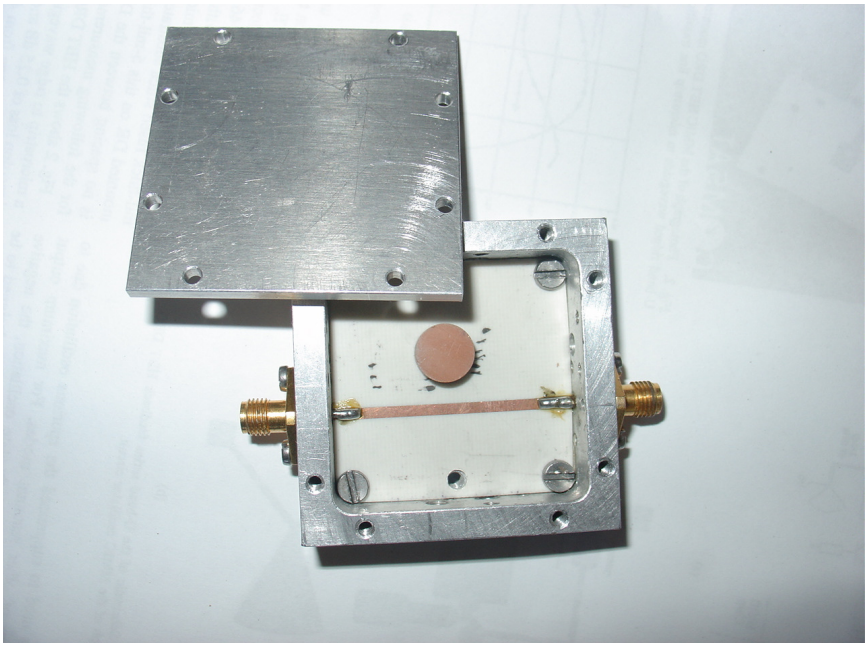

Figure 3. 18 A photo of the DR coupled to one microstrip line

Figure 3.18 shows the metal enclosure, the microstrip line, and the DR and SMA connectors.

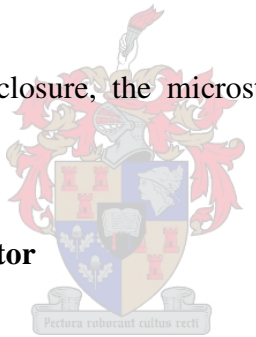

3.9 The D8300 series Resonator

D8300 Dielectric Resonators for Base Station Applications.

3.9.1 Description

Trans-Tech claims that the patented D8300 material represents one of the best products for UHF cellular radio applications, and has the best Q, versus. cost trade-off for PCS/PCN applications near 1.9 GHz. A wide variety of temperature coefficients are available.

3.9.2 Material Characteristics supplied by manufacturer

Table 3. 2 Material characteristics of the D8300 series dielectric resonator

Dielectric Constant	35.0 - 36.5
Temperature Coefficient of Resonant Frequency (tf) (ppm/°C)	-3 to +9
Q (1/tan d) Min. at 850 MHz	>28,000
Q (1/tan d) Min. at 4300 MHz	>9,500
Insulation Resistance (Volume Resistance) (Ohm-cm) at	25 °C 10^13
Coefficient of Thermal Expansion (ppm/°C) (20 - 200 °C)	10
Thermal Conductivity (cal/cm sec °C) at 25 °C	0.0045
Density (g/cm)	>4.65
Water Absorption (%)	<0.01
Composition	Barium Titanate
Colour	Rust

The S_{21} of the test device was measured at different spacings from the microstrip line. The measured data is shown in figure 3.19. The closer the DR is to the microstrip line, the higher the resonant frequency, but the lower the Q factor.

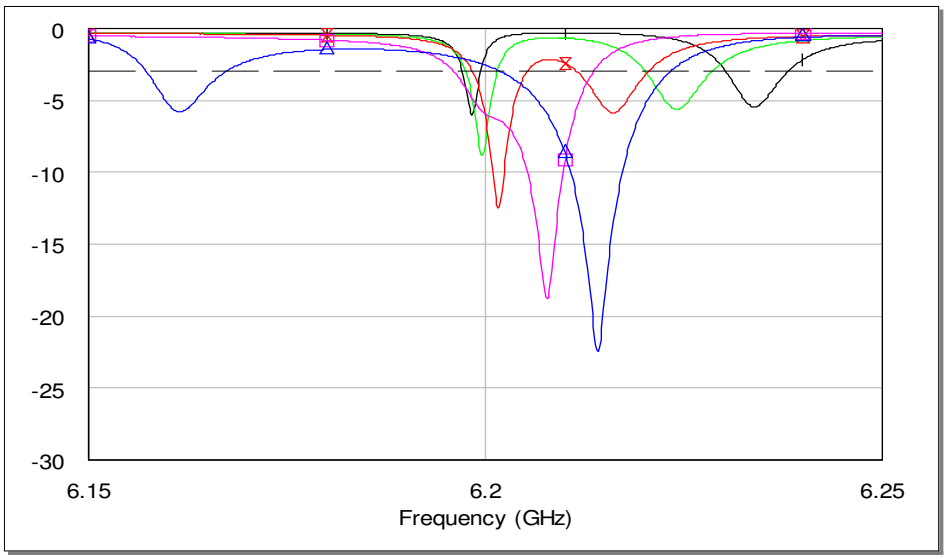

Figure 3. 19 Measured S_{21} of the 6.22GHz DR

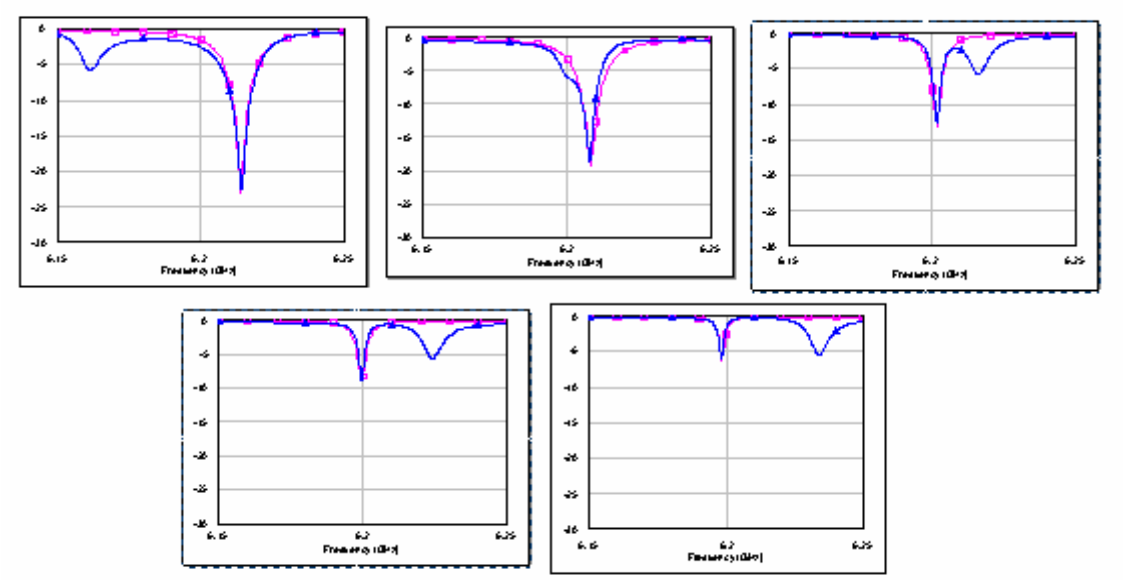

Figure 3. 20 The DR fit of modelled and measured S_{21}

Figure 3.21 shows the relation between the spacing between the microstrip line, the DR and the Q factor. The further the DR is from the microstrip line, the higher the Q factor. Figure 3.20 shows the fit between the measured and modelled data.

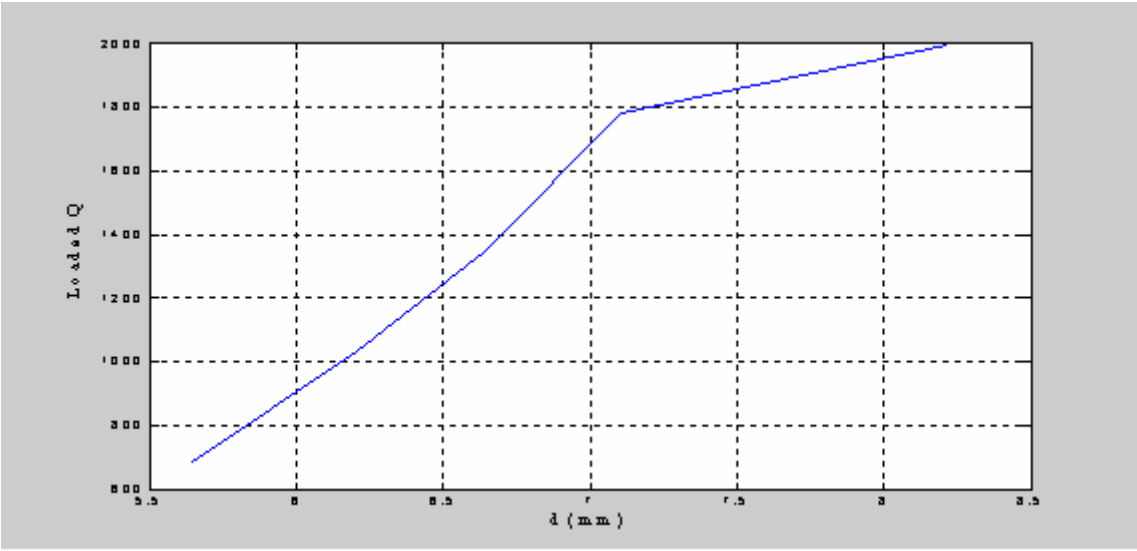

Figure 3. 21 Relation between the spacing and the loaded quality factor

Table 3.3 shows the required parameter which should be known about the DR at a certain distance from the microstrip line. The electric model parameters that are required for the simulation are also shown.

Table 3. 3 Measured and calculated parameters of the D 8300 series resonator

d(mm)	fo(GHz)	QL	N	R(ohm)	L(pH)	C(pF)	Qo	L_0(dB)
5.65	6.22255	683.796	1.03	1400	6.99	93.85	1928.3	3.8
6.21	6.21295	1035.49	1.21	1160	3.8988	168.31	2661.2	4.28
6.64	6.20415	1345	1.63	910	2.8571	230.33	3349.1	4.46
7.105	6.2011	1780.134	2.13	795	1.6191	406.84	3773.9	5.54
8.22	6.1992	1996	2.8	740	1.0958	601.53	3696.4	6.75

3.10 The D8700 Series Resonator

D8700 Series Temperature Stable Dielectric Resonators

3.10.1 Description

The D8700 series is designed for use from 5.5 GHz to 32 GHz and features excellent loss characteristics. This series offers a wide selection of temperature coefficients of resonant frequency for easier circuit compensation and a Q greater than 10,000 at 10 GHz for high stability DRO designs up to millimetre wave frequencies.

3.10.2 Material Characteristics supplied by manufacturer

Table 3. 4 Material characteristics of the D8700 series dielectric resonator

Dielectric Constant	28.2 - 31.0
Temperature Coefficient of Resonant Frequency (tf) (ppm/°C)	0 to +4
Q (1/tan d) Min. at 10.0 GHz	>10,000
Insulation Resistance (Volume Resistivity) (Ohm-cm) at 25 °C	>10^14
Coefficient of Thermal Expansion (ppm/°C) (20 - 200 °C)	10
Thermal Conductivity (cal/cm sec °C) at 25°C	0.006
Specific Heat (cal/g °C)	0.07
Density (g/cm)	7.6
Water Absorption (%)	<0.01
Vickers Hardness No. (kg/mm)	700
Flexural Strength (psi)	10,000
Composition	Ba, Zn, Ti-oxide (perovskite)
Colour	Yellow

The S_{21} of the test device was measured at different spacings from the microstrip line. The measured data is shown in figure 3.22. The closer the DR is to the microstrip line, the higher the resonant frequency, but the lower the Q factor.

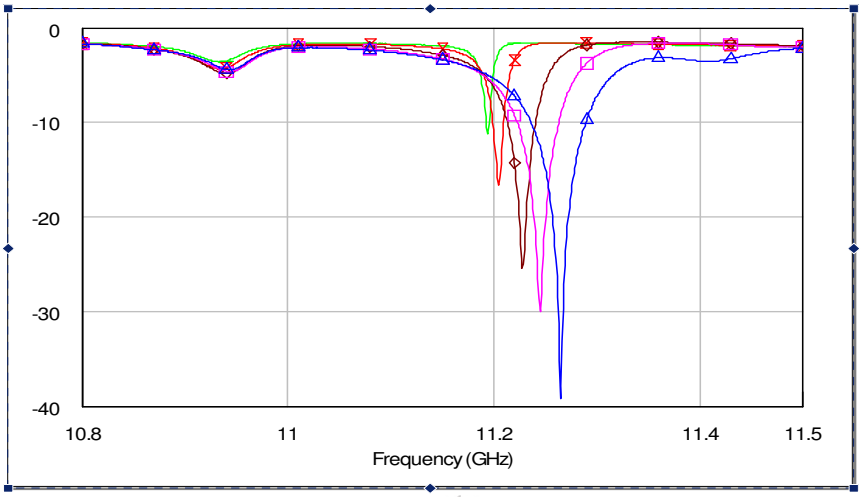

Figure 3. 22 Measured S_{21} of the 11.2 GHz DR

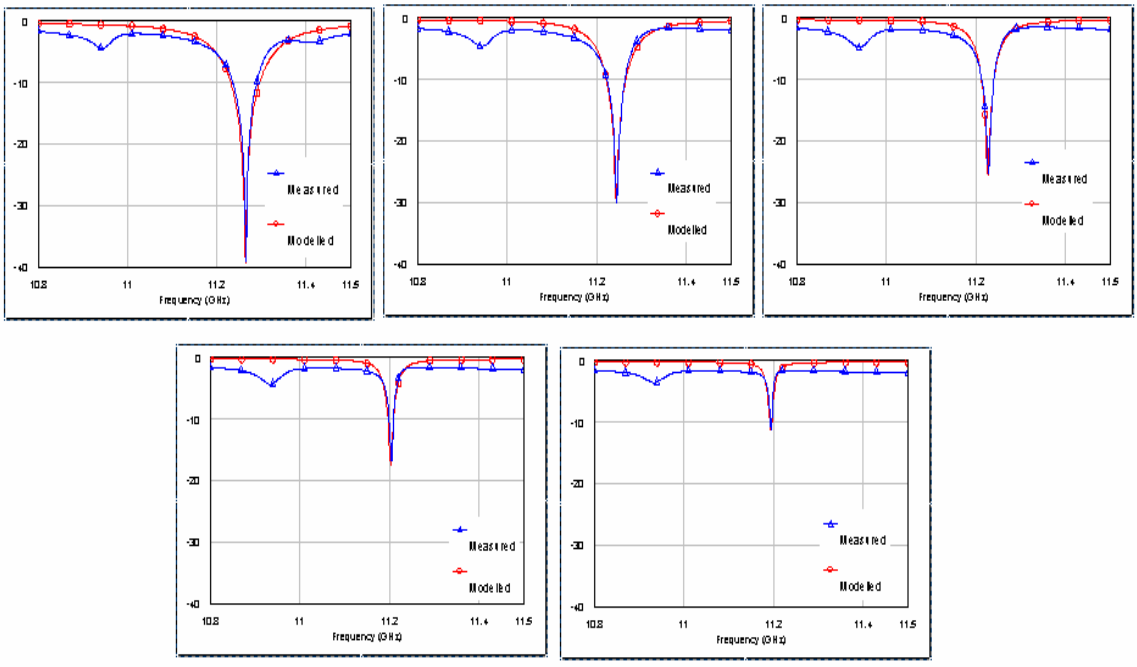

Figure 3. 23 The DR fit of modelled and measured S_{21}

Figure 3.23 shows the fit between the measured and modelled data.

Figure 3.24 shows the relationship between the spacing between the microstrip line and the DR, and the Q factor. The bigger the distance between the DR and the microstrip line, the higher the Q factor.

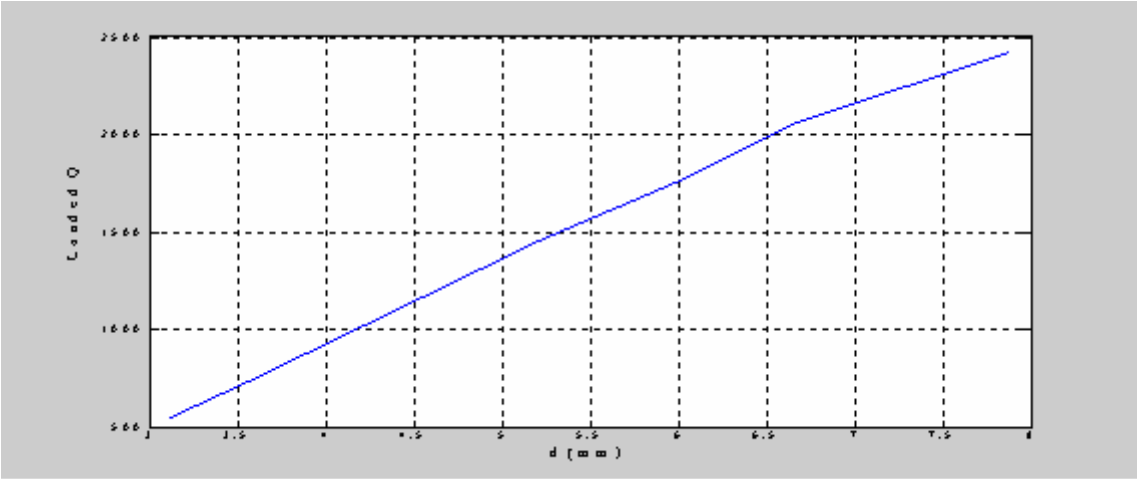

Figure 3. 24 Relation between the spacing and the loaded quality factor

Table 3.5 shows the required parameters of the DR at a certain distance from the microstrip line. The electric model parameters those are required for the simulations are also shown.

Table 3. 5 Measured and calculated parameters of the D8700 series resonator

d(mm)	fo(GHz)	QL	N	R(ohm)	L(pH)	C(pF)	Qo	L_0(dB)
3.125	11.21	544.5	0.325	2560	6,6	30.408	2178	2.5
3.57	11.187	735.98	0.425	799	3.9647	51.051	2207.9	3.5
5.21	11.159	1449.2	0.5	274	1.53	132.92	3710	4.3
5.94	11.151	1756.3	0.505	116	0.8806	231.33	4303.9	4.60
6.68	11.1459	2064.05	0.525	64	0.60766	335.55	3880.4	6.67

3.11 Conclusion

It is clear that it is very important to test the DR and find its important properties and its electric model in order to gain a better understanding of the functioning of DRs. CST can be used to determine the size of the DR at a given frequency before using it. Choosing the dimensions of the packaging is very important in order to avoid unwanted modes. The fit between measured and modelled data was shown.

CHAPTER 4

Procedure of designing series feedback DROs

4.1 Basic Design Configurations

The DR can easily be integrated with the uniplanar circuit by placing it on the substrate. Oscillators stabilized with a DR (DROs) can be divided into two groups. The DR is used as a band rejection filter (DR coupled to a single line) or as an external feedback device (DR placed between two lines). A stabilized GaAs FET oscillator using a dielectric resonator as a band rejection filter is reported by Abe et al. at 6 GHz [36] and by Sun and Wei at X-band frequency [37]. Some oscillators based on a DR as a feedback element have also been reported by. [38] present a DRO at 2 GHz based on a silicon bipolar transistor amplifier. Oscillators was developed using GaAs FETs at 6 GHz [39] and. at 9-14 GHz [40].

Thus, there are two common topologies for designing a Dielectric Resonator Oscillator (DRO). The first is the reflection mode (series feedback). In this mode the resonator acts as an open circuit at the resonant frequency and reflects power in the line into an unstable active element. The active element could be bipolar junction transistor (BJT), field effect transistor (FET), hetero junction a bipolar transistor (HBT) or high electron-mobility transistors (HEMT). When low-noise is desired rather than speed, a BJT should be used. The other devices are faster and most commonly used in high frequency applications, but they exhibit more noise than a BJT. The transistor is made unstable by meeting the negative resistance criteria for oscillation.

For series feedback the transistor gain must be higher, because the coupling from the resonator to the microstrip-line isn't very strong and the source cannot be directly connected to the ground potential. Therefore the parallel feedback configuration is a good choice if the output power is the major concern. However, the series feedback DRO has better phase noise and can to be electrically tuned more easily.

Both configurations will be designed and built. The series feedback procedure will be discussed in this chapter while the parallel feedback procedure will be discussed in chapter 5. The DRO design is based on scattering parameters. MWO is used to simulate the circuit before it is actually built. This gives a close approximation of the behaviour of the circuit and allows for quicker detection of design errors that could be fatal later during the design. The design procedure for the series type is done in detail in the following section and the parallel type is described in chapter 5.

4.2 Design procedure for the Series Feedback DRO

In this section seven basic steps for series resonator oscillator design will be described. These steps will then be applied to two examples in the following sections. The design procedure of a 50 ohm matched series feedback DROs using MWO can be broken down into the following steps:

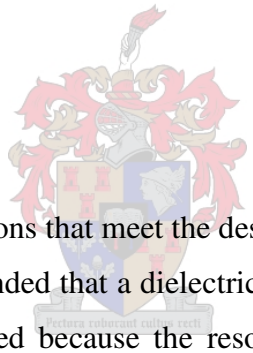

Step 1: Resonator

A suitable resonator with dimensions that meet the design frequency and size limitations must be procured. It is recommended that a dielectric resonator with a lower frequency than the design frequency be used because the resonator may actually resonate at a higher frequency depending on the height of the aluminium enclosure [32]. Also, design goals can be met by varying the distances d and H in Figure.4.1. The distance of the dielectric resonator from the microstrip line and aluminium enclosure affects the resonator impedance, resistance, inductance and the coupling factor which influence the resonant frequency. The dielectric resonator can be characterized by using software from the manufacture that will determine the R, L, and C values of the resonator or can be can characterized more accurately using the magnitudes of s-parameters measurement namely S21 of the resonator when it is coupled to a microstrip line, measured with a scalar network analyser [32, 34, 41]. The distance (d) between the resonator and the microstrip line to achieve the desired resonant frequency must be determined. In this thesis, the model is extracted using the measured scattering parameters data (see chapter 3). An alternative approach characterizes the resonator by

placing it at the furthest possible distance from the microstrip line and varying H with a tuning screw. A network analyzer must be used in order to get the s-parameters of the resonator when it is coupled to a microstrip line. This will then be used in MWO simulations.

Since the design will be at high frequency, substrates specially designed for RF should be used. The important features are substrate uniformity and a low loss coefficient, such as found in Rogers 4003 substrates,

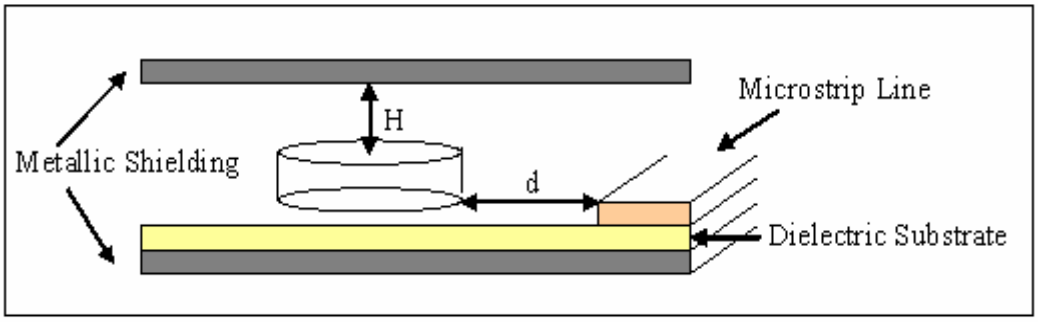

Figure 4. 1 Dielectric resonator on board and parameters that determine the resonant frequency

There is a trade-off between the output power and the phase noise for DROs. The more energy is stored in the dielectric resonator, the better the phase noise, however more of the active device's power is dissipated in the DR, leaving less for the output. Therefore, the DR should be placed far enough from the microstrip line to give high Q which will guarantee a good phase noise but not too far, so that there will be enough power at the output of the DRO [27].

The phase noise can be improved as suggested in [42] by coupling the DR to a microstrip line of impedance higher than 50 ohm.

Step 2: Active Device

An active element must be chosen, which will allow oscillation at the desired frequency and provide sufficient power to sustain oscillation or meet any power specification. This is achieved by viewing the scattering parameters measured with the network analyzer or provided by the manufacturer (see section 2.7 in chapter 2).

The active part must be unstable (K<1 and B1<0) or potentially unstable (K < 1 & B1>0). If not, feedback must be added to make the active part unstable. The feedback can be a short stub connecting the source of the transistor to ground.

Table 4.1 shows the type of the input impedance of the feedback microstrip line when the feedback is short circuit stub or open circuit stub.

Table 4. 1 Input impedance of a short-circuited or an open-circuited stub

Length	Short-circuit	Open circuit
$0 < L < \lambda/4$	Inductive	Capacitive
$\lambda/4 < L < \lambda/2$	Capacitive	Inductive

Step 3: DC Biasing

A dc bias circuit must be constructed to bias the active element at the correct operating point to be able to sustain oscillation. Also, dc blocking capacitors must be fixed on the output line to block dc.

Radial stubs are often used in these bias circuits. The purpose of a radial stub is to provide a resonant short circuit. The radial stub is widely used as a bypass capacitor in the bias circuit of microstrip amplifiers and oscillators [43].

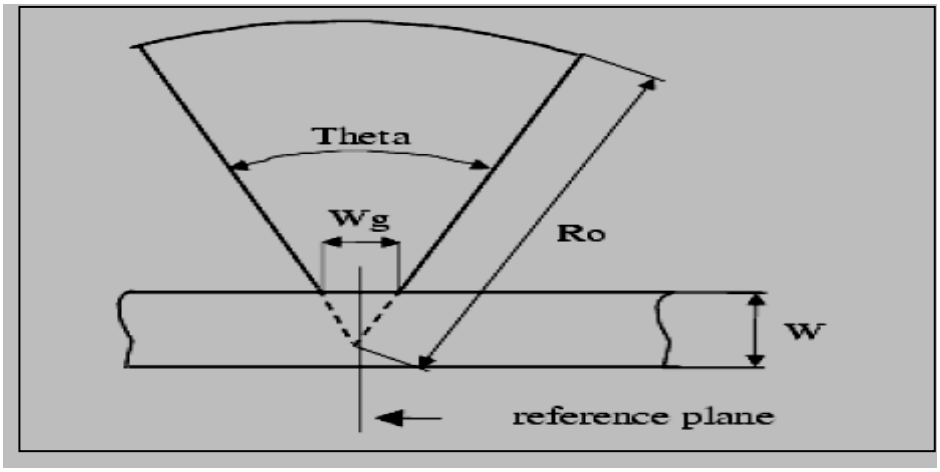

Figure 4. 2 Radial stub Schematic

Where

a) Ro is the outer radius of the stub.

b) W is the microstrip line width.

c) Wg is the width of crossing of stub and microstrip line.

c) Theta is the angle of the stub.

Step 4: DR Position

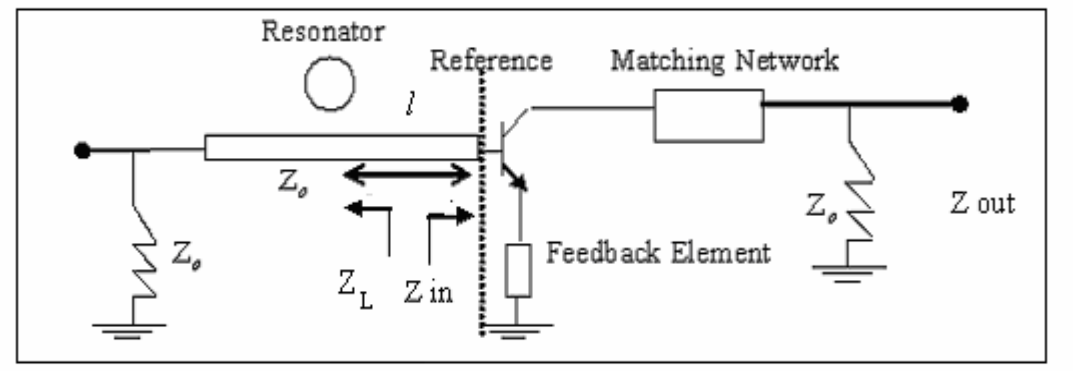

Figure 4. 3 DRO schematic

The exact position of the DR along the microstrip line, as shown in figure 4.3, must be determined

If we observe the transistor, we will find

$$Z_{in} = R_{in} + jX_{in} \tag{4.1}$$

If we observe the resonator side, we will see an open circuit, Z_L would be high. The equation becomes.

$$Z_L = j\frac{Z_O}{\tan(\beta l)} = jZ_O \cot(\beta l) \tag{4.2}$$

where β is the wavenumber and *l is* the microstrip line length

From the oscillation condition

$$X_L = -X_{in} \tag{4.3}$$

Then,

$$X_{in} = -Z_o \cot(\beta l) \text{ or } -Z_o \cot(\theta) \tag{4.4}$$

where length the microstrip line in degree is $\theta = \beta l$

$$\theta = \tan^{-1}\left(\frac{Z_o}{-X_{in}}\right) \tag{4.5}$$

Then to write *l* in terms of λ, the following formula is used:

$$l = x\lambda \tag{4.6}$$

where $x = \frac{\theta}{360}$ and $\lambda = \frac{c}{f_o\sqrt{\varepsilon_e}}$, and ε_e is the effective dielectric constant of the substrate.

Step 5: Matching

The matching is done in such a way that the reflection, looking at the input and the output, should be more than unity (S_{11} and S_{22} >1). The condition here will be S_{11} >100 and S_{22} >100 for a 50 ohm load, since it was shown that this condition is enough to ensure oscillation [44]. The stability circle of both the input and the output of the oscillator must be drawn on a Smith chart in order to make sure that 50 ohm at both sides lies in the unstable region especially at the output port. In order to obtain a Z_{out} (looking into the output of the DRO) that allows negative resistance for oscillation.

This step will become clearer after looking at the design example which will follow later.

If the oscillating conditions change, step 5 must be repeated.

Step 6: PCB and Measurement

After doing the simulation using MWO, the DRO circuit must be constructed in order to measure its performance. The measurement should include the resonant frequency and its power, the harmonics and spur levels, the frequency pushing, and the phase noise.

Step 7: Frequency Tuning

The oscillator will most probably not operate at the exact design frequency. The frequency must then be tuned using a tuning screw. A tuning screw is connected to a metal plate, which will be placed above the resonator. Screwing in and out will change the L, C, and R of the dielectric resonator, which will then determine the frequency of the resonator. When the metal plate is moved to increase or decrease the distance to the resonator, the frequency will increase and decrease respectively.

4.2.1 Design example one

The first example is to design a DRO at a frequency of approximately 6.22 GHz by following the above design procedure. The frequency was used because of the availability of the resonators.

Step 1: Resonator

This step deals with the dielectric resonators and due to its importance, it was done in detail in chapter 3 section 3.10. The resonator that was used is the 8300 series resonator from Trans-Tech with a resonance frequency of approximately 6.22 GHz. The substrate that was used is Rogers 4003 with an ε_r of 3.38, height of 0.8128 mm and tanδ of

0.0027. The important DR characteristics that are required for the design are summarized in table 3.3. The extracted parallel RLC model is used in the simulation using MWO

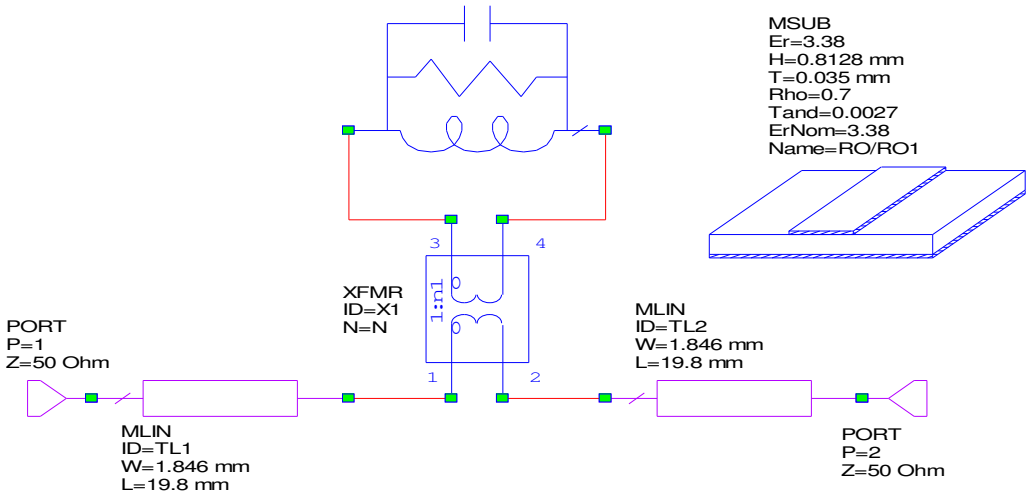

Figure 4. 4 The Simulation model of the DR

Step2: Active Device

The decision was made to use a HEMT device: a 2 – 18 GHz ultra low noise pseudomorphic HEMT (ATF-36077) from Agilent Technologies. This device has a typical noise figure of 0.5 dB and 12 dB associated gain at 12 GHz. Reasons for choosing the active part were given in chapter 2 (section 2.6). The scattering parameters were provided at the typical operating point (Vds=1.5V Vgs=-0.2V, and Id=10mA).

The first significant difference between the active components of the parallel and the series feedback topologies of oscillators is that the series feedback oscillator needs an unstable transistor as opposed to the stable amplifier of the parallel feedback type. The design starts with the data sheet of the transistor from which the Rollet stability factor (K) is calculated. This was calculated as being less than unity, thus the device is conditionally stable at 6.22 GHz, which means that it will be unstable for certain load

and source terminations. It is suggested that this number be reduced even further [45]. This is accomplished by adding capacitive feedback to the source of the transistor by means of a short-circuit stub. The MWO plot of K and B1 is shown in figure 4.5.

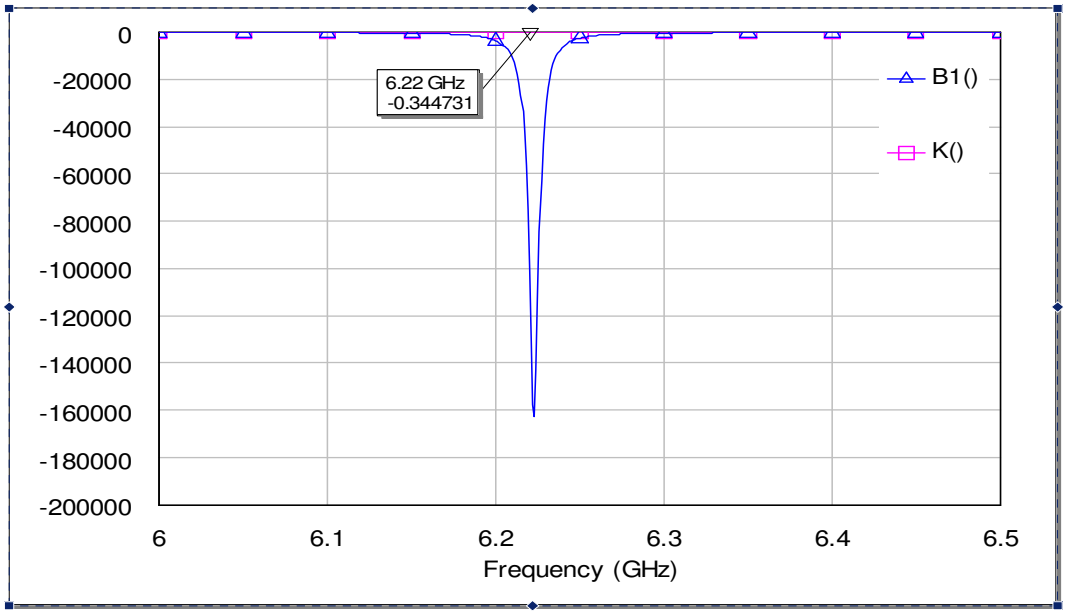

Figure 4. 5 MWO plot of K and B1 after adding the series feedback

Figure 4.5 shows the K and B1 values at the designed frequency. The K and B1 are both less than unity at 6.22 GHz.

Step 3: DC Biasing

In this step the dc bias of the active part is discussed. The radial stub was designed at the desired frequency using MWO to block the ac at around 6.22 GHz as shown in Figure 4.7.

The biasing conditions of the transistor are given in the data sheet as V_{GS} = -0.2V, V_{DS} = 1.5V and I_{DS} = 10mA. Some basic DC biasing networks for FET's are given by [45]. The one that is suitable for low noise, high gain applications, which is shown in figure

4.5, was chosen. It requires positive (for the drain voltage) and negative (for the gate voltage) power supplies.

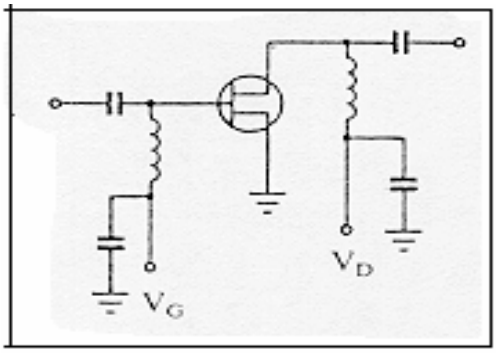

Figure 4. 6 Biasing Network.

The inductors in Figure 4.5 are RF chokes designed to keep RF signals from reaching the DC power supplies. Another simple form of RF choke is the end or shunt connected microstrip radial stub that can be seen in figure 4.2 [32, 46].

The stub converts the open circuit at the outer edge of the radial part to a short circuit at the 100 ohm microstrip line. This short circuit is then converted to an open circuit at the a quarter wave length along the microstrip line. It is this part that is connected to the circuit and that will let DC pass but will act as an open circuit at the quarter wavelength frequency

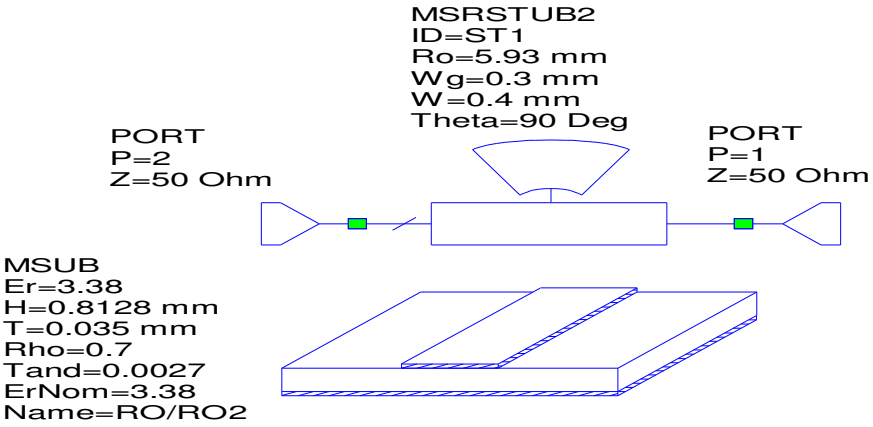

Figure 4. 7 The Radial Stub Schematic in MWO

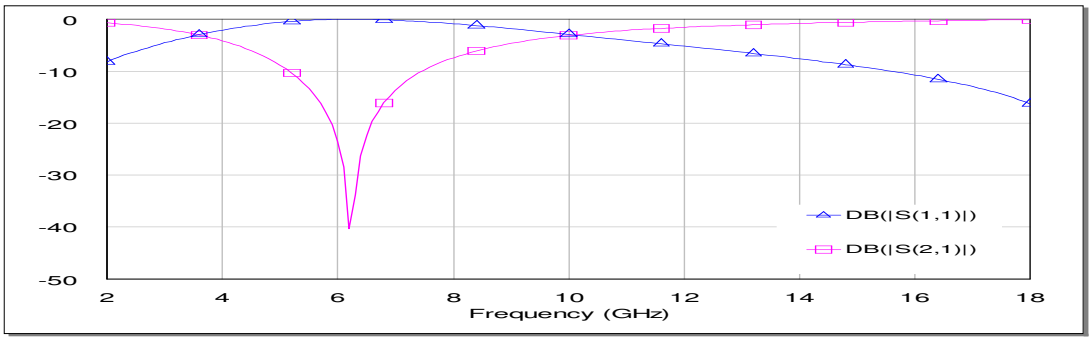

Figure 4. 8 Plot of the radial stub response

The radial sub is designed using MWO at the designed frequency. The dimensions of the radial stub are as follows:

a) R_0= 5.93 mm

b) W=0.4 mm

c) Wg= 0.3 mm

d) Theta= 90 Deg

The next step was to put on the dc blocking capacitors on the main transmission line to the output load. A 47 pf 0603 capacitor was initially used. It was found that it has more losses. Figure 4.9 shows a typical measurement of a 47 pf 0603 a 15 pf 0402 capacitors when used as a dc blocks.

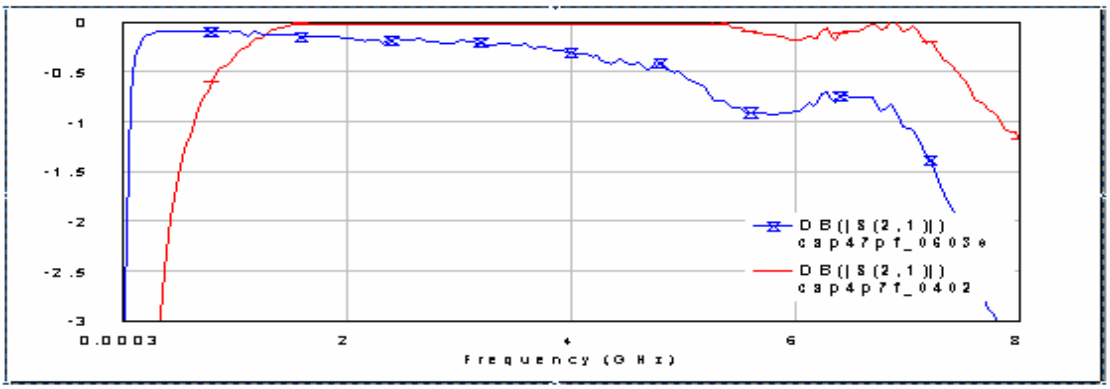

Figure 4. 9 MWO Plot of S_{21} of the 47 pf 0603 and the 15pf 0402 surface mount capacitors

So, the decision was made to use the smaller sized 0402 capacitor, which will have less inductance associated with it. Figure 4.10 shows that this capacitor is well suited for the dc blocking as most of the signal was transmitted through the capacitors.

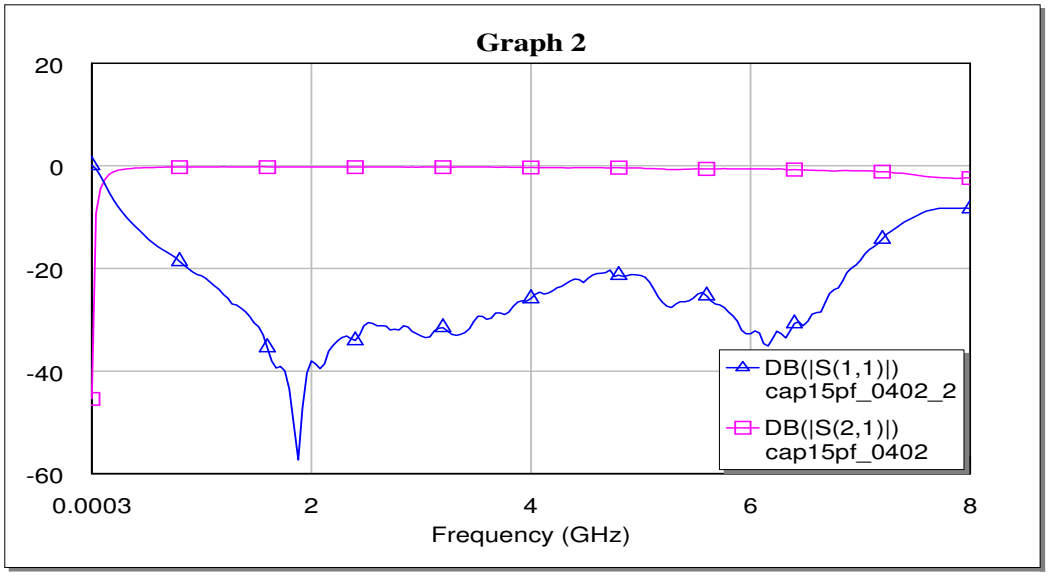

Figure 4. 10 MWO Plot of S_{21} and S_{11} of the 15 pF 0402 surface mount capacitor

Step 4: DR Position

By looking at the input impedance of the active part side, X(*l*) can be determined, which will be used to calculate the length (*l*) of the microstrip line at where the DR should be placed. This is done using the formulas which was provided in section 4.2, step 4.

Figure 4.11 shows the real and imaginary impendence looking at the gate of the active part. The real part must be negative and the imaginary part is used to calculate the distance from the gate to where the DR should be positioned.

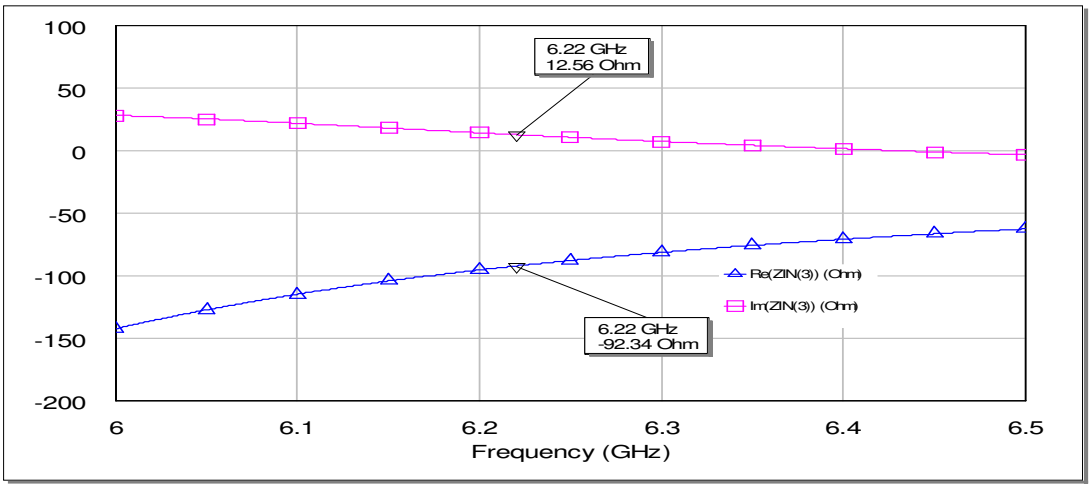

Figure 4. 11 MWO plot of the input impedance of the active part looking at the base

If X_{in} = 12.56 then X*l*=-12.56 which gives that *l*=0.2892 λ

Which means that *l*= 7.6mm at 6.22GHz.

Step 5: Matching

This step matches the oscillator circuit to a 50 ohm load. Such a step will ensure maximum reflection at the load looking into the oscillator output circuit. It is important to ensure that 50 ohm lies in the unstable region by looking at the instability circle of the oscillator. This will ensure a small negative resistance at the oscillator port.

The matching network is a single stub that matches the oscillator circuit to a 50 ohm load such that the reflection is high at the load looking into the oscillator output circuit. It was added to the output and optimised using MOW. The matching stub can be seen in the final layout in figure 4.14.

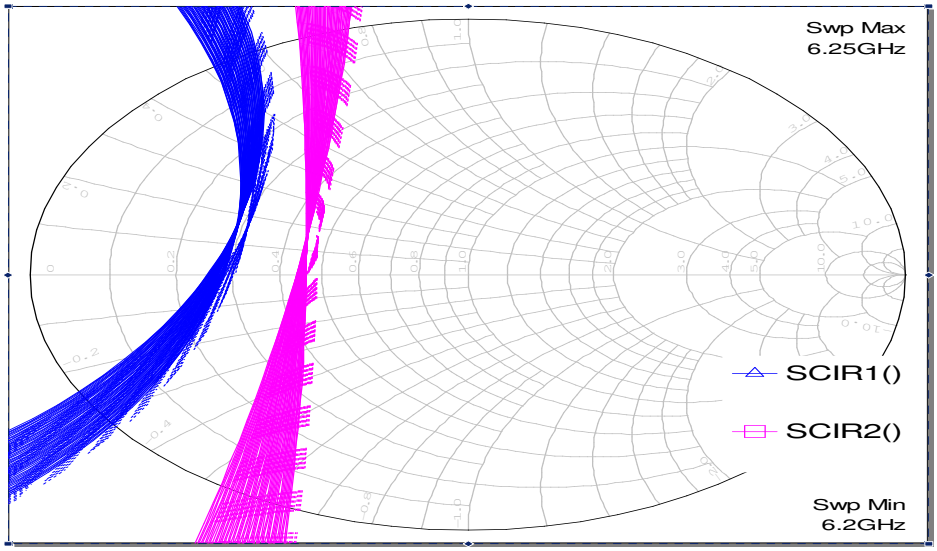

Figure 4. 12 Stability circles of the oscillator circuit (output is in red)

The reflection at both sides of the oscillator should be a 100 or more for the series DRO to ensure oscillation. The stability circles of the oscillator are shown in figure 4.12. 50 ohm should lie in the unstable region. The reflections are shown in figure 4.13.

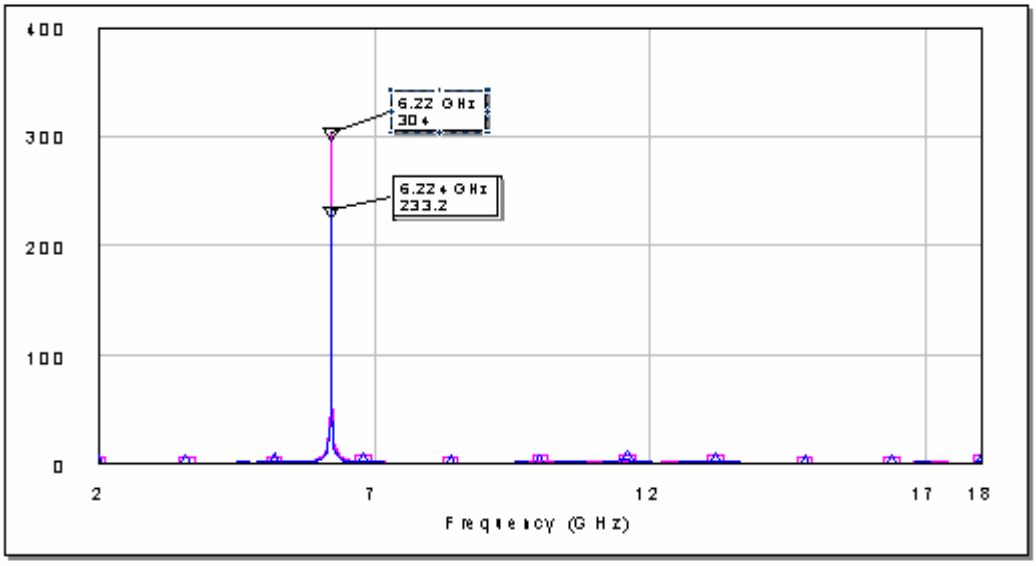

Figure 4. 13 Reflections at both sides of the oscillator

Step 6: PCB and Measurement

The DRO was built and tested. Figure 4.14 shows the final layout of the PCB of the DRO drawn on AutoCAD. C1, C2, C5, and C6 are decoupling capacitors where C1 and C5 are 100nf 0603 capacitors and C2 and C6 are 47 pf 0603 capacitors. The DC block capacitors C3 and C4 are 15 pf 0402 capacitors. T is the ATF 36077 HEMT from Agilent.

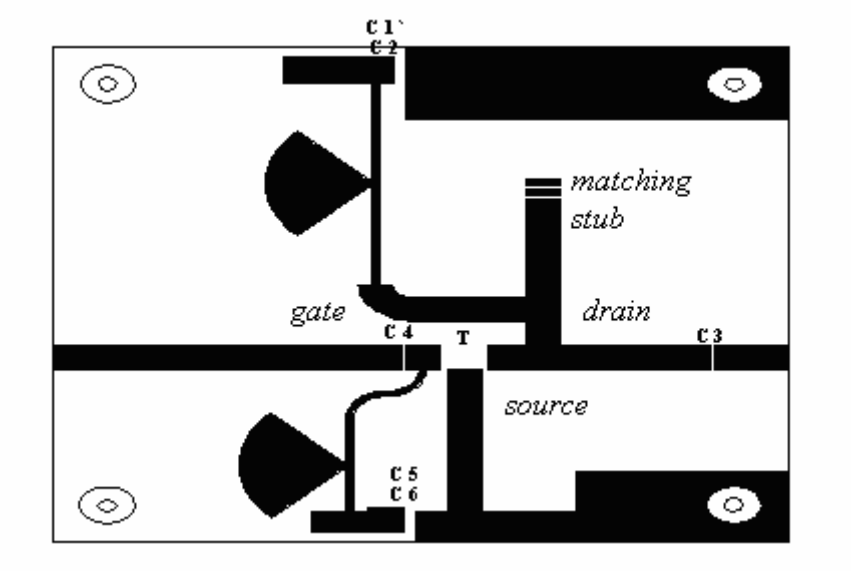

Figure 4. 14 The 6.22GHz DRO PCB AutoCAD layout

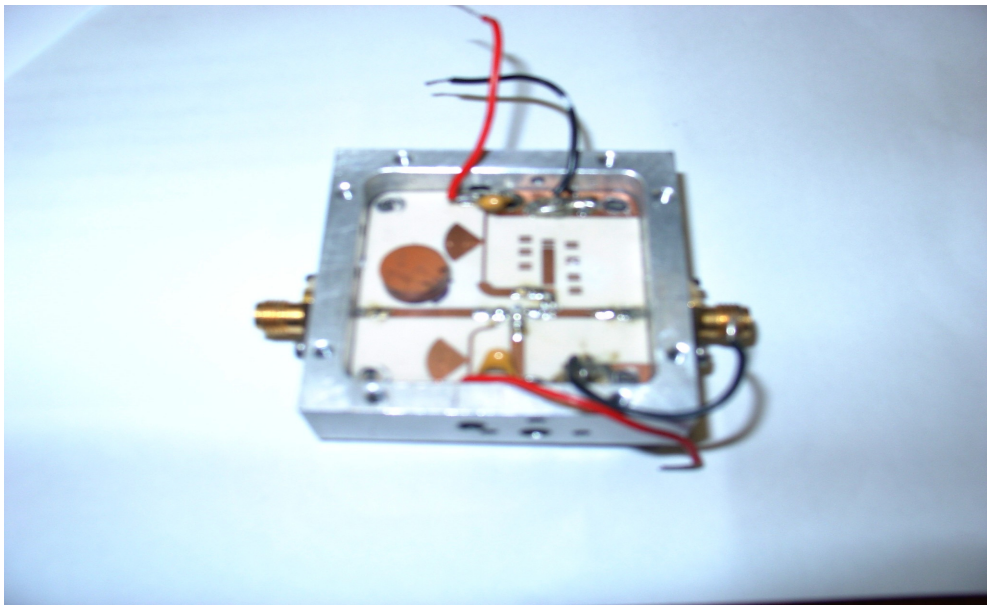

Figure 4. 15 The 6.22GHz DRO Photo

The actual measurement of the DRO which was done using HP 8562A spectrum analyzer with 30 dB attenuation (Att), 100 kHz resolution bandwidth (RBW) and 100 kHz video bandwidth (VBW) can be seen in figure 4.16. It shows the fundamental, the second and third harmonics. The fundamental is approximately 8 dBm, the second harmonic is roughly -20 dBc and the third harmonic -23 dBc. The spurious level is around -74 dBc (the noise floor of the spectrum analyser is about -77 dB).

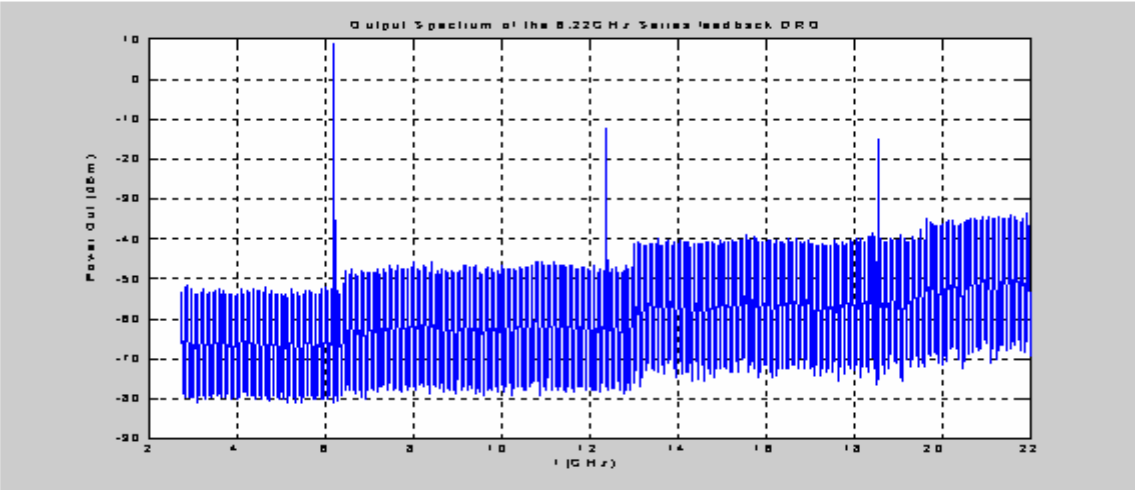

Figure 4. 16 Output spectrum of the DRO

Figure 4.17 shows the fundamental component only measured with 30 dB Att, 30 kHz RBW and 30 kHz VBW.

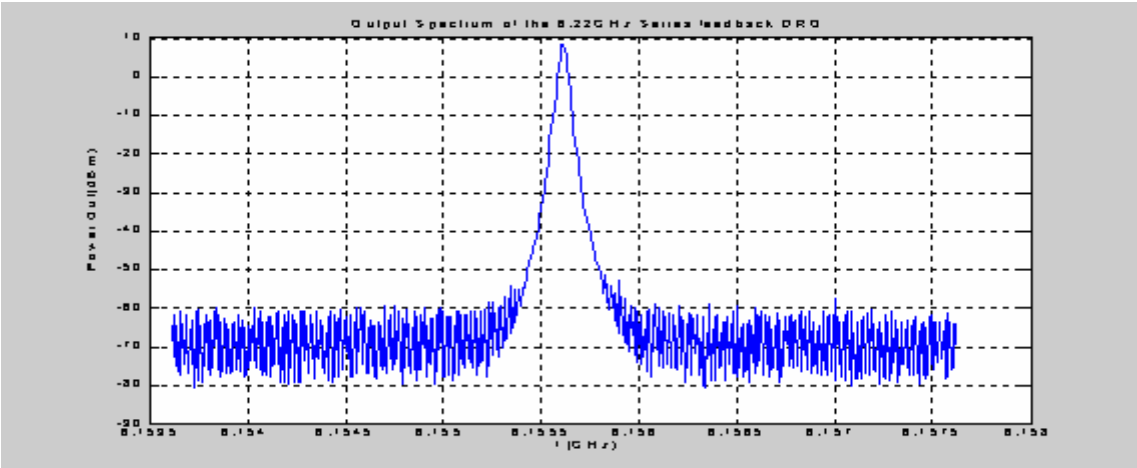

Figure 4. 17 The Spectrum of the fundamental

In figure 4.18, the phase noise of the DRO is shown. It is -100 dBc at 10 kHz away from the carrier and -120 dBc at 100 kHz away from the carrier. The measurement was done using PN9000B phase noise measurement system using the delay line method.

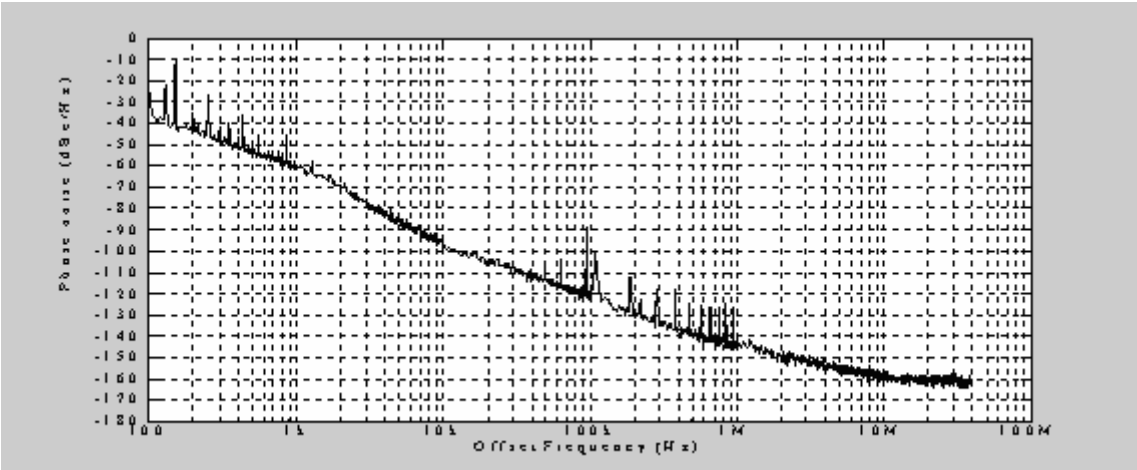

Figure 4. 18 The 6.22 GHz DRO phase noise

Step 8: Frequency Tuning

The DRO is a fixed frequency oscillator with its frequency determined by the resonator material permittivity, resonator dimensions, and the shielding conditions. However, the frequency of oscillation can be tuned over a narrow frequency range mechanically. Use is made of the fact that the frequency of the resonator is highly sensitive to the shielding. A tuning screw is inserted from the top cover of the aluminium enclosure, right above the DR. Increasing the tuning screw depth will increase the frequency of the DR. Caution should be taken to keep the distance between the DR and the tuning screw at least half the DR height in order not to degrade the DR quality factor. Typically, 1 to 5 percent tuning range can be achieved in practice. However, tuning more than 5 percent is not advisable; otherwise the FM noise and the output power will be affected [32]. Any tuning greater than 5 percent of the resonant frequency will result in a significant reduction in the unloaded Q (5 percent tuning equal approximately 75 percent of maximum unloaded Q) [33]. Tuning the DRO of about 9 percent is shown in figure 4.19. The pushing was investigated by varying the input voltage and observing the change in the resonant frequency and found to be less than 1 MHz/volt for the 6.22 GHz DRO.

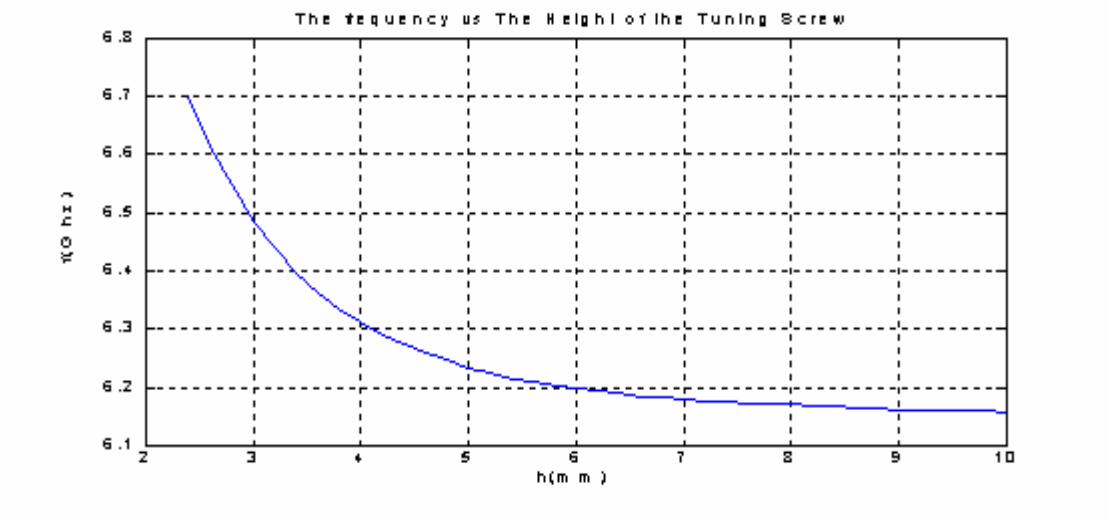

Figure 4. 19 The 6.22 GHz DRO frequency tuning

4.2.2 Design Example Two

The very exact procedure was used to design another series feedback DRO at a higher frequency which is 11.2 GHz. The layout is shown in figure 4.20. In figure 4.20, C1, C2, C5, and C6 are decoupling capacitors where C1 and C5 are 100 nf 0603 capacitors and C2 and C6 are 47 pf 0603 capacitors. The DC block capacitors C3 and C4 are 4.7 pf 0402 capacitors. T is ATF 36077 HEMT from Agilent.

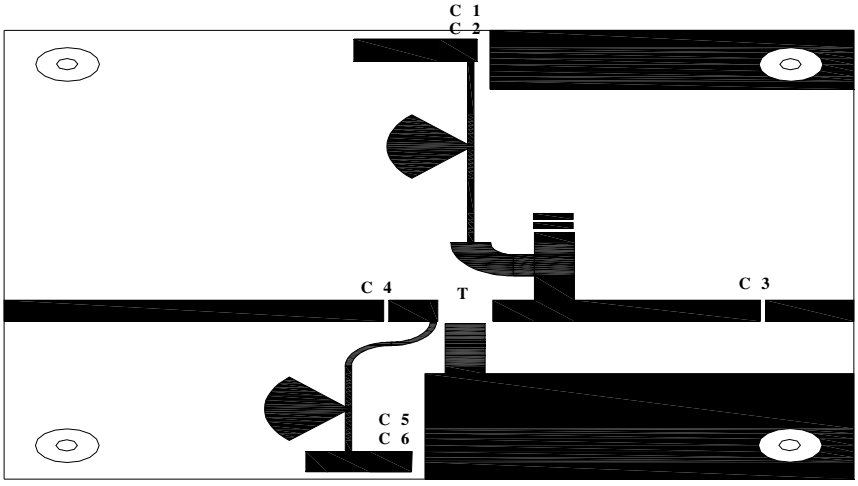

Figure 4. 20 The 11.2 GHz DRO PCB AutoCAD layout

Figure 4.21 is an actual photo of the 11.2GHz DRO.

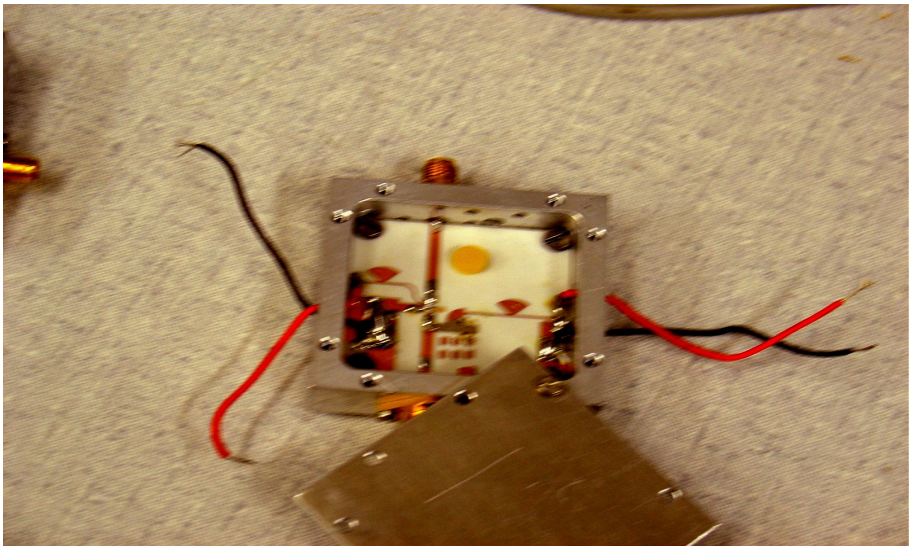

Figure 4. 21 The 11.2 GHz DRO Photo

The measurements which are shown in figure 4.22 were done using FSEK 30 spectrum analyser from ROHDE and SCHWARZ with 30 dB Att, 100 kHz RBW and 100 kHz VBW. It shows the fundamental, the second and third harmonics. The fundamental is approximately 4 dBm, the second harmonic is roughly -22 dBc and the third harmonic -34 dBc. The spurious level is less than -65 dBc (the noise floor of the spectrum analyser is about -70 dB). Figure 4.23 which shows the fundamental component only was measured using HP 8562A spectrum analyser with 30 dB Att, 100 kHz RBW and 100 kHz VBW settings.

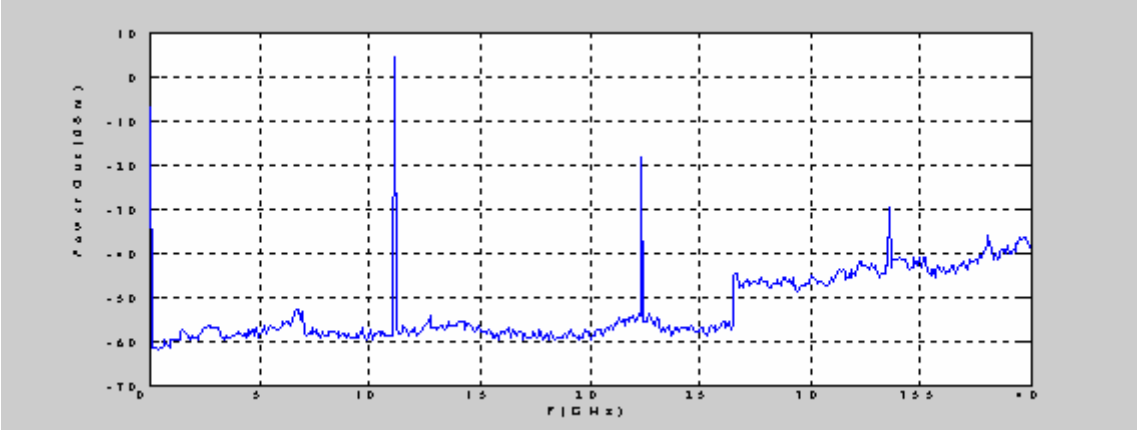

Figure 4. 22 Output Spectrum of the 11.2 GHz DRO (30dB attenuation ,100 kHZ RBW and 100kHz VBW)

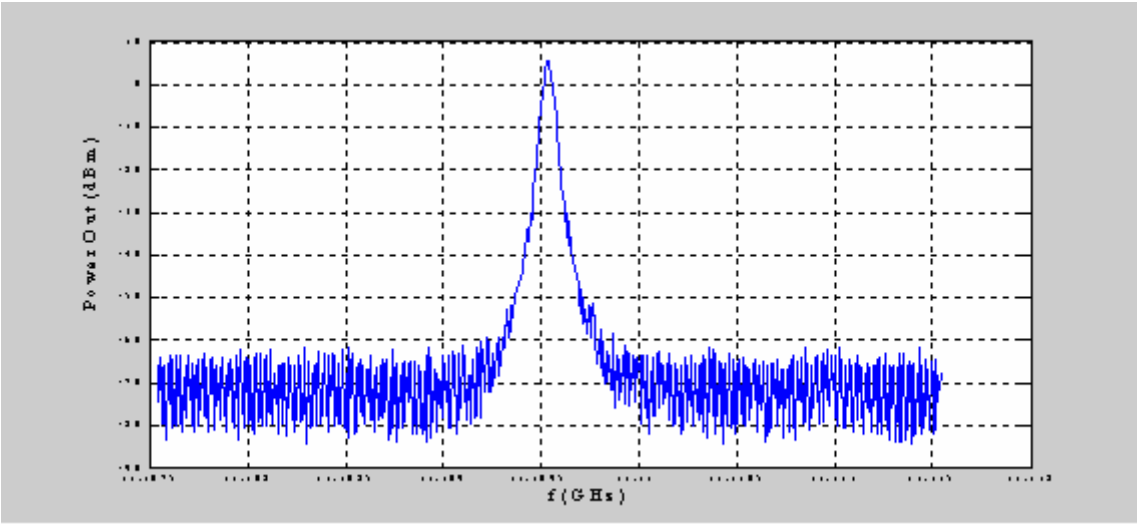

Figure 4. 23 Output spectrum of the 11.2 GHz DRO for the fundamental (30dB att ,100 kHZ RBW and 100kHz VBW)

In figure 4.24, the phase noise of the DRO which is measured using PN9000B phase noise measurement system using the delay line method, is shown. It is -93 dBc/Hz at 10 kHz away from the carrier and -112 dBc/Hz at 100 kHz away from the carrier. The measurement was done with same device and method. The pushing is 1.5 MHz/volt.

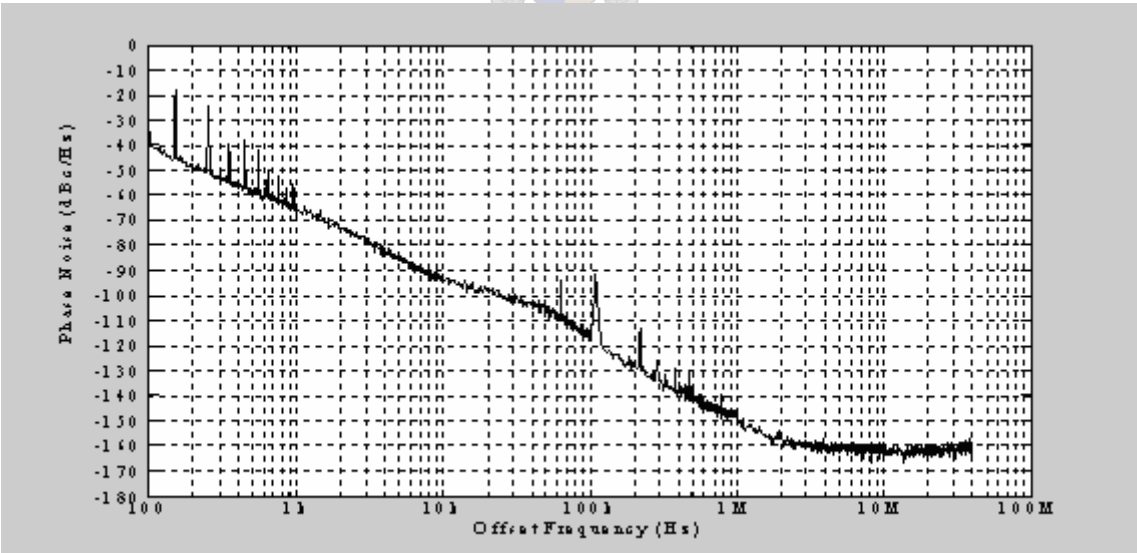

Figure 4. 24 The 11.2 GHz DRO phase noise

The tuning of the 11.2 GHz DRO by approximately 200 MHz is shown in figure 4.25.

.

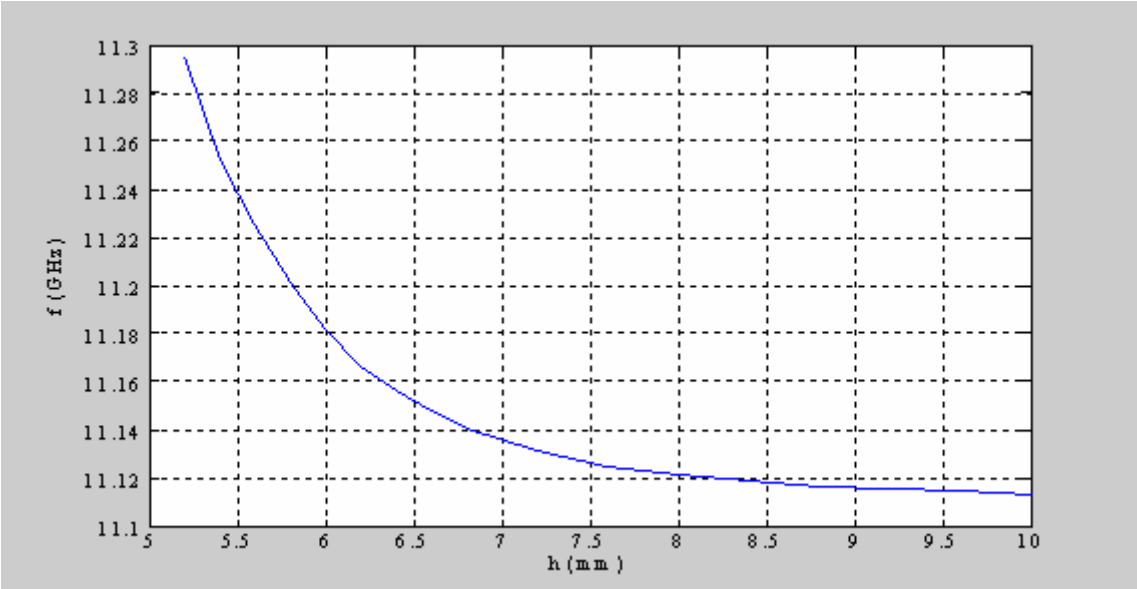

Figure 4. 25 The 11.2 GHz DRO frequency tuning

4.3 Coclusion.

The procedure described above was used to design DROs at two different frequencies starting with a fairly low frequency then increasing the frequency.

The frequency of the first DRO is at approximately 6.22 GHz and the second one is at around 11.2 GHz. The design of the first oscillator is illustrated in detail while only the experimental results are shown for the second design. For the first DRO roughly 8 dBm output power was achieved while maintaining a high Q. This was done by moving the DR away from the microstrip line until almost half of the power is consumed by the loss of the resonator which will guarantee a good phase noise performance and high Q.

A phase noise of -120 dBc/Hz at 100 kHz offset from the carrier was achieved while using an output power of about 8 dBm for the 6.22 GHz DRO. If both high output power and phase noise are needed, a buffer amplifier should be used.

The 11.2 GHz output power of approximately 4 dBm was achieved with a phase noise of -112 dBc/Hz. The second harmonic level is -22 dBc and the third harmonic level is -34 dBc. The pushing was found to be less than 1 MHz/volt for the 6.22 GHz and 1.5 MHz/volt for the 11.2 GHz DROs.

The fact that DRO can be tuned mechanically is one of its main advantages since it is easy to tune the frequency of the DRO by mounting a screw above the DRO. The tuning range of the 6.22 GHz DRO is roughly 500 MHz and 200 MHz for the 11.2 GHz DRO.

The Results obtained compare well to published DROs performance especially the phase noise [5, 27, 47, 48]. A phase noise of -120 dBc/Hz at 100 kHz for oscillators up to 8 GHz and -110 dBc/Hz at 100kHz for oscillators below 12 GHz were reported.

Table 4. 2 The series feedback DROs features

	Unit	6.22 GHZ DRO	11.2 GHZ DRO
Supply Voltage Vds Vgs	 Volt Volt	 1.5 -0.2	 1.5 -0.2
Supply Current	mA	10	10
Output Power	dBm	8	4
Second Harmonic	dBc	-20	-22
Third Harmonic	dBc	-23	-34
Phase noise 10kHz 100kHz	 dBc/Hz dBc/Hz	 -90 -120	 -80 -112
Frequency Pushing	MHz/Volt	1	1.5
Spurious Level	dBc	<-75	<-65

For the schematics of both DROs refer to Appendix B.

CHAPTER 5

Procedure of designing parallel feedback DROs

5.1 Introduction

The second way to realize a stable oscillator is by using the dielectric resonator coupled simultaneously to two microstrip lines as a parallel feedback for the amplifier. In this case, the output matching circuits for a common source transistor are designed to obtain a high enough gain amplifier around the oscillator frequency. Positive feedback between the input and the output should be used to create stable oscillations. This is done by feeding a part of the output signal back to the input by using the dielectric resonator as a transmission filter.

5.2 Principle of oscillator

To obtain the correct operation of the oscillator, this one must satisfy two conditions must be satisfied.

The two startup conditions are summarised in the following formulas:

For Start up condition:

$$G_A - L_F > 0 \tag{5.1}$$

where G_A and L_F are the amplifier gain and the feedback circuit loss at f_o.

$$\varphi_A + \varphi_F = 2n\pi, \quad \text{(n integer)} \tag{5.2}$$

where φ_A and φ_F are respective insertion phases of the amplifier and the feedback network at f_o.

For Steady state conditions:

$$G_A - L_F = 0 \tag{5.3}$$

5.3 The design procedure

Step 1: Resonator

The design frequency must be set and then a dielectric resonator manufacturer must be contacted about the availability of a resonator with the dimensions that meet the design frequency and size limitations of the board with the microstrip line. It is recommended that a dielectric resonator with a lower frequency than the design frequency be used because the resonator may actually resonate at a higher frequency depending on the height of the aluminium enclosure [32]. The distance of the dielectric resonator from the microstrip line and aluminium enclosure affect the resonator impedance, resistance, inductance, and coupling factor which influence the resonant frequency. The dielectric resonator can be characterized by using software from the manufacture that will determine the R, L, and C values of the resonator or can be can characterized more accurately using the magnitudes of s-parameters measurement namely S21 of the resonator when it is coupled to a microstrip line, measured with a scalar network analyser [32, 34, 41]. The distance (d) the resonator should be placed away from the microstrip line to achieve the desired resonant frequency but in this thesis, the model is extracted using the measured scattering parameters data (see chapter 3). Network Analyzer must be used in order to get the scattering parameters of the resonator when it is coupled to a microstrip line which will be used in MWO simulations.

Step 2: Active Device

An active element is chosen, which will allow oscillation at the desired frequency and provide sufficient power to sustain oscillation or meet any power specification. This is achieved by viewing the scattering parameters obtained with the Network Analyzer or provided by the manufacturer (see section 2.7 in chapter 2).

The transistor must be stable at the resonant frequency. There is always a way to make a transistor stable, usually suggested by the manufacturer either in the datasheet or in an application note.

Step 3: Phase Shift

Decide which transistor configuration suits the design (see chapter 2 section 2.2). Calculate the phase shift of the transistor (φ_A) for the chosen configuration which is, in this case, a common source configuration. The gate to the drain phase shift must be checked at after grounding the source.

Step 4: Amplifier Design

Design an amplifier with a wide enough gain margin at the resonant frequency. It must include the feedback stubs but not the resonator as shown in the figure 5.1. R_L is used to limit the spurious and to simulate an infinite line, since it is chosen to be 50 ohm.

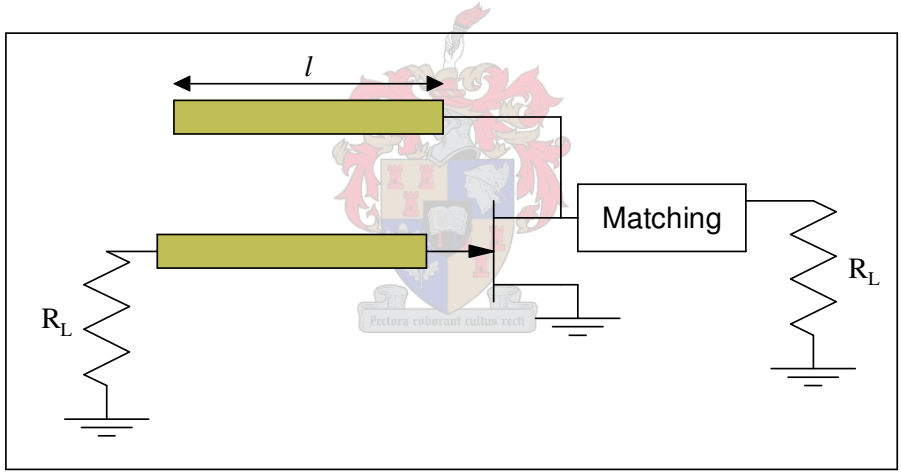

Figure 5. 1 Amplifier circuit

Step 5: Adding the DR model and Matching

Add the resonator RLC model to the circuit as shown in the figure 5.2. A negative resistance must be seen when looking into the output of the oscillator circuit. The reflection should be more than unity.

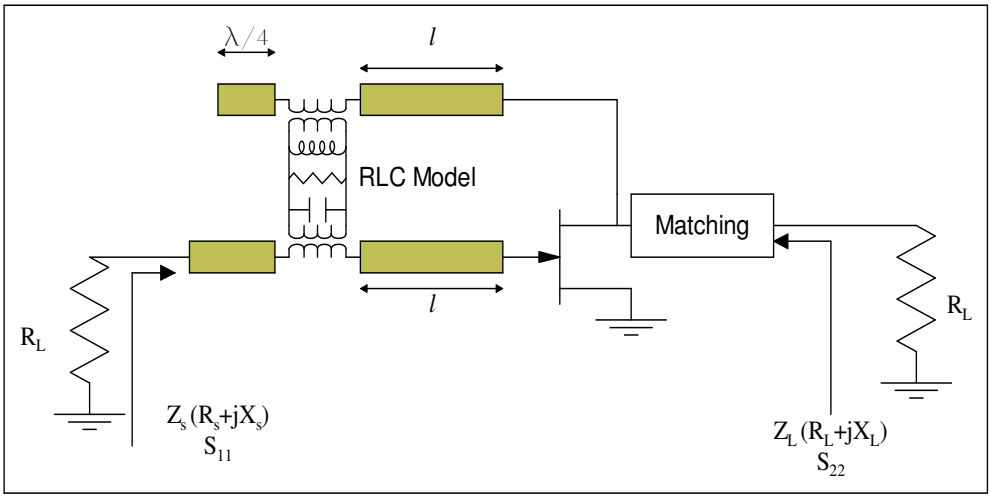

Figure 5. 2 Amplifier circuit after adding the resonator RLC model

Step 6: PCB and Measurement

Draw a PCB layout and have it manufactured. Then build it and take the measurements. The measurement should include the resonant frequency and its power, the harmonics and spurs levels, frequency pushing, and the phase noise.

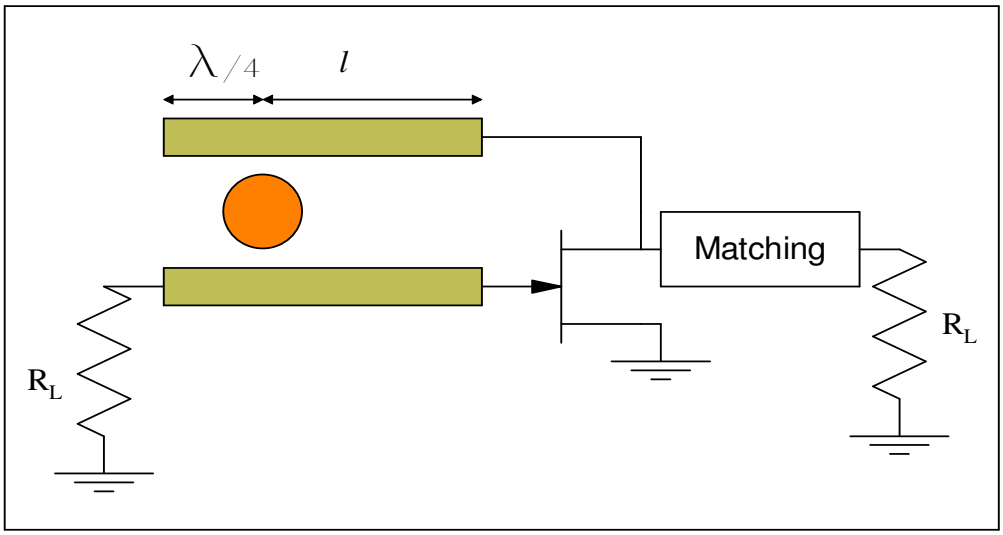

Figure 5. 3 Parallel feedback DRO schematic

Step 7: Frequency Tuning

The frequency must be tuned using a tuning screw since the oscillator will most probably not operate at the exact design frequency. A tuning screw is connected to a metal plate, which is placed above the resonator. Screwing in and out will change the L, C, and R of the dielectric resonator, which will then determine the frequency of the resonator. When the metal plate is moved to increases or decreases the distance to the resonator, the frequency will increase and decrease respectively.

5.3.1 Design Example One

Step 1: Resonator

This step deals with the dielectric resonators and due to its importance, it was done in detail in chapter 3 section 3.10. The resonator that was used is the 8300 series resonator from Trans-Tech at with a frequency of approximately 6.22 GHz. The substrate that was used is Rogers 4003 with an ε_r of 3.38, height of 0.8128 mm and tanδ of 0.0027. The important DR characteristics that are required for the design are table 3.2. The extracted parallel RLC model is used in the simulation using MWO.

Step 2: Active Device

The decision was made to use a HEMT (ATF-36077) from Agilent Technologies. (see chapter 2 section 2.6). The s-parameters were provided at the typical operating point (Vds=1.5V, Vgs=-0.2V, and Id=10mA).

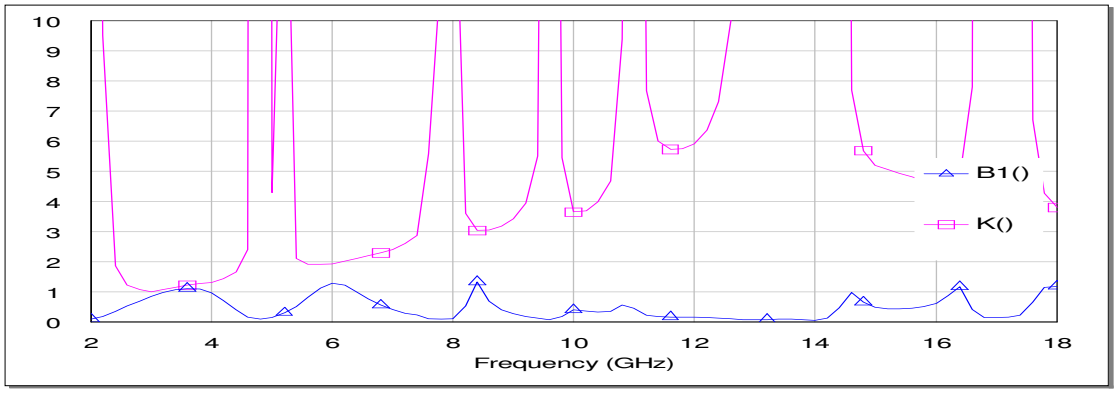

Figure 5. 4 MWO plot of K and B1 for The Amplifier

Figure 5.4 shows that the transistor became stable my adding a small resistor (8 ohm) between the matching and the drain of the transistor as suggested by the application note [51]. The resistor needs a 0.08 V extra voltage so the power supply must be 1.58 V

Step 3: Phase Shift

Figure 5.5 shows that the phase shift of the transistor is approximately 85 degrees, thus the feedback should be -85 degrees.

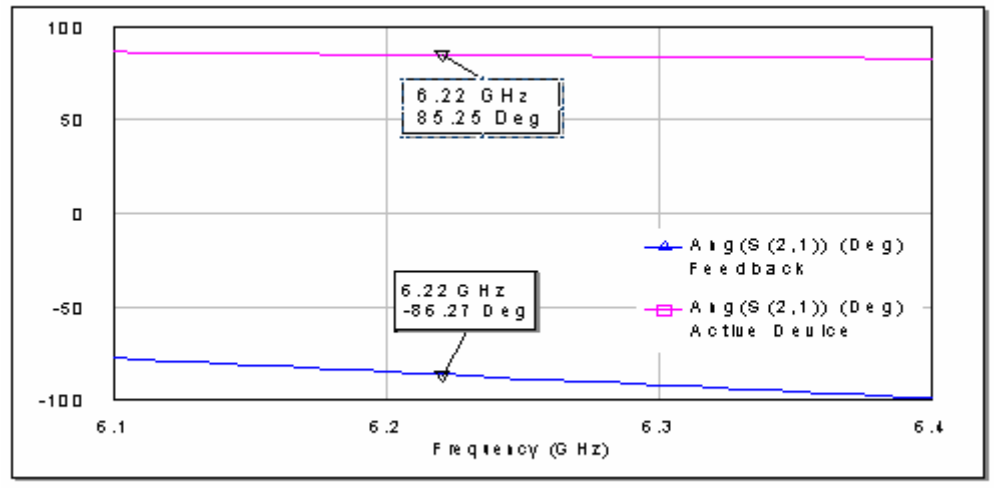

Figure 5. 5 Phase shift of the common source transistor at 6.22 GHz

Step 4: Amplifier Design

The amplifier is designed at 6.22 GHz. It has some gain bandwidth of approximately 1 GHz around the designed frequency. The gain at 6.22 GHz is approximately 10 dB. Figure 5.6 shows the frequency response of the amplifier with gain around the design frequency indicated with markers.

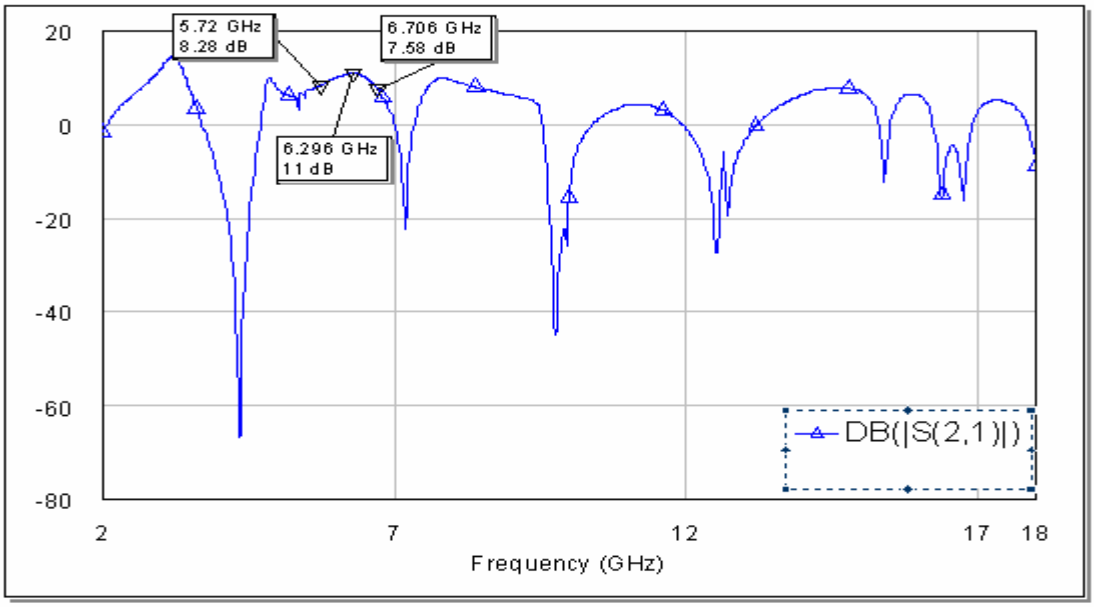

Figure 5. 6 S_{21} of the 6.22 GHz amplifier

Step 5: Adding the DR model and Matching

After designing the amplifier the model of the DR is added as shown in figure 5.2. The reflections at both sides of the DRO must be more than unity. Figure 5.7 shows that S_{11} and S_{22} are more than 32 at 6.22 GHz. (See figure 5.2 for the position of S_{11} and S_{22} on the diagram).

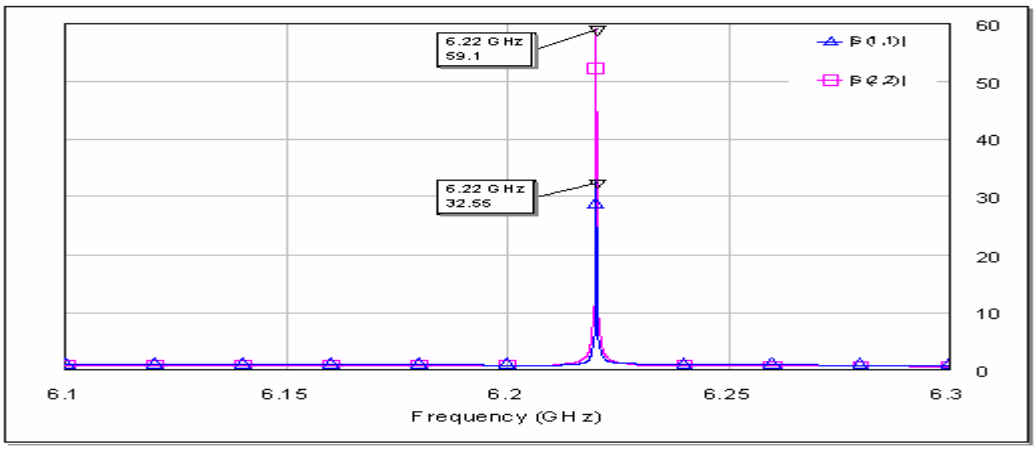

Figure 5. 7 S_{11} and S_{22} of the 6.22 GHz DRO

A small negative resistance must be seen at the output of the DRO. Figure 5.8 shows that a negative resistance can be seen at the output of the 6.22 GHz DRO and the imaginary part is close to zero.

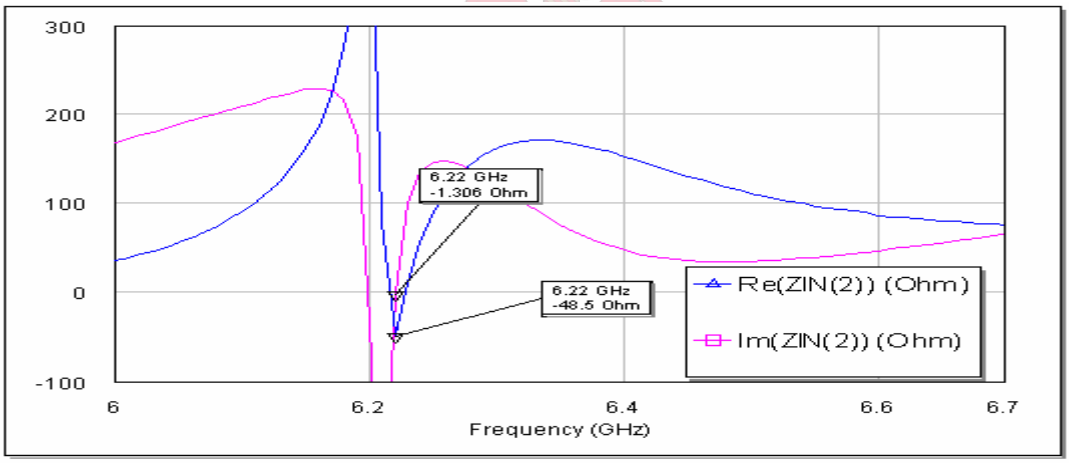

Figure 5. 8 The output impedance of the 6.22 GHz DRO

Step 6: PCB and Measurement

The PCB layout was done using AutoCAD. Figure 5.9 shows the final layout of the PCB of the DRO drawn on AutoCAD. C1, C2, C5, and C6 are decoupling capacitors where C1 and C5 are 100nf 0603 capacitors and C2 and C6 are 47 pf 0603 capacitors.

The DC block capacitors C3 and C4 are 15 pf 0402 capacitors. T is Agilent HEMT ATF 36077 Transistor and R is 8-29 ohm.

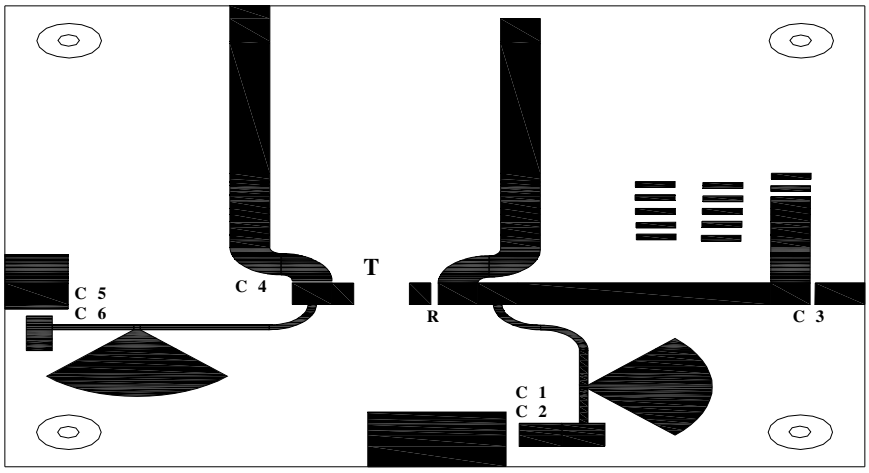

Figure 5. 9 The 6.22 GHz DRO PCB AutoCAD layout

Figure 4.10 is an actual photo of the 6.22 GHz DRO.

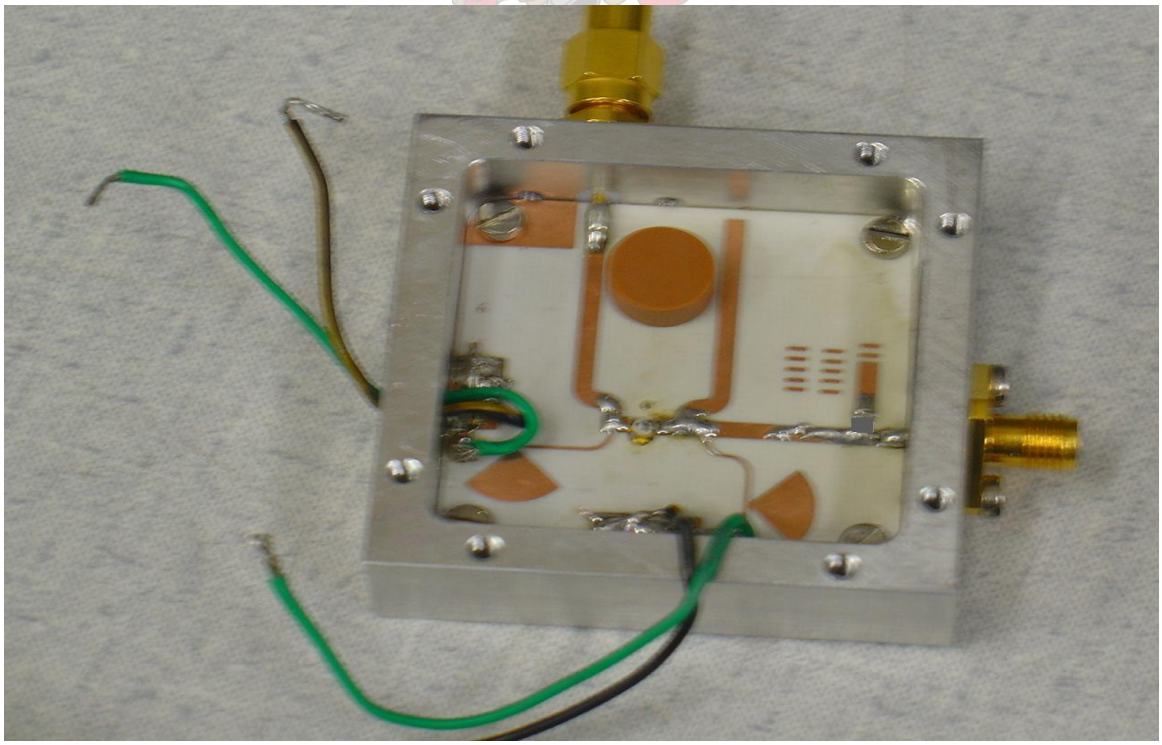

Figure 5. 10 The 6.22 GHz DRO Photo

The actual measurement of the DRO can be seen in figure 5.11. It shows the fundamental, the second and third harmonics using HP 8562A spectrum analyzer with 30 dB Att, 100 kHz RBW and 100 kHz VBW. The fundamental is approximately 8 dBm, the second harmonic is roughly -20 dBc and the third harmonic -23 dBc. The spurious level is around -74 dBc (the noise floor of the spectrum analyser is -78.5 dB). Figure 5.12 shows the fundamental component only with 20 dB Att, 30 kHz RBW and 30 kHz VBW.

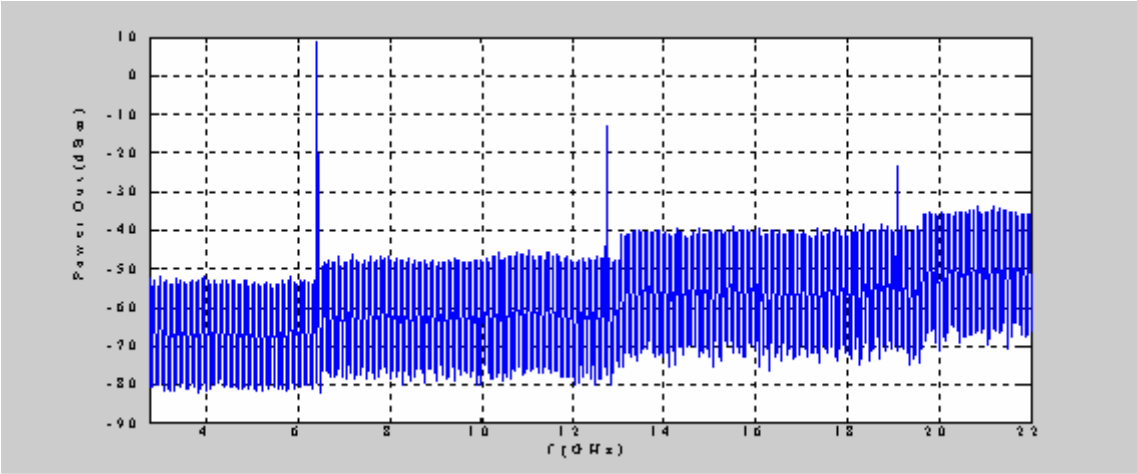

Figure 5. 11 Output spectrum of the 6.22 GHz DRO

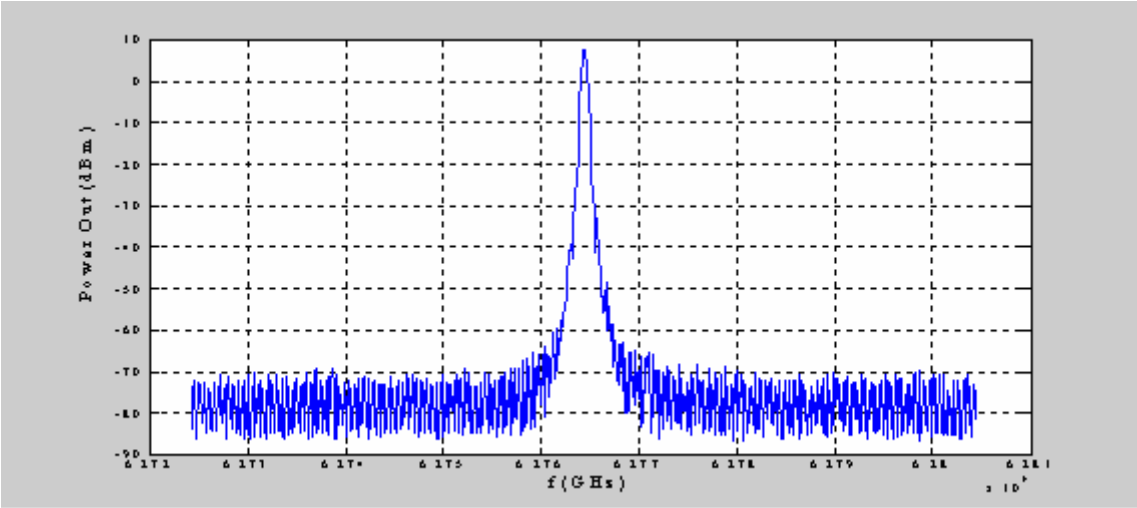

Figure 5. 12 The spectrum of the fundamental of the 6.22 GHz DRO

One of important characteristics of a DRO is the phase noise at 10 kHz or further away from the carrier. The phase noise of a DRO depends on the active device, the coupling of the oscillation power to the DR, and the amount of power delivered to the load. [52]

The pushing was investigated by varying the input voltage and observing the change in the resonant frequency and found to be less than 1 MHz/volt for the 6.22 GHz DRO. Figure 5.13 shows the phase noise of the 6.22 GHz which oscillator agrees with the typical phase noise given by [52]. It is -90 dBc/Hz at 10 kHz away from the carrier and -120 dBc/Hz at 100 kHz away from the carrier. The phase noise was measured using PN9000B phase measurement system using the delay line method.

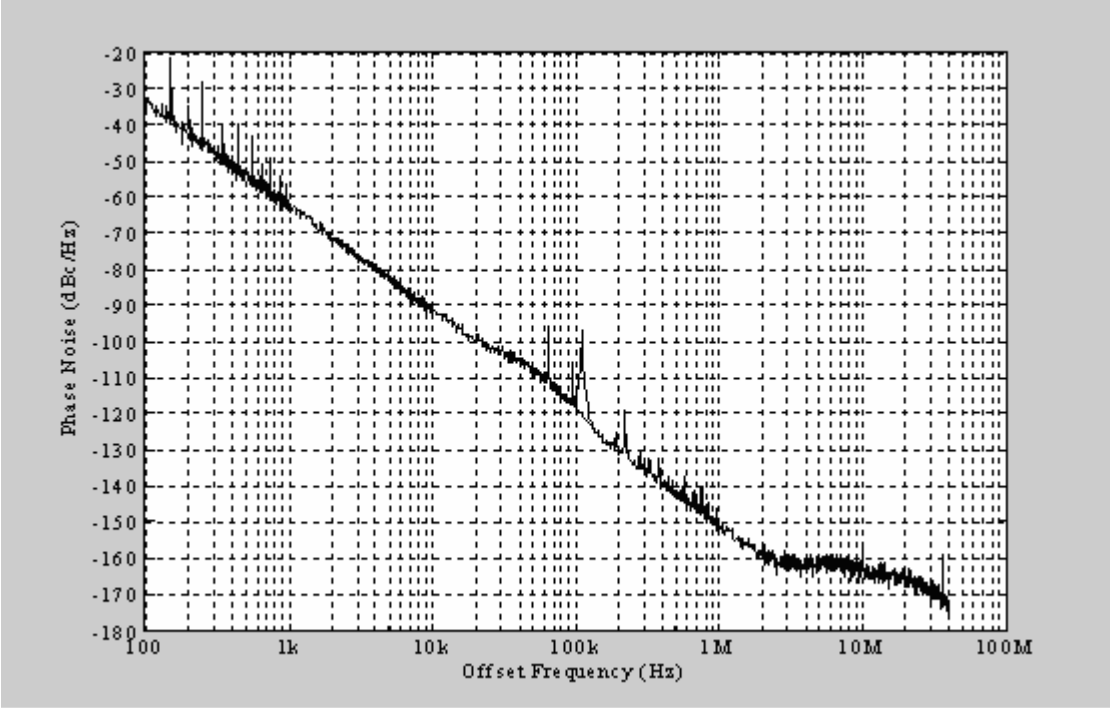

Figure 5. 13 The 6.22 GHz DRO phase noise

Step 7: Frequency Tuning

Basically, the DRO is a fixed frequency oscillator with its frequency determined by the resonator material permittivity, resonator dimensions, and the shielding conditions. However, the frequency of oscillation can be tuned mechanically over a narrow

frequency range. Use is made by the fact that the frequency of the resonator is highly sensitive to the shielding. A tuning screw is inserted from the top cover of the aluminium enclosure, right above the DR. The increase of the tuning screw depth will increase the frequency of the DR. Caution should be taken to keep the distance between the DR and the tuning screw at least half the DR height in order not to degrade the DR quality factor. Tuning the DRO of about 420 MHz is shown in figure 5.14.

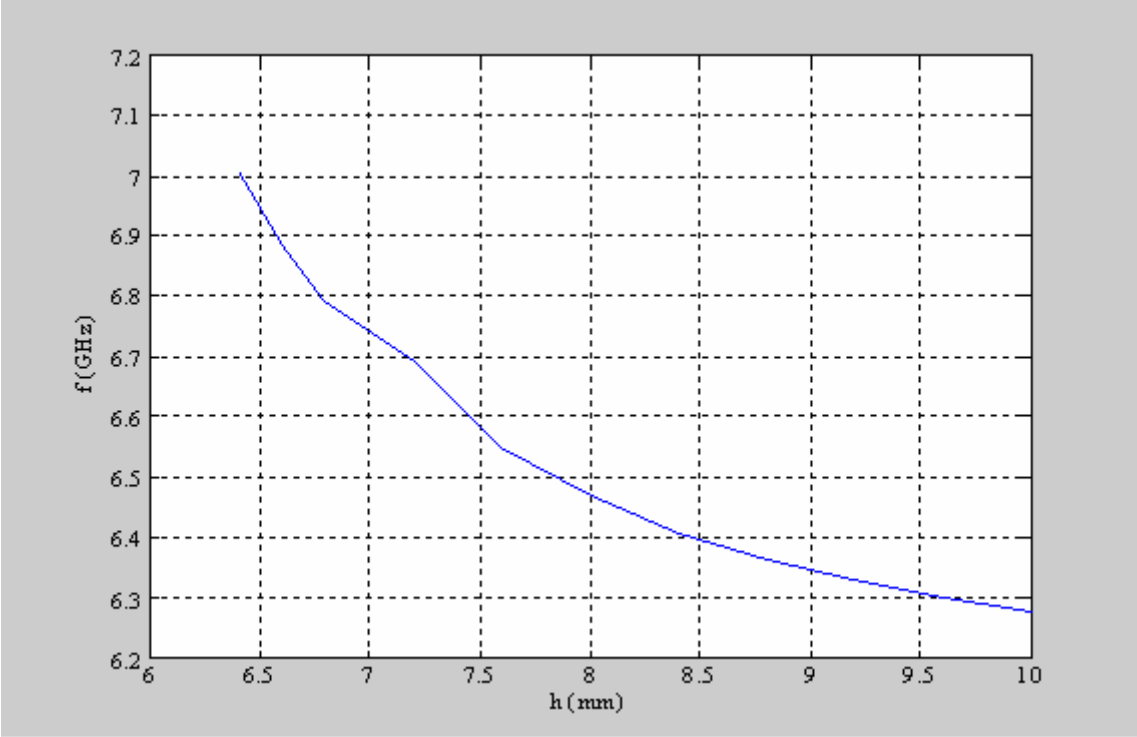

Figure 5. 14 Frequency tuning of the 6.22 GHz DRO

5.3.2 Design Example Two

The PCB layout have been done using AutoCAD and manufactured. The DRO was built and tested. Figure 5.15 shows the final layout of the PCB of the DRO drawn on AutoCAD. C1, C2, C5, and C6 are decoupling capacitors where C1 and C5 are 100nf 0603 capacitors and C2 and C6 are 47 pf 0603 capacitors. The DC block capacitors C3 and C4 are 4.7 pf 0402 capacitors. T is Agilent HEMT ATF 36077 Transistor and R is 8-29 ohm.

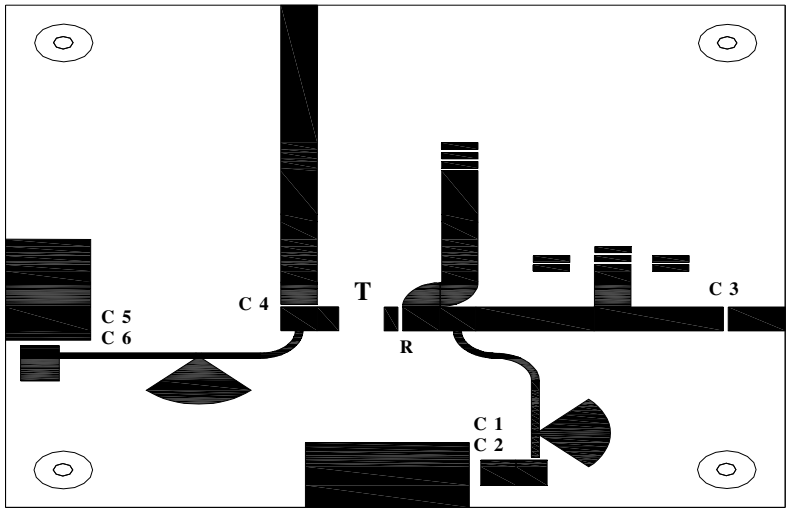

Figure 5. 15 The 11.2 GHz DRO PCB AutoCAD layout

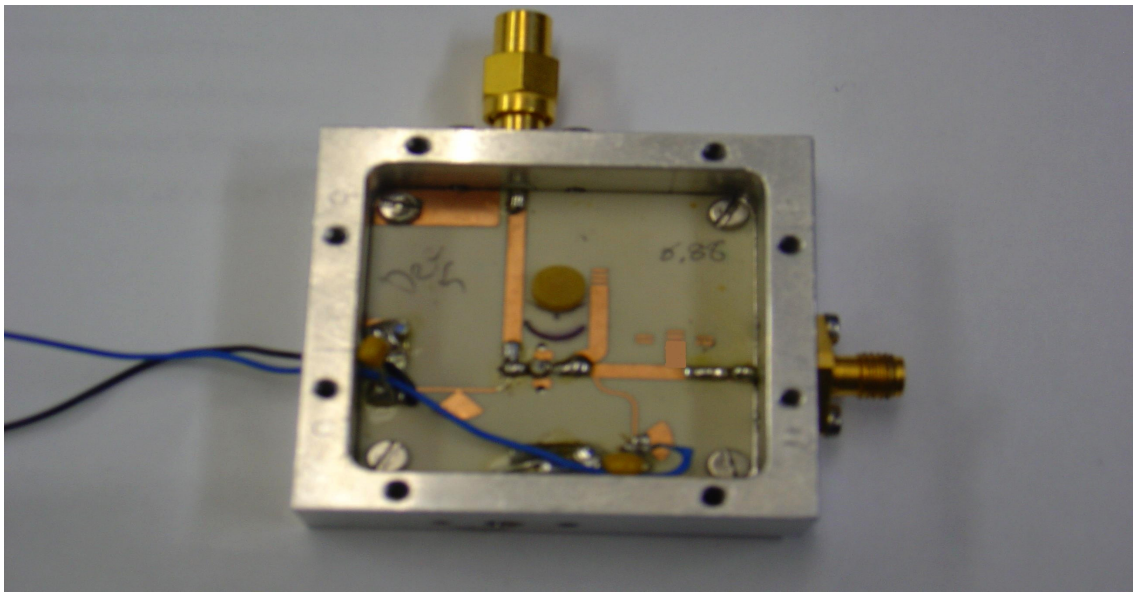

Figure 5. 16 The 11.2 GHz DRO Photo

The actual measurement of the DRO can be seen in figure 5.17. It shows the fundamental, the second and third harmonics which are measured using FSEK 30 spectrum analyser from ROHDE and SCHWARZ with 30 dB Att, 100 kHz RBW and 100 kHz VBW.. The fundamental is approximately 8 dBm, the second harmonic is roughly -21 dBc and the third harmonic -34 dBc with 30 dB Att, 100 kHz RBW and 100 kHz VBW. The spurious level is around -65 dBc (the noise floor of the spectrum

analyser was about -70 dB). Figure 5.18 shows the fundamental component only with 30 dB Att, 30 kHz RBW and 30 kHz VBW.

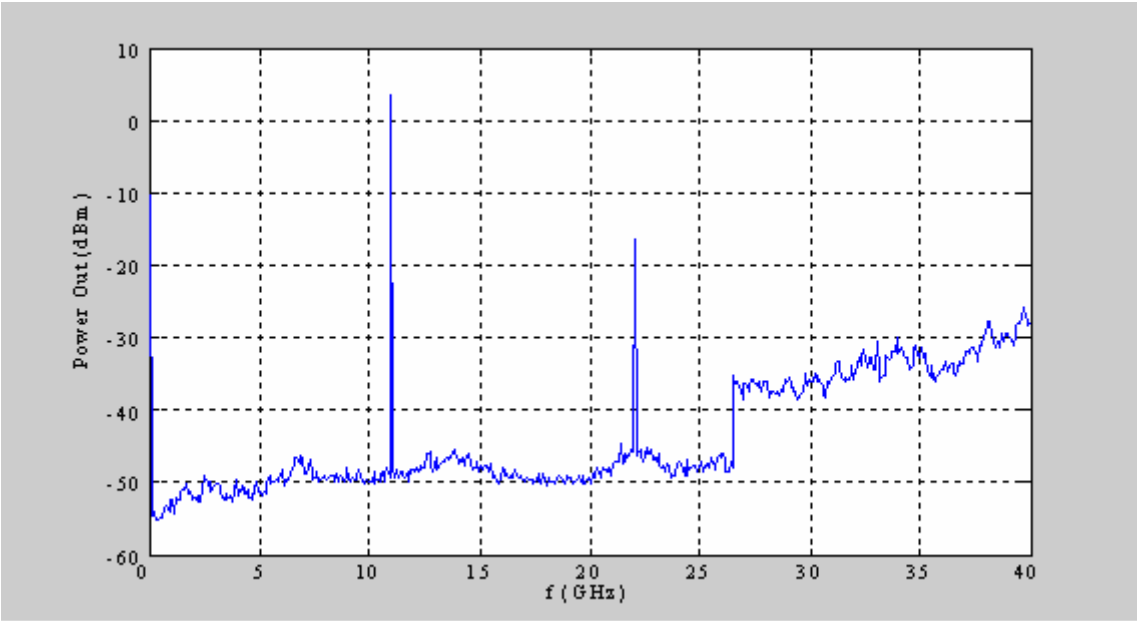

Figure 5. 17 Output spectrum of the 11.2 GHz DRO

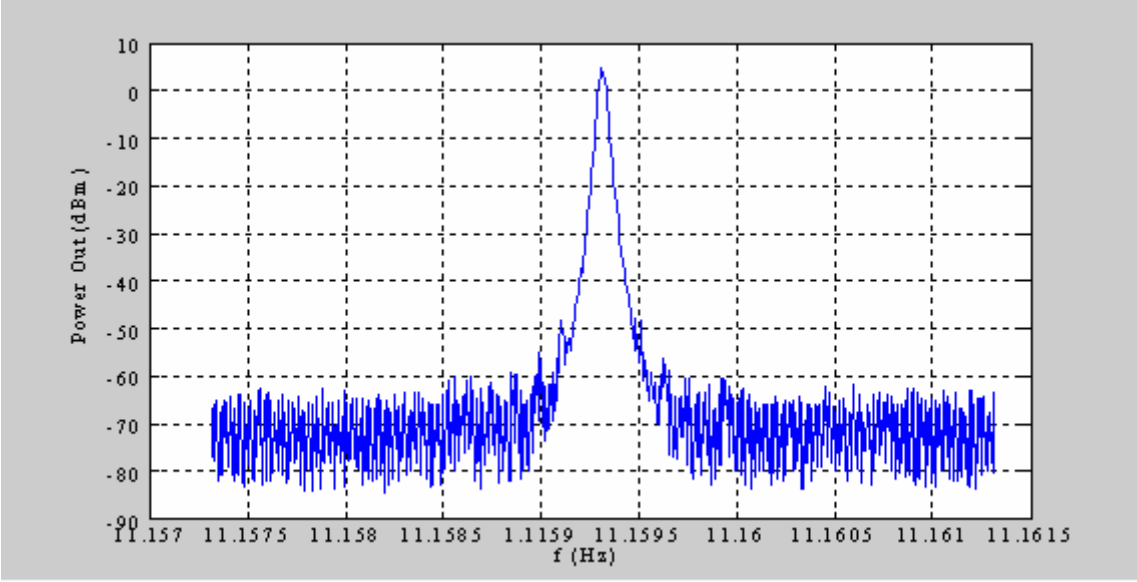

Figure 5. 18 The Spectrum of the fundamental of the 11.2 GHz DRO

The pushing was investigated by and found to be less than 1.5 MHz/volt for the 11.2 GHz DRO. The phase noise of the 6.22 GHz is shown in figure 5.19. which also agree with the typical phase noise given by [52]. It is -80 dBc/Hz at 10 kHz away from the carrier and -110 dBc/Hz at 100 kHz away from the carrier. The phase noise was measured using PN9000B phase measurement system using the delay line method.

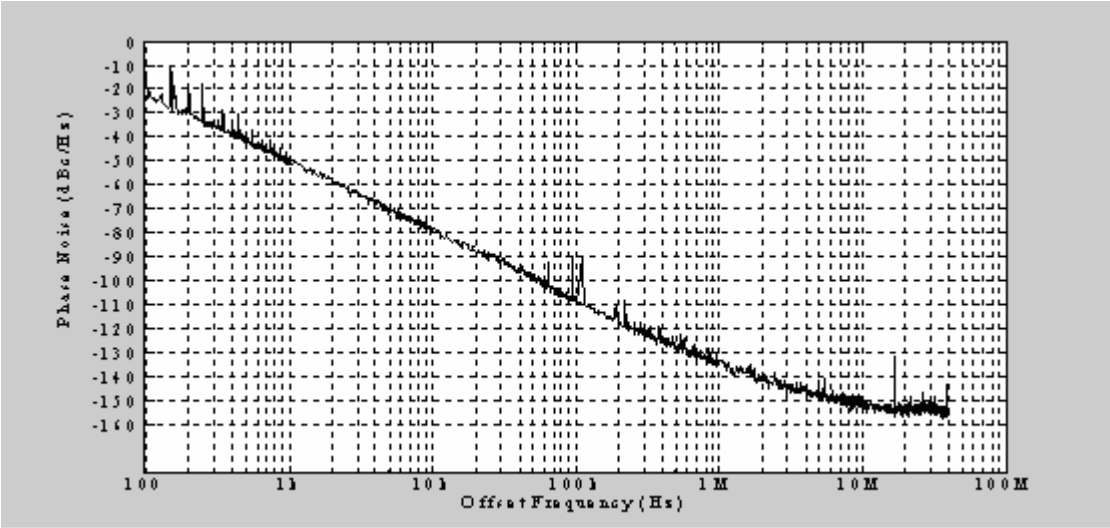

Figure 5. 19 The 11.2 GHz DRO phase noise

The result of tuning the DRO of about 200 MHz for the 11.2 GHz DRO is shown in figure 5.20

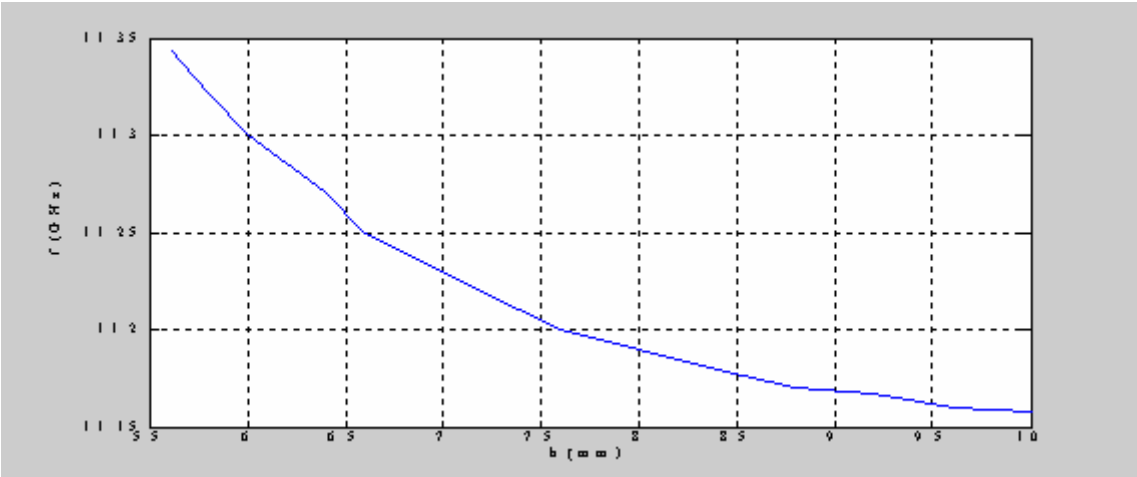

Figure 5. 20 Frequency tuning of the 11.2 GHz DRO

5.4 Conclusion

The procedure of designing parallel feedback DROs was used to design DROs at two different frequencies starting with a fairly low frequency and then increasing the frequency.

The frequency of the first DRO is at approximately 6.22 GHz and the second one is at around 11.2 GHz. The design of the first DRO is illustrated in detail while only the layout and the experimental results are shown for the second since a very exact procedure is used. For the first DRO roughly 8 dBm output power was achieved while maintaining a high Q. This is done by increasing the distance between the two microstrip lines that the DR is coupled to until almost half of the power is consumed by the loss of the resonator, this will guarantee a good phase noise performance and high Q.

A phase noise of -120 dBc/Hz at 100 kHz offset from the carrier was achieved while having an output power of about 8 dBm for the 6.22 GHz DRO. If both high output power and phase noise are needed, a buffer amplifier should be used.

The 11.2 GHz output power of approximately 4 dBm was achieved with a phase noise of -110 dBc/Hz. The second harmonic level is -21 dBc and the third harmonic level is -34 dBc.

The pushing was found to be less than 1 MHz/volt for the 6.22 GHz and 1.5 MHz/volt for the 11.2 GHz DROs.

The fact that the DRO can be tuned mechanically is one of its main advantages since it is easy to tune the frequency of the DRO by only mounting a screw above the DRO. The tuning range of the 6.22 GHz is roughly 420 MHz and 200 MHz for the 11.2 GHz.

The Results obtained compare well to published DROs performance especially the phase noise[38, 49, 50]. A phase noise of -120 dBc/Hz at 100 kHz for oscillators up to

10 GHz and -103 dBc/Hz and -110 dBc/Hz at 100kHz for oscillators below 12 GHz were reported in publications and application notes.

Table 5. 1 The parallel feedback DROs features

	Unit	6.22 GHZ DRO	11.2 GHZ DRO
Supply Voltage			
Vds	Volt	1.58	1.58
Vgs	Volt	-0.2	-0.2
Supply Current	mA	10	10
Output Power	dBm	8	4
Second Harmonic	dBc	-20	-22
Third Harmonic	dBc	-23	-34
Phase noise			
10kHz	dBc/Hz	-90	-80
100kHz	dBc/Hz	-120	-110
Frequency Pushing	MHz/Volt	1	1.5
Spurious Level	dBc	<-75	<-65

For the schematics for both DROs refer to Appendix B.

.

CHAPTER 6

Conclusion

First a thorough study of dielectric resonator oscillators was undertaken thus providing a background and motive for using DROs. Oscillators were discussed in general in the second chapter of this thesis, to provide the reader with the necessary information. In the third chapter, dielectric resonators were concentrated on. The important properties of dielectric resonators were measured using a network analyzer. From the measured data, the electric model of the dielectric resonator was extracted and it was used in the simulation.

The procedure of designing series feedback dielectric resonators was discussed in detail in the fourth chapter and the procedure was validated by two examples. These two examples were designed by using two dielectric resonators, each at a different frequency. The carrier power, pushing, tuning and the phase noise of the oscillators were shown, in addition, the harmonics and the spurs levels were measured and documented.

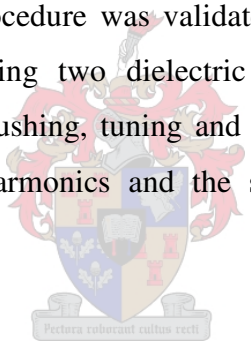

In the fifth chapter the design procedure for parallel feedback dielectric resonators was discussed in detail and validated by two examples. These two examples were designed in a similar way to the series feedback dielectric resonator oscillator by using two dielectric resonators at two different frequencies. As in the case of series feedback dielectric resonators, the parameters of the oscillators were measured and documented.

The aim of the study was to develop a procedure for designing dielectric resonator oscillators. This aim was achieved by setting the procedure and then testing it with four designs of different types and frequency. One of the main issues in the design that became evident is the unwanted modes caused by the dielectric resonator packaging. It was shown that, by carefully analysing the resonator packaging and coupling, an accurate and reliable model can be obtained to ensure a successful

oscillator design. Both types, the series feedback DRO and the parallel feedback DRO worked well.

Refrences

[1] R. D. Richtmyer, "Dielectric Resonators," *Journal of Applied Physics*, vol. 10, pp. 391-398, June1939.

[2] S. B. Cohn, "Microwave Bandpass Filters Containing High-Q Dielectric Resonators," *IEEE Transaction On Microwave Theory and Techniques*, vol. MTT-16, pp. 218-227, April 1968.

[3] J. K. Plourde and C. Ren, "Application of Dielectric Resonators in Microwave Components," *IEEE Transactions on Microwave Theory and Techiques*, vol. MTT-29, pp. 754-770, August 1981.

[4] R. R. Bonetti and A. E. Atia, "Analysis of Microstrip Circuits Coupled to Dielectric Resonators," *IEEE Transactions on Microwave Theory and Techiques*, vol. MTT-29, pp. 1333-1337, December 1981.

[5] A. P. S. Khanna, "Review of Dielectric Resonator Oscillator Technology," *41st Annual Frequency Control Symposium, IEEE*, pp. 478-486, 1987.

[6] T. Tokumitsu, "K-band and millimetre-wave MMICs for emerging commercial wireless applications," *IEEE Transactions On Microwave Theory and Techniques*, vol. 49, pp. 2066-2072, November 2001.

[7] M. K. Siddik, A. K. Shaema, L. G. Callejo, and R. Lai, "High power and high efficiency monolithic power amplifier at 28 GHz for LMDS application," *IEEE Transactions On Microwave Theory and Techniques*, vol. 46, pp. 2226-2232, December 1998.

[8] P. Heide, "Commercial microwave sensor technology – an emerging business," *Microwave Journal*, vol. 42, pp. 348-352, May 1999.

[9] J. A. Kielb and O. Pulkrabek, "Application of a 25 GHz FMCW radar for industrial and process level measurement," *IEEE International Microwave Symposium Digest*, vol. MTT-22, pp. 281-284, 1999.

[10] H. Meinel, "Automotive millimetre-wave radar history and present status," *in proceeding 0f 28th European Microwave Conference*, pp. 619-629, 1998.

[11] Y. Campos-Roca, L. Verweyen, M. Neumann, M. Fernandez-Barciela, M. C. Curras-Francos, E. Sanchez, A. Huelsmann, and M. Schlechtweg, "Coplanar PHEMT MMIC frequency multipliers for 76 GHz automotive radar," *I IEEE Microwave Guided Wave Letters*, vol. 9, pp. 242-244, February 1999.

[12] "Phase-locked DRO achieves low noise and cost at 26 GHz," *Microwave & RF*, pp. 144-148, June 2000.

[13] P. Guillon, B. Byzery, and M. Chaubet, "Coupling Parameters Between Dielectric Resonator and a Microstripline," *IEEE Transactions on Microwave Theory and Techiques*, vol. MTT-33, pp. 222-226, March 1985.

[14] H. C. Duran, U. Lott, H. Benedickter, and W. B. Achtold, "A K-band DRO in coplanar layout with dry and wet etched In PHEMT's," *IEEE International Microwave Symposium Digest*, vol. MTT-21, pp. 861-864, June 1998.

[15] P. J. Garner, M. J. Howes, and C. M. Snowden, "Ka-band and MMIC PHEMT-based VCO's with low phase-noise properties," *IEEE Transaction On Microwave Theory and Techniques*, vol. 46, pp. 1531-1535, October 1998.

[16] H. Takamura, H. Matsumoto, and K. Wakino, " Low Temperature Properties of Microwave Dielectrics," *Japaneese Journal of Applied Physics*, vol. 28, pp. 21-23, 1989.

[17] H. Abe, "A GaAs MESFET oscillator quasi-linear design method," *IEEE Transaction On Microwave Theory and Techniques*, vol. MTT-34, pp. 19–25, January 1986.

[18] R. W. Rhea, *Oscillator Design and Computer Simulation* 2ed. Atlanta: Noble Publishing, 1995.

[19] G. R. Basawapatna, "A unified approach to the design of wide-band microwave solid-state oscillators," *IEEE Transactions on Microwave Theory and Techniques*, vol. MTT-27, pp. 379-385, May 1979.

[20] F. Pergal, "Detail a colpitts vco as a tuned one-port," *Microwaves*, vol. 18, pp. 110-115, April 1979.

[21] D. M. Pozar, *Microwave Engineering*, 2 ed. New York: John Wiley & Sons Inc, 1998.

[22] G. V. Vendelin, *Design of Amplifiers and Oscillators by the S-Parameter Method*. New York: Wiley, 1982.

[23] G. D. Vendelin, A. M. Pavio, and U. L. Rohde, *Microwave Circuit Design Using Linear and Nonlinear Techniques*. New Jersey: Wiley, 2005.

[24] E. L. Holzman, *Solid State Microwave Power Oscillator Design*. Boston: Artech House, 1992.

[25] S. A. Maas, *Nonlinear Microwave Circuits*. Norwood: Artech House, 1988.

[26] M. Regis, O. Llopis, and J. Graffeuil, "Nonlinear Modeling and Design of Bipolar Transistors Ultra Low Phase Noise Dielectric Resonator Oscillator," *IEEE Transactions on Microwave Theory and Techniques*, vol. 46, pp. 1589-1593, October 1998.

[27] Y. Chen and T. Kajita, "DRO State of the Art," *Applied Microwave*, pp. 69-77, Spring 1990.

[28] R. G. Rogers, *Phase Noise Microwave Oscillator Design*. Boston: Artech House, 1991.

[29] M. Pouysugar, G. Graffeuil, J. Sautereau, and J. Fortera, "Comparative Study of Phase Noise in HEMT an MESFET Microwave Oscillators," *IEEE International Microwave Symposium Digest*, vol. 2, pp. 557 - 560, 1988.

[30] X. Zhang, D. Sturzebecher, and A. Daryoush, "Comparison of the Phase Noise Performance of HEMT and HBT Based Oscillators," *IEEE International Microwave Symposium Digest*, vol. MTT-21, pp. 697 - 700, 1995.

[31] G. Gonzalez, *Microwave transistor amplifiers: Analysis and design*, 2nd ed: Prentice Hall, 1997.

[32] D. Kajfez and P. Guillon, *Dielectric Resonators*, 2nd ed. Atlanta: Noble, 1998.

[33] "Dielectric Resonators - A Designer Guide to Microwave Dielectric Ceramics," Trans-Tech Inc. Publication No. 50080040, Rev 2, October 1990.

[34] D. Kajfez and E. J. Hwan, "*Q*-Factor Measurement with Network Analyzer," *IEEE Transactions on Microwave Theory and Techiques*, vol. MTT-32, pp. 666-670, July 1984.

[35] Y. Komatsu and Y. Murakami, "Coupling Coefficient Between Microstrip Line and Dielectric Resonator," *IEEE Transaction On Microwave Theory and Techniques*, vol. MTT-08, pp. 34-40, January 1983.

[36] H. Abe, Y. Takayama, A. Higashisaka, and H. Takamizawa, "A Highly Stabilized Low-Noise GaAs FET Integrated Oscillator with a Dielectric Resonator in the C-Band," *IEEE Transactions on Microwave Theory and Techiques*, vol. MTT-26, pp. 156-162, March 1978.

[37] J. Sun and C. Wei, "A Highly Stabilized GaAs FET reflection type Oscillator with a Dielectric Resonator in X-Band," *Microwave Journal*, vol. 35, pp. 72-80, April 1992.

[38] M. Loboda, T. Parker, and G. Montress, "Frequency Stability of L-Band, Two-Port Dielectric Resonator Oscillators," *IEEE Transactions on Microwave Theory and Techiques*, vol. MTT-35, pp. 1334-1339, December 1987.

[39] T. Saito, Y. Arai, Y. Itoh, T. Nishikawa, and H. Komizo, "A 6 GHz Highly Stabilized GaAs FET Oscillator Using a Dielectric Resonator," *IEEE International Microwave Symposium Digest*, vol. 79, pp. 197-199, April 1979.

[40] O. Ishihara, T. Mori, H. Sawano, and M. Nakatani, "A Highly Stabilized GaAs FET Oscillator Using a Dielectric Resonator Feedback Circuit in 9-14 GHz," *IEEE Transactions on Microwave Theory and Techiques*, vol. MTT-28, pp. 817-824, Aug. 1980

[41] A. Khanna and Y. Garault, "Determination of Loaded, Unloaded, and External Quality Factors of a Dielectric Resonator Coupled to a Microstrip Line," *IEEE Transactions on Microwave Theory and Techiques*, vol. MTT-31, pp. 261-264, March 1983.

[42] M. Lee, K. Ryu, and I. Yom, "Phase Noise Reduction of Microwave HEMT Oscillators Using a Dielectric Resonator Coupled by a High Impedance Inverter," *ETRI Journal*, vol. 23, pp. 199-201, December 2001.

[43] S. L. March, "Analyzing lossy radial-line stubs," *IEEE Transactions on Microwave Theory and Techiques*, vol. MTT-33, pp. 269-271, March 1985.

[44] "*Microwave Oscillator Design*," Agilent Technologies Application Note A008.

[45] P. C. L. Yip, *High-Frequency Circuit Design and Measurements*: Chapman & Hall, 1990.

[46] F. Giannini, R. Ruggieri, and J. Vrba, "Shunt-connected microstrib radial stubs," *IEEE Transactions on Microwave Theory and Techiques*, vol. MTT-34, pp. 363-366, March 1986.

[47] I. Yom, D. Shin, K. Ryu, S. Oh, and M. Lee, "Phase-Noise Reduction of Voltage-Controlled Dielectric Resonator Oscillator for the X-Band," *Microwave and Optical Technology Letters*, vol. 47, pp. 515-518, December 2005.

[48] K. Kamozaki, "4GHZ Miniaturized Low Noise Dielectric Resonator Stabilized Oscillator," *IEEE Transaction On Microwave Theory and Techniques*, vol. MTT-14, pp. 1305-1308, 1992.

[49] "Dielectric Resonator Oscillator (DRO) at 10 GHz," SIEMENS Application note No. 002.

[50] S. Ha, C. Ahn, K. Lee, and H. U, "Improved Structure of a DRO for High Output Power and Low Phase Noise," *Microwave and Optical Technology Letters*, vol. 41, pp. 68-70, April 2004.

[51] "L Band Amplifier using the ATF-36077 Low Noise PHEMT," Agilent Technologies Application Note 1128.

[52] C. Y. Ho and T. Kajita, "DRO State of the Art," *Applied Microwave*, pp. 69-80, Spring 1990.

Appendix A Datasheet of ATF 36077

Agilent Technologies
Innovating the HP Way

2–18 GHz Ultra Low Noise Pseudomorphic HEMT

Technical Data

ATF-36077

Features

- **PHEMT Technology**
- **Ultra-Low Noise Figure:**
  0.5 dB Typical at 12 GHz
  0.3 dB Typical at 4 GHz
- **High Associated Gain:**
  12 dB Typical at 12 GHz
  17 dB Typical at 4 GHz
- **Low Parasitic Ceramic Microstrip Package**
- **Tape-and-Reel Packing Option Available**

Applications

- **12 GHz DBS LNB (Low Noise Block)**
- **4 GHz TVRO LNB (Low Noise Block)**
- **Ultra-Sensitive Low Noise Amplifiers**

Note: 1. See Noise Parameter Table.

Description

Agilent's ATF-36077 is an ultra-low-noise Pseudomorphic High Electron Mobility Transistor (PHEMT), packaged in a low parasitic, surface-mountable ceramic package. Properly matched, this transistor will provide typical 12 GHz noise figures of 0.5 dB, or typical 4 GHz noise figures of 0.3 dB. Additionally, the ATF-36077 has very low noise resistance, reducing the sensitivity of noise performance to variations in input impedance match, making the design of broadband low noise amplifiers much easier. The premium sensitivity of the ATF-36077 makes this device the ideal choice for use in the first stage of extremely low noise cascades.

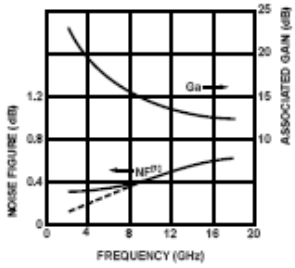

Figure 1. ATF-36077 Optimum Noise Figure and Associated Gain vs. Frequency for V_{DS} = 1.5 V, I_D = 10 mA.

77 Package

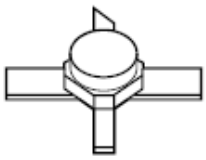

Pin Configuration

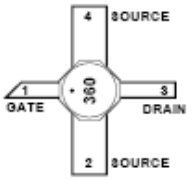

The repeatable performance and consistency make it appropriate for use in Ku-band Direct Broadcast Satellite (DBS) Television systems, C-band Television Receive Only (TVRO) LNAs, or other low noise amplifiers operating in the 2-18 GHz frequency range.

This GaAs PHEMT device has a nominal 0.2 micron gate length with a total gate periphery (width) of 200 microns. Proven gold based metalization systems and nitride passivation assure rugged, reliable

Agilent Technologies
Innovating the HP Way

2–18 GHz Ultra Low Noise Pseudomorphic HEMT

Technical Data

ATF-36077

Features

- **PHEMT Technology**
- **Ultra-Low Noise Figure:**
  0.5 dB Typical at 12 GHz
  0.3 dB Typical at 4 GHz
- **High Associated Gain:**
  12 dB Typical at 12 GHz
  17 dB Typical at 4 GHz
- **Low Parasitic Ceramic Microstrip Package**
- **Tape-and-Reel Packing Option Available**

Applications

- **12 GHz DBS LNB (Low Noise Block)**
- **4 GHz TVRO LNB (Low Noise Block)**
- **Ultra-Sensitive Low Noise Amplifiers**

Note: 1. See Noise Parameter Table.

Description

Agilent's ATF-36077 is an ultra-low-noise Pseudomorphic High Electron Mobility Transistor (PHEMT), packaged in a low parasitic, surface-mountable ceramic package. Properly matched, this transistor will provide typical 12 GHz noise figures of 0.5 dB, or typical 4 GHz noise figures of 0.3 dB. Additionally, the ATF-36077 has very low noise resistance, reducing the sensitivity of noise performance to variations in input impedance match, making the design of broadband low noise amplifiers much easier. The premium sensitivity of the ATF-36077 makes this device the ideal choice for use in the first stage of extremely low noise cascades.

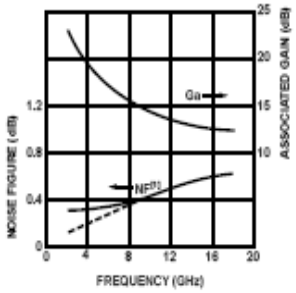

Figure 1. ATF-36077 Optimum Noise Figure and Associated Gain vs. Frequency for V_{DS} = 1.5 V, I_D = 10 mA.

77 Package

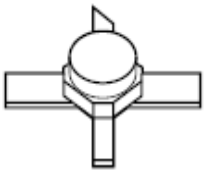

Pin Configuration

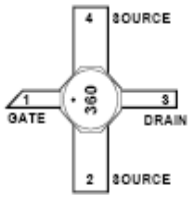

The repeatable performance and consistency make it appropriate for use in Ku-band Direct Broadcast Satellite (DBS) Television systems, C-band Television Receive Only (TVRO) LNAs, or other low noise amplifiers operating in the 2-18 GHz frequency range.

This GaAs PHEMT device has a nominal 0.2 micron gate length with a total gate periphery (width) of 200 microns. Proven gold based metalization systems and nitride passivation assure rugged, reliable devices.

2

ATF-36077 Absolute Maximum Ratings

Symbol	Parameter	Units	Absolute Maximum[1]
V_{DS}	Drain – Source Voltage	V	+3
V_{GS}	Gate – Source Voltage	V	-3
V_{GD}	Gate-Drain Voltage	V	-3.5
I_D	Drain Current	mA	I_{dss}
P_T	Total Power Dissipation[3]	mW	180
$P_{in\,max}$	RF Input Power	dBm	+10
T_{ch}	Channel Temperature	°C	150
T_{STG}	Storage Temperature	°C	-65 to 150

Thermal Resistance[2,3]:
$\theta_{ch-c} = 60°C/W$

Notes:
1. Operation of this device above any one of these parameters may cause permanent damage.
2. Measured at $P_{diss} = 15$ mW and $T_{ch} = 100°C$.
3. Derate at 16.7 mW/°C for $T_C > 139°C$.

ATF-36077 Electrical Specifications,

$T_C = 25°C$, $Z_O = 50\ \Omega$, $V_{ds} = 1.5$ V, $I_{ds} = 10$ mA, (unless otherwise noted).

Symbol	Parameters and Test Conditions		Units	Min.	Typ.	Max.
NF	Noise Figure[1]	f = 12.0 GHz	dB		0.5	0.6
G_A	Gain at NF[1]	f = 12.0 GHz	dB	11.0	12.0	
g_m	Transconductance	$V_{DS} = 1.5$ V, $V_{GS} = 0$ V	mS	50	55	
I_{dss}	Saturated Drain Current	$V_{DS} = 1.5$ V, $V_{GS} = 0$ V	mA	15	25	45
$V_{p\,10\,\%}$	Pinch-off Voltage	$V_{DS} = 1.5$ V, $I_{DS} = 10\%$ of I_{dss}	V	-1.0	-0.35	-0.15

Note:
1. Measured in a fixed tuned environment with Γ source = 0.54 at 156°; Γ load = 0.48 at 167°.

ATF-36077 Characterization Information,

$T_C = 25°C$, $Z_O = 50\ \Omega$, $V_{ds} = 1.5$ V, $I_{ds} = 10$ mA, (unless otherwise noted).

Symbol	Parameters and Test Conditions		Units	Typ.
NF	Noise Figure (Tuned Circuit)	f = 4 GHz f = 12 GHz	dB dB	0.3[2] 0.5
G_A	Gain at Noise Figure (Tuned Circuit)	f = 4 GHz f = 12 GHz	dB dB	17 12
$S_{12\,off}$	Reverse Isolation	f = 12 GHz, $V_{DS} = 1.5$ V, $V_{GS} = -2$ V	dB	14
P_{1dB}	Output Power at 1 dB Gain Compression	f = 4 GHz f = 12 GHz	dBm dBm	5 5
$V_{GS\,10\,mA}$	Gate to Source Voltage for $I_{DS} = 10$ mA	$V_{DS} = 1.5$ V	V	-0.2

Note:
2. See noise parameter table.

3

ATF-36077 Typical Scattering Parameters,
Common Source, Z_O = 50 Ω, V_{DS} = 1.5 V, I_D = 10 mA

Freq.	S_{11}		S_{21}			S_{12}			S_{22}	
GHz	Mag.	Ang.	dB	Mag.	Ang.	dB	Mag.	Ang.	Mag.	Ang.
1.0	0.99	-17	14.00	5.010	163	-36.08	0.016	78	0.60	-14
2.0	0.97	-33	13.81	4.904	147	-30.33	0.030	66	0.59	-28
3.0	0.94	-49	13.53	4.745	132	-27.25	0.043	54	0.57	-41
4.0	0.90	-65	13.17	4.556	116	-25.32	0.054	43	0.55	-54
5.0	0.86	-79	12.78	4.357	102	-24.04	0.063	33	0.53	-66
6.0	0.82	-93	12.39	4.162	88	-23.17	0.069	24	0.50	-78
7.0	0.78	-107	12.00	3.981	75	-22.58	0.074	16	0.48	-89
8.0	0.75	-120	11.64	3.820	62	-22.17	0.078	8	0.46	-99
9.0	0.72	-133	11.32	3.682	49	-21.90	0.080	1	0.44	-109
10.0	0.69	-146	11.04	3.566	37	-21.71	0.082	-6	0.42	-119
11.0	0.66	-159	10.81	3.473	25	-21.57	0.083	-13	0.40	-129
12.0	0.63	-172	10.63	3.401	13	-21.44	0.085	-19	0.38	-139
13.0	0.61	175	10.50	3.349	1	-21.32	0.086	-25	0.37	-149
14.0	0.60	161	10.41	3.315	-12	-21.19	0.087	-32	0.35	-160
15.0	0.58	147	10.36	3.296	-24	-21.04	0.089	-39	0.33	-171
16.0	0.57	131	10.34	3.289	-37	-20.87	0.091	-47	0.31	177
17.0	0.56	114	10.34	3.289	-50	-20.69	0.092	-55	0.29	164
18.0	0.57	97	10.35	3.291	-64	-20.53	0.094	-65	0.26	148

ATF-36077 Typical "Off" Scattering Parameters,
Common Source, Z_O = 50 Ω, V_{DS} = 1.5 V, I_D = 0 mA, V_{GS} = -2 V

Freq.	S_{11}		S_{21}			S_{21}			S_{22}	
GHz	Mag.	Ang.	dB	Mag.	Ang.	dB	Mag.	Ang.	Mag.	Ang.
11.0	0.96	-139	-14.2	0.19	-43	-14.2	0.19	-43	0.97	-125
12.0	0.95	-152	-14.0	0.20	-56	-14.0	0.20	-56	0.97	-137
13.0	0.94	-166	-13.8	0.20	-69	-13.8	0.20	-68	0.96	-149

Agilent Technologies
Innovating the HP Way

ATF-36077 Typical Noise Parameters,

Common Source, $Z_O = 50\ \Omega$, $V_{DS} = 1.5$ V, $I_D = 10$ mA

Freq. GHz	F_{min}[1] dB	Γ_{opt} Mag.	Γ_{opt} Ang.	R_n/Z_o -
1	0.30	0.95	12	0.40
2	0.30	0.90	25	0.20
4	0.30	0.81	51	0.17
6	0.30	0.73	76	0.13
8	0.37	0.66	102	0.09
10	0.44	0.60	129	0.05
12	0.50	0.54	156	0.03
14	0.56	0.48	-174	0.02
16	0.61	0.43	-139	0.05
18	0.65	0.39	-100	0.09

Note:
1. The F_{min} values at 2,4, and 6 GHz have been adjusted to reflect expected circuit losses that will be encountered when matching to the optimum reflection coefficient (Γ_{opt}) at these frequencies. The theoretical F_{min} values for these frequencies are: 0.10 dB at 2 GHz, 0.20 dB at 4 GHz, and 0.29 dB at 6 GHz. Noise parameters are derived from associated s parameters, packaged device measurements at 12 GHz, and die level measurements from 6 to 18 GHz.

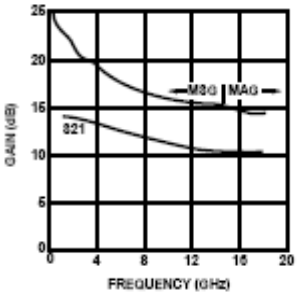

Figure 2. Maximum Available Gain, Maximum Stable Gain and Insertion Power Gain vs. Frequency. $V_{DS} = 1.5$ V, $I_D = 10$ mA.

77 Package Dimensions

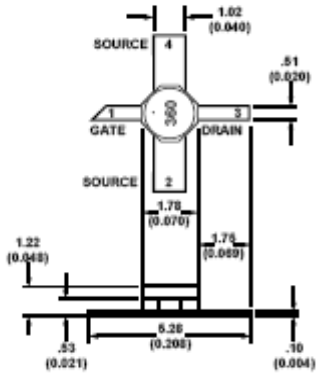

TYPICAL DIMENSIONS ARE IN MILLIMETERS (INCHES).

Part Number Ordering Information

Part Number	No. of Devices	Container
ATF-36077-TR1[2]	1000	7" Reel
ATF-36077-STR	10	strip

Note:
2. For more information, see "Tape and Reel Packaging for Semiconductor Devices," in "Communications Components" Designer's Catalog.

www.semiconductor.agilent.com
Data subject to change.

Obsoletes 5962-0193E
5965-8726E (11/99)

Appendix B: DROs schematics

a) The 6.22 GHz series feedback DRO

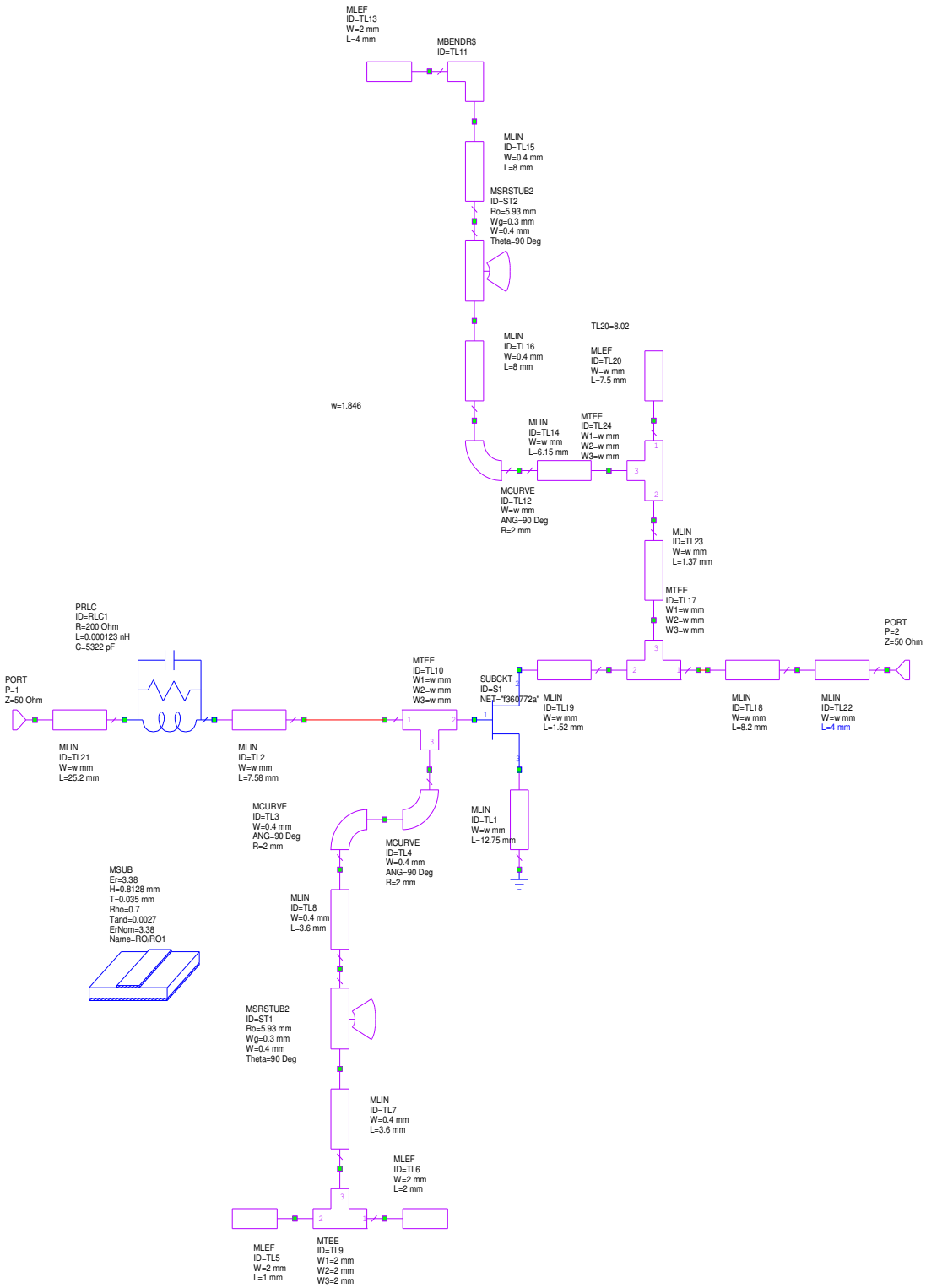

b) The 11.2 GHz series feedback DRO schematic

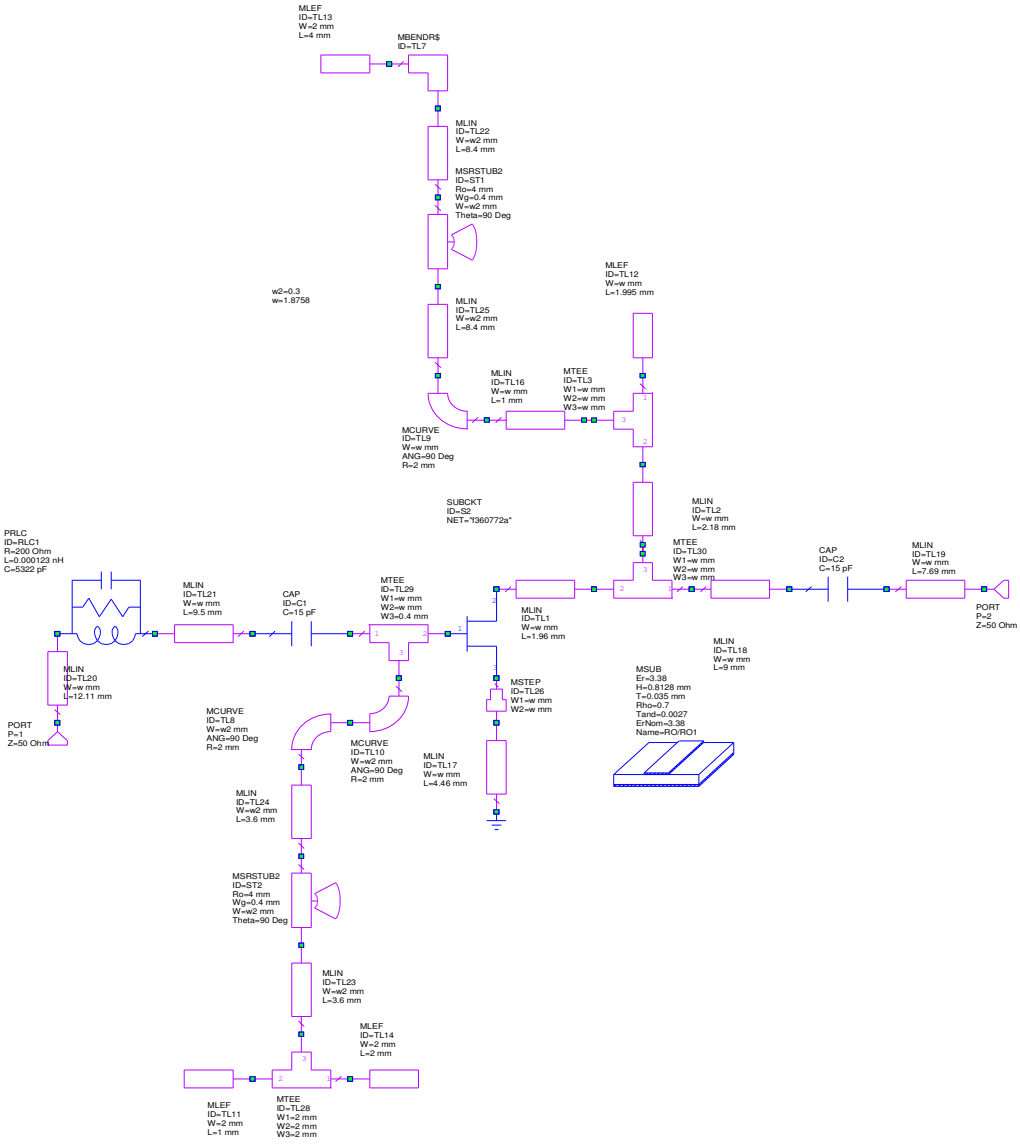

c) The 6.22 GHz parallel feedback DRO schematic

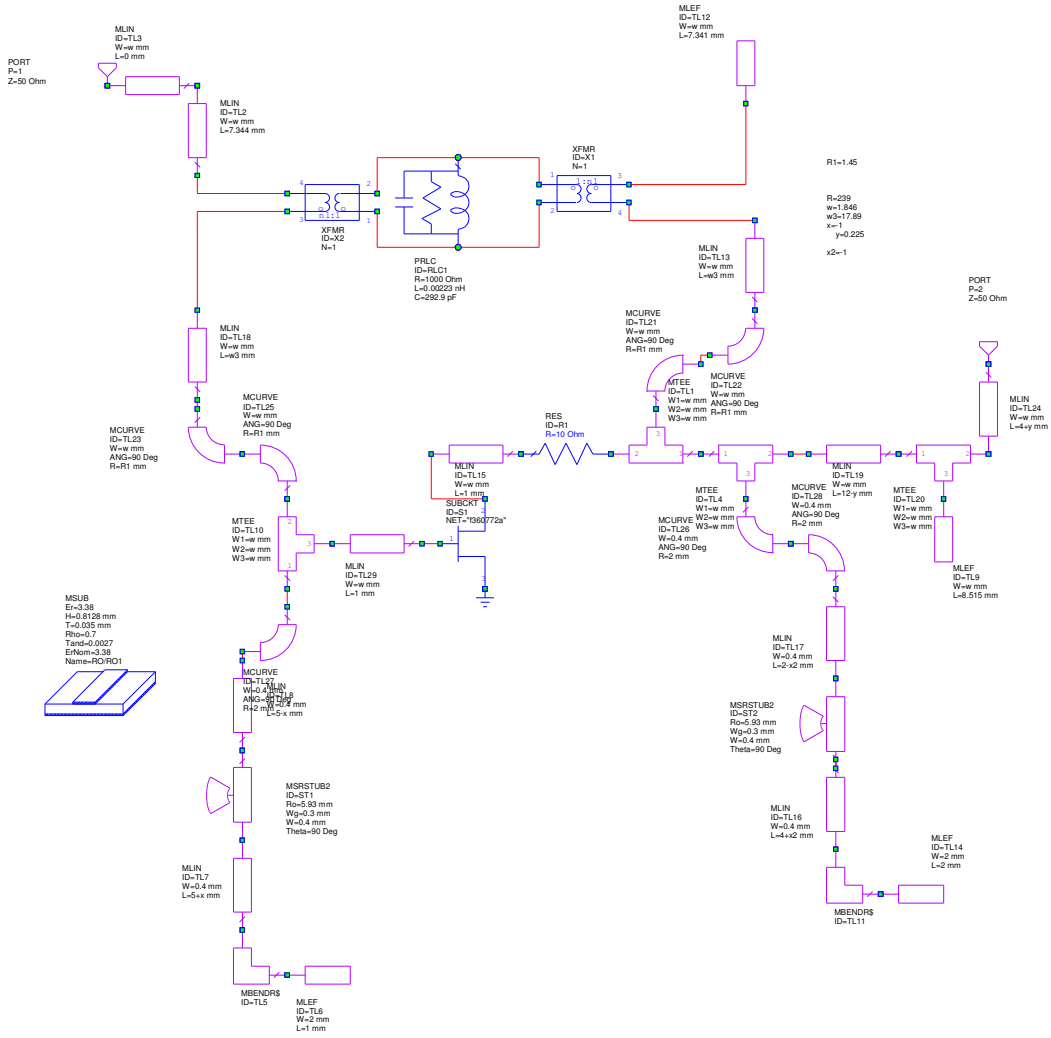

d) The 11.2 GHz parallel feedback DRO schematic

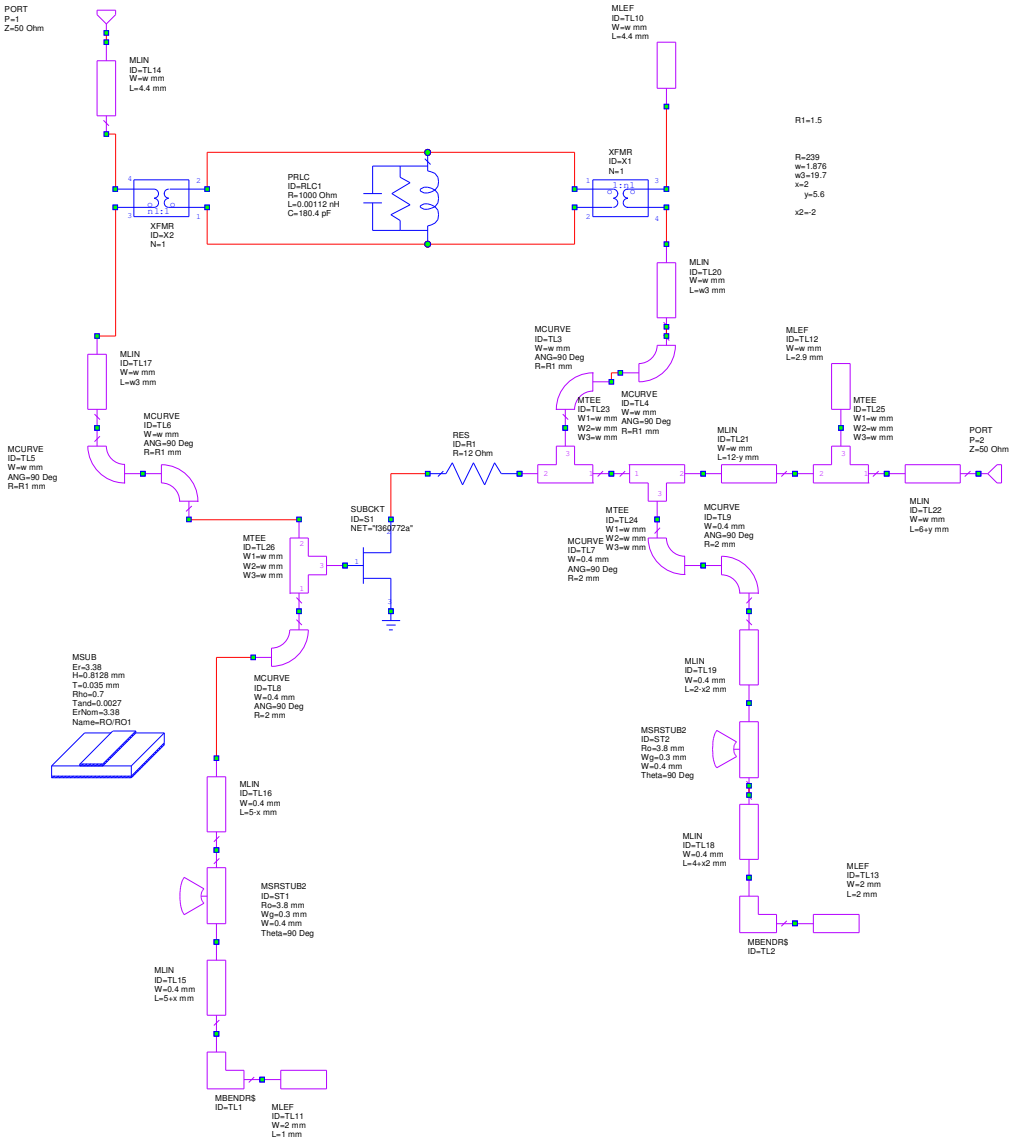

Appendix C: Resonant Modes for the metal cavity

```
clc
close all
clear all

a=40e-3; %width
%b=20.195e-3;% hi
b= 10e-3; % Hieght
d=40e-3;% Length
 c=3e8;
  m=1:10;
n=1:10;
P=1:10;

mind=1;
nind=1;
Pind=1;

for i=1:size(m,2)
   for j=1:size(n,2)
      for k=1:size(P,2)
         f(i,j,k)                                                                    =
(c/(2*pi)).*sqrt(((m(1,i)*pi)/a).^2+((n(1,j)*pi)/b).^2+((P(1,k)*pi)/d).^2)/1e9;
         if(f(i,j,k)>=0 && f(i,j,k)<=20)
            disp('****************')
            disp('      m        n        P      f');
            disp({i     j     k    f(i,j,k)});
            disp('****************')
         end
      end
   end
end
```

Appendix C

The Resonant Modes of the Metal Cavity:

****

m	n	P	f
1.0000	1.0000	1.0000	15.9099

****

****

m	n	P	f
1.0000	1.0000	2.0000	17.1847

****

****

m	n	P	f
1.0000	1.0000	3.0000	19.1213

****

****

m	n	P	f
2.0000	1.0000	1.0000	17.1847

****

****

m	n	P	f
2.0000	1.0000	2.0000	18.3712

****

****

m	n	P	f
3.0000	1.0000	1.0000	19.1213

****